

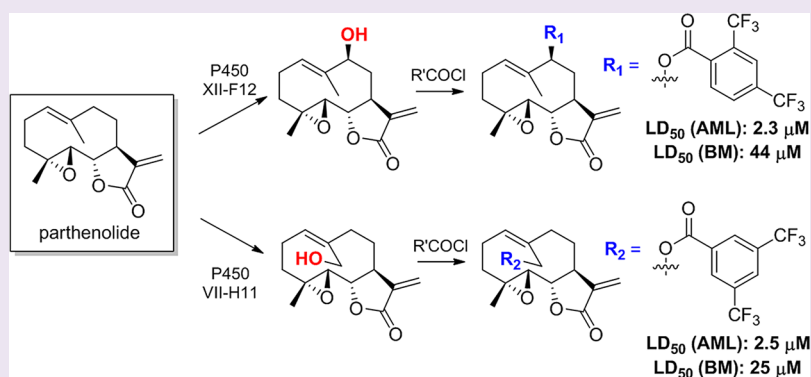
# Discovery of Potent Parthenolide-Based Antileukemic Agents Enabled by Late-Stage P450-Mediated C—H Functionalization

Joshua N. Kolev,<sup>†</sup> Kristen M. O'Dwyer,<sup>‡</sup> Craig T. Jordan,<sup>‡,§</sup> and Rudi Fasan<sup>\*,†</sup>

<sup>†</sup>Department of Chemistry, University of Rochester, Rochester, New York 14627, United States of America

<sup>‡</sup>Department of Hematology/Oncology, School of Medicine and Dentistry, University of Rochester, Rochester, New York 14627, United States of America

## S Supporting Information



**ABSTRACT:** The sesquiterpene lactone parthenolide has recently attracted considerable attention owing to its promising antitumor properties, in particular in the context of stem-cell cancers including leukemia. Yet, the lack of viable synthetic routes for re-elaborating this complex natural product has represented a fundamental obstacle toward further optimization of its pharmacological properties. Here, we demonstrate how this challenge could be addressed via selective, late-stage *sp*<sup>3</sup> C—H bond functionalization mediated by P450 catalysts with tailored site-selectivity. Taking advantage of our recently introduced tools for high-throughput P450 fingerprinting and fingerprint-driven P450 reactivity prediction, we evolved P450 variants useful for carrying out the highly regioselective hydroxylation of two aliphatic sites (C9 and C14) in parthenolide carbocyclic backbone. By chemoenzymatic synthesis, a panel of novel C9- and C14-modified parthenolide analogs were generated in order to gain initial structure–activity insights on these previously inaccessible sites of the molecule. Notably, some of these compounds were found to possess significantly improved antileukemic potency against primary acute myeloid leukemia cells, while exhibiting low toxicity against normal mature and progenitor hematopoietic cells. By identifying two ‘hot spots’ for improving the anticancer properties of parthenolide, this study highlights the potential of P450-mediated C—H functionalization as an enabling, new strategy for the late-stage manipulation of bioactive natural product scaffolds.

The past decade has witnessed an increasing interest for the natural product class of sesquiterpene lactones, a group of plant-derived 15-carbon terpenoids arising from the biosynthetic assembly of three isoprene units and containing a lactone ring either *cis*- or *trans*-fused to the carbocyclic skeleton.<sup>1,2</sup> Among them, parthenolide (**1**, PTL, Scheme 1) has attracted particular attention owing to its promising potential as an anticancer agent.<sup>3,4</sup> In recent studies, PTL was found capable of inducing robust apoptosis in primary acute myelogenous leukemia (AML) cells, proving to be equally effective among all subpopulations within primary AML specimens, including the so-called leukemia stem cells (LSCs).<sup>5–7</sup> LSCs are believed to play a crucial role not only in the genesis of AML<sup>8,9</sup> but also in the clinical relapse of AML patients following traditional chemotherapy<sup>10</sup> due to their reduced responsiveness to chemotherapeutic agents that kill actively cycling cells.<sup>11–13</sup> Thus, the LSC-targeting ability of PTL makes this molecule

particularly relevant toward the development of more effective treatments for AML and other hematologic malignancies. In addition, PTL was found to possess notable antiproliferative properties against many other types of human cancers, including breast,<sup>14,15</sup> lung,<sup>16</sup> prostate,<sup>17</sup> liver,<sup>18,19</sup> brain,<sup>20</sup> pancreas,<sup>21</sup> and bone<sup>22</sup> cancer.

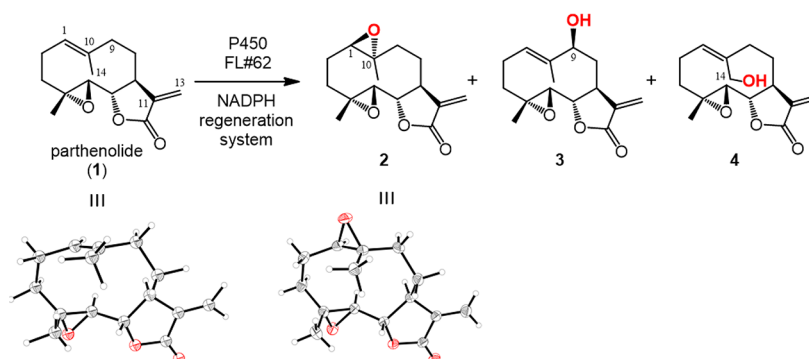
The anticancer properties of parthenolide has been primarily associated to its ability to inhibit the transcription factor NF- $\kappa$ B,<sup>23–25</sup> which is known to control multiple tumor-related processes such as inflammation, proliferation, angiogenesis, and metastasis.<sup>4</sup> However, additional mechanisms have been recently found to lie at the basis of the pharmacological effect of this molecule in cancer cells, which include activation of

Received: August 22, 2013

Accepted: October 22, 2013

Published: November 8, 2013

Scheme 1. Chemical Structure of Parthenolide (1, PTL) and of the Oxidation Products Obtained from Reaction with P450<sub>BM3</sub> Variant FL#62<sup>a</sup>



<sup>a</sup>Product distribution: 77% 2; 13% 3; 10% 4. X-ray crystal structures of 1<sup>63</sup> and 2 (this study) are shown.

p53<sup>5,26</sup> and proapoptotic Bcl-2 proteins,<sup>27</sup> induction of oxidative stress,<sup>18,28,29</sup> and alteration of epigenetic mechanisms.<sup>30,31</sup>

Owing to the promising anticancer properties of PTL, and in particular to its ability to target cancer stem cells, there is currently a high interest in re-elaborating this natural product scaffold to obtain derivatives with enhanced potency and improved drug-like properties. Previous efforts in this direction have taken advantage of the reactivity of the  $\alpha$ -methylene- $\gamma$ -lactone moiety, resulting in the preparation of various C13-modified PTL analogs.<sup>7,32–36</sup> However, the  $\alpha$ -methylene- $\gamma$ -lactone moiety is also critical for mediating PTL pharmacological effects, serving as an electrophilic center in Michael-type addition reactions with sulphhydryl groups in the various cellular components (e.g., NF- $\kappa$ B, I $\kappa$ K, glutathione) targeted by the molecule.<sup>23,24,28,37</sup> As a result, the tolerance of this site to functionalization has been limited, with the corresponding C13-substituted derivatives often exhibiting a large decrease or complete loss of biological activity compared to PTL.<sup>7,32–36</sup> As an exception, a few C13-amino adducts, and in particular 11,13-dehydro-13-dimethylamino-parthenolide (DMAPT),<sup>7,32</sup> has been shown to retain comparable anticancer activity to PTL, while presenting improved oral bioavailability due to the increased water-solubility of the amine adduct.<sup>7</sup> Notably, DMAPT has advanced to clinical trials for the treatment of AML and other hematologic malignancies. Despite this progress, improvements in PTL anticancer potency have not been achieved to date, posing a barrier to the development of more effective and selective parthenolide-based anticancer agents.

Based on our previous work,<sup>38,39</sup> we envisioned that P450-mediated C–H functionalization could provide a means to expand opportunities for the functional re-elaboration of the PTL scaffold toward this goal. Cytochrome P450 enzymes constitute an attractive catalytic platform for the oxyfunctionalization of unactivated C–H bonds in organic molecules,<sup>40–48</sup> complementing and often extending beyond the scope of chemical oxidation reagents and catalysts.<sup>49</sup> In particular, methodologies for high-throughput P450 active-site mapping (“P450 fingerprinting”) and P450 reactivity prediction recently introduced by our group have provided a way to guide and accelerate the development of P450 catalysts with fine-tuned regio- and stereoselectivity,<sup>38,39</sup> a key requirement toward the application of these biological catalysts for synthetic applications.<sup>49</sup> Here, we demonstrate how these tools proved useful in

rapidly generating a panel of engineered P450 variants, derived from the bacterial, catalytically self-sufficient CYP102A1 (*B. megaterium*),<sup>50</sup> for the highly regio- and stereoselective oxidative activation of two  $sp^3$  C–H sites (C9 and C14) as well as of the C<sub>1</sub>,C<sub>10</sub> double bond in PTL carbocyclic skeleton. Using these catalysts, a series of novel, C9- and C14-substituted parthenolide derivatives were made available by chemo-enzymatic synthesis for activity evaluation in assays with primary AML specimens. Importantly, these studies demonstrate that both the C9 and C14 positions constitute ‘hot spots’ for improving the antileukemic potency of parthenolide, while granting high selectivity against malignant cells over normal mature and progenitor hematopoietic cells.

## RESULTS AND DISCUSSION

**Parthenolide Oxidation via a Substrate-Promiscuous P450<sub>BM3</sub> Variant.** In previous studies,<sup>38</sup> we found that a substrate-promiscuous variant of the fatty acid monooxygenase P450<sub>BM3</sub> (*B. megaterium*),<sup>50</sup> called FL#62, is able to oxidize a broad range of bulky compounds, including decaline-based terpenes. Accordingly, we expected that our target compound, parthenolide, could be equally well accepted by this P450 as a substrate for oxidation. Gratifyingly, FL#62 was found to be capable of efficiently oxidizing PTL, supporting more than 1000 total turnovers (TTN) and producing a mixture of three monooxygenated products in 77:13:10 ratio as determined by GC-MS. Structural elucidation by NMR and X-ray crystallography revealed that the major product consisted of 1(R),10(R)-epoxy-parthenolide (2, 77%), while the two minor products consisted of 9(S)-hydroxy-parthenolide (3, 13%) and 14-hydroxy-parthenolide (4, 10%), respectively (Scheme 1). The stereochemical configuration of the newly formed oxirane ring in 2 was determined by X-ray crystallographic analysis (Scheme 1). On the other hand, the observation of NOEs between the 9(H) and 1(H) protons allowed for the unambiguous assignment of the *S* configuration to the C9 carbon in 3. In contrast to FL#62, wild-type P450<sub>BM3</sub> showed minimal PTL-oxidation activity (30 TTN), producing the epoxide 2 as the only product.

Compounds 2 and 3 correspond to naturally occurring derivatives of parthenolide,<sup>51,52</sup> whereas compound 4 has been previously obtained as a minor product (4%) from microbial metabolism of PTL.<sup>53</sup> The hydroxylation products 3 and 4 were of particular interest to us, as they can provide two valuable intermediates, not accessible via currently available

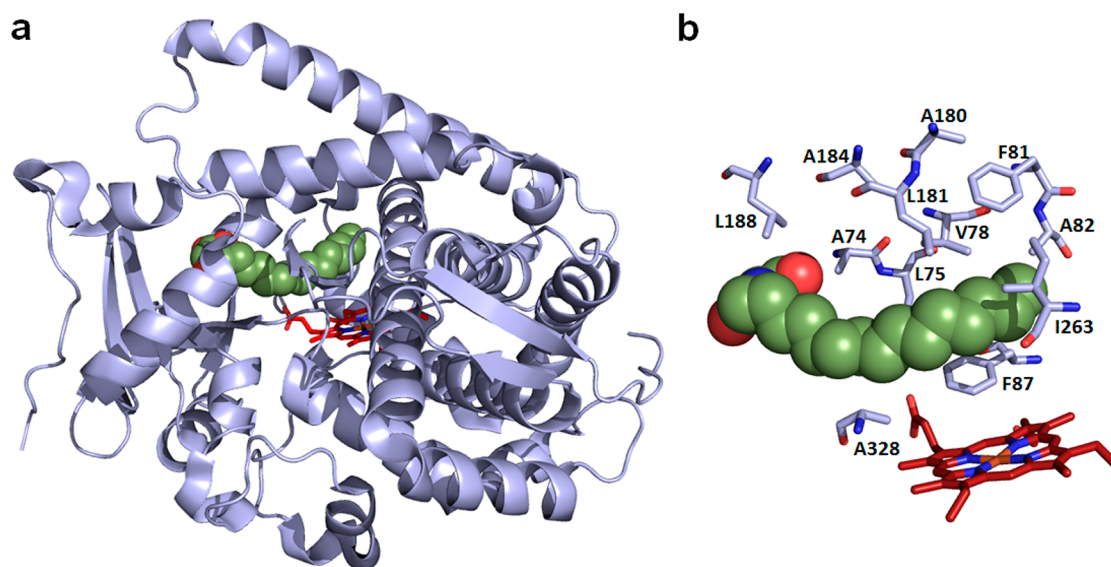


**Figure 1.** (a) Crystal structure of P450<sub>BM3</sub> heme domain in complex with N-palmitoylglycine (PDB code 1JPZ). The heme prosthetic group is displayed in red (stick model) and the enzyme-bound substrate in green (sphere model). (b) Close-up view of the enzyme active site, in which the amino acid residues targeted for mutagenesis in this study are highlighted.

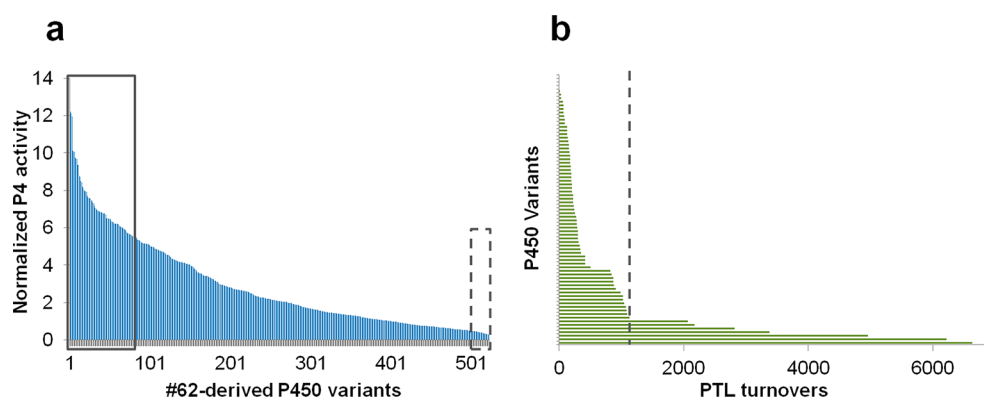


**Figure 2.** Fingerprint-based prediction of parthenolide reactivity via fingerprint single component analysis (SCA). (a) Ranking of the 522 FL#62-derived P450 variants according to their normalized activity on the decaline-based probe P4 (SI Figure S1). The 75 top-ranking (solid box) and 20 bottom-ranking (dotted box) variants are highlighted. (b) Total turnovers in PTL oxidation for the 75 top-scoring P450 variants arranged from the least to the most active variant. TTN value for FL#62 is indicated for comparison (dotted line).

synthetic methods, for re-elaboration of parthenolide carbocyclic skeleton by chemoenzymatic means. Indeed, while chemical oxidation of the allylic site C14 in parthenolide has been reported (with SeO<sub>2</sub> and *t*-BuOOH),<sup>54</sup> this transformation is accompanied by a Z→E isomerization of the 1,10-double bond, leading to an important structural reorganization of the 10-membered ring of the molecule.<sup>55</sup> Interestingly, the sites targeted by FL#62 (i.e., *si* face of 1,10 C=C bond, pro-*S* C(9)—H bond, and C(14)—H bond) are localized within the same region of the molecule, as evinced from inspection of the crystal structure of 2 (Scheme 1). While the expanded active site of FL#62 is likely at the basis of the poor regio/stereocontrol in the oxidation of this and other substrates,<sup>38,39</sup> the preferential formation of 2 over 3 and 4 is likely to arise from the higher reactivity of the electron-rich olefinic group compared to the neighboring allylic positions, C9 and C14, to P450-catalyzed oxidation. This electronic bias notwithstanding, our previous success in fine-tuning the site-selectivity of artemisinin-hydroxylating P450 variants suggested that P450 catalysts with improved site-selectivity toward each of the positions targeted by FL#62, and in particular the two, less

activated aliphatic C—H sites, could be obtained via re-elaboration of the enzyme active site in combination with our recently introduced P450 fingerprint-based tools<sup>38,39</sup> to expedite this process.

**Prediction of PTL Oxidation Reactivity via Fingerprint Single Component Analysis (SCA).** In the course of previous work, over 500 functionally diverse P450 catalysts derived from FL#62 were obtained via a two step process involving (a) simultaneous site-saturation mutagenesis of multiple ‘first-sphere’ active-site residues (i.e., 74, 78, 81, 82, 87, 181, and 184, Figure 1), followed by (b) high-throughput mapping of the active site configuration of the resulting engineered P450 variants by means of a panel of five structurally diverse chromogenic probes (compounds P1–P5, Supporting Information (SI) Figure S1). Through this process, a collection of 522 FL#62-derived P450s featuring a unique active site geometry and thus unique regio- and stereoselectivity properties (as derived from the uniqueness of their fingerprint profile)<sup>38</sup> were thus made available for the search of more selective PTL-oxidizing P450 catalysts in the context of this work.

Table 1. Amino Acid Mutations and Catalytic Properties of Parthenolide-Oxidizing P450 Variants<sup>a</sup>

variant	amino acid substitutions <sup>b</sup>							product distribution (%)			TTN	product form. rate <sup>c</sup>	coupling efficiency (%) <sup>d</sup>	K <sub>D</sub> (μM)
	78	81	82	87	180	181	184	2	3	4				
FL#62	A	S	V	A	T	L	V	77	13	10	1042 ± 98	234 ± 23	55.8	243 ± 9
III-D4	F	V	A					90	7	3	4980 ± 430	214 ± 31	29.5	193 ± 67
II-C5	T	I	A					29	68	3	1370 ± 153	59 ± 9	37.5	56 ± 12
XI-A11	T	I	T					22	77	1	1710 ± 116	44 ± 2	60.8	340 ± 21
XII-F12	T	I	T		A			19	80	1	1310 ± 71	27 ± 1	25.8	229 ± 38
II-E2	N	F	A					26	20	53	1055 ± 59	176 ± 12	42.9	289 ± 116
VII-H11	N	F	A		A	A	S	17	2	81	420 ± 46	21 ± 3	31.1	478 ± 109
XII-D8	N	F	A	V	A	A	S	4	0	95	60 ± 8	2 ± 0.6	1.4	n.d.

<sup>a</sup>Mean values and standard deviations are calculated from triplicate experiments. <sup>b</sup>Compared to P450<sub>BM3</sub>, FL#62 carries the following mutations: V78A, F81S, A82 V, F87A, P142S, T175I, A180T, A184 V, A197 V, F205C, S226R, H236Q, E252G, R255S, A290 V, L353 V. <sup>c</sup>Rates are measured over initial 30 s and expressed as mole product per mole P450 per minute. <sup>d</sup>Ratio between product formation rate and NADPH oxidation rate in the presence of parthenolide.

We recently reported two complementary methods for predicting P450 reactivity based on the analysis of their fingerprints. A first one, suitable for probe-related target substrates, utilizes the fingerprint component corresponding to the probe most closely related, structurally, to the target substrate as a predictor of enzyme reactivity toward this molecule (referred to as fingerprint single component analysis, or SCA).<sup>38</sup> More recently, we described a more general approach, applicable to probe-unrelated target molecules, that relies upon the multivariate analysis of fingerprint/substrate reactivity correlations using a randomly chosen training set of P450 variants (fingerprint multiple component analysis, or MCA).<sup>39</sup> In the context of parthenolide, both approaches are feasible, which provided us with an interesting opportunity to compare side-by-side the performance and predictive capability of the two methods.

The Maximum Common Substructure (MCS) algorithm<sup>56,57</sup> is particularly well suited to assess the degree of structural similarity between core-related molecules.<sup>58</sup> Based on this algorithm, the decaline-based probe P4 (Supporting Information (SI) Figure S1) was determined to represent the best predictor of parthenolide reactivity among the fingerprint probe set ( $S_{\text{MCS}} = 0.68$  vs  $S_{\text{MCS}} < 0.4$  against P1, P2, P3, or P5, with  $S_{\text{MCS}}$  ranging from 1 (structural identity) to 0 (max. structural dissimilarity)) via the SCA method. Accordingly, the collection of 522 FL#62-derived P450 catalysts were ranked based on their P4 probe activity in order to prioritize our search for PTL-oxidizing variants with improved regioselectivity (Figure 2a). Guided by these analyses, the 75 top-ranking P450 variants were retrieved from the collection and tested for PTL oxidation activity. Gratifyingly, we found that 81% of these variants (61/75) showed PTL-oxidation activity at synthetically useful levels (>100 TTN; average = 695 TTN, Figure 2b). In addition, a good fraction (21%) exhibited higher PTL oxidation activity than the parent enzyme, with four of them supporting total turnover numbers in excess of 4000 (Figure 2b). In contrast, 90% of the predicted inactive (i.e., bottom-ranking) variants (18/20) were found to be inactive on parthenolide, further supporting the reliability of the SCA predictions.

The parthenolide-oxidizing P450 variants identified in this manner exhibited in most cases diversified regioselectivity properties as expected from their different fingerprint profiles (SI Table S2). Most importantly, P450 catalysts with improved regioselectivity toward each of three target oxidation sites were found. In particular, the triple mutant II-C5 displayed the

largest improvement toward C9 hydroxylation (13% → 68%) while maintaining absolute S stereoselectivity and supporting more catalytic turnovers than FL#62 (Table 1 and SI Table S2). On the other hand, the triple mutant II-E2 represented the best C14-hydroxylating catalyst (10% → 53%) within this generation of variants, supporting over 1000 TTN in parthenolide oxidation (Table 1 and SI Table S2). Finally, a P450 variant with improved regioselectivity and absolute stereoselectivity for production of 1(R),10(R)-epoxy-PTL (2), III-D4, was also found at this stage, this variant also exhibiting a nearly 5-fold increase in catalytic activity compared to the parent enzyme FL#62 (4980 vs 1042 TTN).

**Parthenolide Reactivity Prediction via Fingerprint Multiple Component Analysis (MCA).** To compare the relative performance of MCA vs SCA toward prediction of parthenolide reactivity, a training set consisting of 20 parthenolide-active P450 variants, including FL#62, was first assembled (SI Table S3). Then, a fingerprint-based predictive model of PTL reactivity was generated by correlating the fingerprints with the experimentally determined PTL oxidation activities (measured in TTNs) across the training set using multiple linear regression analysis (MLR), as described previously (SI Figure S2a).<sup>39</sup> Using this model, the P450 catalysts in the 522-member collection were ranked according to their predicted PTL reactivity (SI Figure S2b). Experimental testing of the 75 top-ranking variants revealed that 62 of them (83%) were capable of PTL oxidation at synthetically useful levels (TTN > 100), supporting an average of 807 TTN (SI Figure S2c). To further probe the MCA-based predictions, the 20 bottom-ranking variants were also tested. Within this group, only six (30%) were found to be active (avg. TTN: 163). Interestingly, the group of 75 top-ranking P450s as defined by MCA largely overlapped with that based on SCA (64%) and included the best C9- and C14-hydroxylating variants (i.e., II-C5 and II-E2, respectively) previously identified by the latter method. None of the 27 variants uniquely found by MCA show further improved regioselectivity toward these positions. Based on these results, we conclude that both methods performed equally well in guiding the search for PTL oxidizing P450 catalysts.

**Selective P450 Catalysts for C9 and C14 Hydroxylation.** To achieve further improvements in regioselectivity for C9 hydroxylation, II-C5 was used as the parent enzyme for the construction of a series of single mutant libraries via site-saturation mutagenesis (NNK degenerate codon) of positions

82, 87, 180, 181, 184, 263, and 328 (Figure 1). These positions correspond to 'first-sphere' active site residues (based on the available P450<sub>BM3</sub> crystal structure<sup>59</sup>) that, with the exception of residue 82, have remained unmodified as compared to FL#62. High-throughput fingerprinting of these libraries (609 total recombinants screened) followed by fingerprint comparative analysis revealed the occurrence of 111 unique-fingerprint variants. Upon screening of these variants, three P450 catalysts with improved C9-selectivity (65–75%) were found, with the best one, XI-A11, also exhibiting higher catalytic activity than the parent enzyme II-C5 (1710 vs 1040 TTN, Table 1). As expected, each of these variants carried a single active-site mutation, namely A82T (in XI-A11), A87S, and T180A. The latter two beneficial mutations were then introduced into XI-A11, alone and in combination. Among the resulting variants, XII-F12, which corresponds to XI-A11(T180A), emerged as the best catalyst for C9-hydroxylation, being able to produce the desired product 3 with 80% regioselectivity, absolute *S*-stereoselectivity, and supporting over 1300 TTN (Table 1).

Using a similar approach, the best C14-hydroxylating variant identified during the first step, II-E2, was selected as the starting point toward generating P450 catalysts that could provide selective access to the C14 aliphatic position. Conveniently, a panel of about 50 functionally diverse, II-E2-derived active-site variants were already available from our previous work.<sup>39</sup> These variants were produced by triple site-saturation mutagenesis of active site residues 74, 181, and 184. Screening of this panel of P450 catalysts against parthenolide led to the discovery of a triple mutant variant, VII-H11, which showed significantly improved regioselectivity toward C14 hydroxylation compared to II-E2 (53% → 81%, Table 1), albeit at the expense of the catalytic activity (420 vs 1055 TTN). In a further round of directed evolution, additional first-sphere active residues left untouched in VII-H11 (i.e., positions 74, 75, 87, 263, and 328) were subjected to site-saturation mutagenesis. From these five single mutant libraries, forty P450 variants were determined to be catalytically active and functionally diverse based on fingerprint analysis. Among these enzymes, XII-D8 represented the best catalyst for C14 hydroxylation, catalyzing the formation of 4 with excellent regioselectivity (95%, Table 1). Interestingly, also in this case, the improvement of C14-regioselectivity was accompanied by a reduction in the catalytic turnover number (Table 1).

Overall, the process outlined above enabled us to achieve our task of obtaining a panel of P450 catalysts with refined site-selectivity for each of the sites oxidized by the initial enzyme, FL#62, in the PTL carbocyclic scaffold (Figure 3). The fact that this goal could be accomplished by analyzing only a minimal fraction (1.8%) of the original engineered enzyme libraries (>16,500 members) highlights the peculiar advantage of the fingerprint-based analysis/prediction tools to guide this process.

#### Characterization of the Evolved P450 Catalysts.

Further experiments were conducted to characterize the best P450 variants for 1,10-epoxidation (III-D4), 9(*S*)-hydroxylation (XI-A11, XII-F12), and 14-hydroxylation (VII-H11, XII-D8), as well as their evolutionary intermediates (II-C5, II-E2), with respect to their kinetic parameters, substrate binding affinity, and coupling efficiency. Sequencing revealed that a small set of active site mutations (3–4), clustered within the back-end region of the heme pocket (i.e., positions 78, 81, 82, (180); Figure 1) were beneficial for steering the regioselectivity of the enzyme toward hydroxylation of the C9 site or toward epoxidation of the 1,10 double bond (Table 1). In comparison,

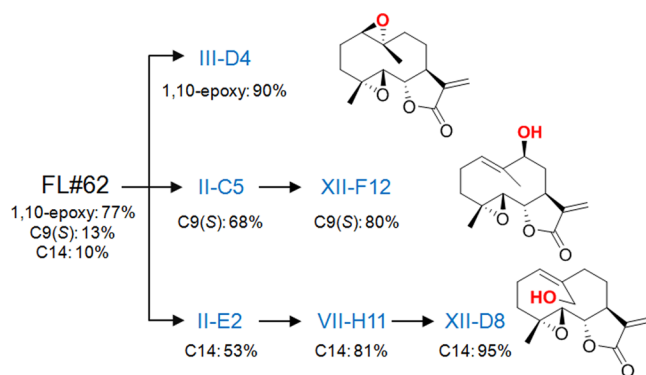


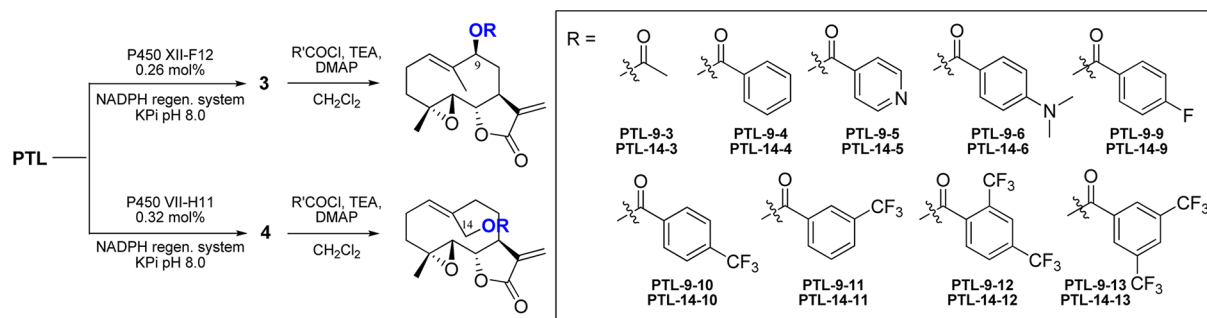
**Figure 3.** Overview of the directed evolution process leading to the selective parthenolide-oxidizing P450 variants.

refinement of C14-regioselectivity required a larger number of amino acid substitutions (6–7), which include modification of the aforementioned positions as well as another cluster of spatially close active site residues (i.e., 180, 181, 184; Figure 1).

The effect of these mutations on the substrate binding affinity ( $K_D$ ) was assessed via substrate-induced heme spin shift experiments (SI Figures S3–S4). These analyses indicated that the parent enzyme FL#62 binds parthenolide with relatively moderate affinity ( $K_D = 243 \mu\text{M}$ , Table 1), although this  $K_D$  value remains within the range of those observed for wild-type P450<sub>BM3</sub> and some fatty acid substrates (e.g., laurate;  $K_D = 270 \mu\text{M}$ ).<sup>60</sup> Comparable equilibrium dissociation constants (190–290  $\mu\text{M}$ ) were measured for most of the improved variants, with the exception of VII-H11, which showed a roughly 2-fold higher  $K_D$ , and XII-D8, which showed no signs of substrate-induced heme spin shift. Thus, these data suggest that, while being beneficial toward improving C14-selectivity, the mutations in the 180/181/184 cluster somewhat weaken the enzyme interaction with PTL.

Across the set of C9- and C14-hydroxylating variants, the progressive increase in site-selectivity was found to be generally accompanied by a decrease in the rate of substrate oxidation (Table 1). Interestingly, a similar trade-off was observed in the context of our previously reported artemisinin-hydroxylating P450s,<sup>39</sup> suggesting that this trend may be a common feature within this class of enzymes. This notwithstanding, all the improved variants, with the exception of VII-H11 and XII-D8, were able to support higher TTN compared to the initial enzyme FL#62, exhibiting coupling efficiencies (= ratio of product formation rate/NADPH oxidation rate) that range from 25% to 60% (Table 1). Interestingly, as noted above, the improvement of site-selectivity toward C14 hydroxylation was accompanied by a reduction in TTN, and in the case of XII-D8, also by a pronounced reduction in coupling efficiency, likely a result of the larger number of active site mutations accumulated by these variants. Nevertheless, the selectivity and catalytic efficiency of VII-H11 were well suited for synthetic purposes as demonstrated below.

**Chemoenzymatic Synthesis of PTL Derivatives.** With the strategy outlined above, three highly regio- and stereoselective P450 catalysts could thus be made available to explore the importance of the 1,10-double bond for parthenolide antileukemic activity (2) as well as provide two new points of entry (3, 4) for further functionalization of this molecule at the C9 and C14 sites via chemoenzymatic synthesis. To isolate sufficient quantities of 3 and 4 for these studies, preparative-scale reactions (100 mg PTL) were carried out using P450

Scheme 2. Chemoenzymatic Synthesis of the C9- and C14-Substituted Parthenolide Derivatives<sup>a</sup>

<sup>a</sup>Designated as PTL-9-(#) and PTL-14-(#), respectively.

variants XII-F12 (0.26 mol %) and VII-H11 (0.32 mol %), respectively, in the presence of a NADPH regeneration system consisting of a thermostable phosphite dehydrogenase<sup>61</sup> and sodium phosphite as sacrificial reductant. VII-H11 was preferred over the more regioselective XII-D8 because of much higher total turnover numbers, making it a superior catalyst for synthetic purposes. From these reactions, about 75 mg of each of the desired oxidation products could be obtained in over 70% isolated yields.

The isolated 9(*S*)-hydroxy- (3) and 14-hydroxy-PTL (4) were then further processed to generate a panel of 9- and 14-substituted parthenolide derivatives (Scheme 2). To this end, direct acylation of 3 and 4 with acid chloride reagents was chosen as a rapid means to explore the accessibility of the C9 and C14 sites to substituents of varying size (e.g., acetyl vs benzoyl group) and to gain initial structure–activity insights on the impact of these modifications on PTL antileukemic activity. Based on the superior performance of the benzoylated analogs PTL-9/14-4 (*vide infra*), a second set of derivatives were prepared in which the benzoyl moiety was substituted with polar or lipophilic groups. Finally, the activity data collected with these compounds inspired the design and synthesis of a third set of parthenolide analogs in which two trifluoromethyl groups are installed at different positions of the benzoyl moiety.

**Antileukemic Activity of the PTL Derivatives.** To evaluate the antileukemic activity of the novel parthenolide derivatives, these compounds were tested against primary acute myelogenous leukemia (AML) cells obtained with informed consent from leukemia patients. In particular, two relapsed refractory AML specimens were utilized, which feature both a normal (AML100510) and a complex karyotype (AML123009), the latter exhibiting reduced sensitivity to PTL ( $LD_{50}$ : 9.7 vs 6.1  $\mu$ M, Table 2). Dose–response curves were obtained by measuring the variation of cell viability at increasing compound concentration using a previously described assay based on cell staining with annexin-V and 7-amino-actinomycin (7-ADD) followed by flow cytometry analysis.<sup>62</sup>

As illustrated in Figure 4a and SI Figure S6, 1(*R*),10(*R*)-epoxy-PTL (2) was found to show a moderate (2-fold) reduction in potency compared to PTL in both AML specimens, possibly due to the slight structural change resulting from epoxidation of the 1,10-double bond as revealed by the crystallographic data (Scheme 1). Interestingly, a complete loss of activity was observed with the two hydroxylated derivatives 3 and 4, clearly pointing at the deleterious effect of introducing a polar, hydroxyl group at either the C9 or C14 site. Similarly, the acetylated derivatives PTL-9-3 and PTL-14-3, featured a

**Table 2.  $LD_{50}$  Values for Parthenolide (PTL) and Its Chemoenzymatic Derivatives against the Two Primary AML Specimens and Healthy Bone Marrow (BM) Cells<sup>a</sup>**

	$LD_{50}$ ( $\mu$ M)	$LD_{50}$ ( $\mu$ M)	$LD_{50}$ ( $\mu$ M)
	AML123009	AML100510	bone marrow
PTL	9.7 (1)	6.1 (1)	>80
2	13.5 (0.7)	13.9 (0.4)	n.d.
3	95 (0.1)	17.4 (0.4)	n.d.
PTL-9-3	>100	24.2 (0.3)	n.d.
PTL-9-4	4.1 (2.4)	6.2 (1.0)	>20
PTL-9-5	6.1 (1.6)	7.2 (0.8)	>50
PTL-9-6	4.8 (2.0)	3.1 (2.0)	>50
PTL-9-9	6.3 (1.5)	2.7 (2.2)	25
PTL-9-10	3.5 (2.7)	4.3 (1.4)	23
PTL-9-11	4.6 (2.1)	6.3 (1.0)	n.d.
PTL-9-12	2.3 (4.2)	3.7 (1.6)	44
PTL-9-13	2.7 (3.6)	5.1 (1.2)	105
4	>100	>100	n.d.
PTL-14-3	>100	12.5 (0.5)	n.d.
PTL-14-4	6.4 (1.5)	7.8 (0.8)	>80
PTL-14-5	20.8 (0.5)	8.7 (0.7)	n.d.
PTL-14-6	5.9 (1.7)	5.4 (1.1)	n.d.
PTL-14-9	6.4 (1.5)	6.2 (1.0)	n.d.
PTL-14-10	3.7 (2.6)	3.1 (2.0)	37
PTL-14-11	7.8 (1.2)	10 (0.6)	n.d.
PTL-14-12	5 (1.9)	9.5 (0.6)	n.d.
PTL-14-13	2.5 (3.9)	3.4 (1.8)	25

<sup>a</sup>The values in parentheses indicate relative activities compared to PTL. n.d. = not determined.

dramatic reduction in antileukemic potency (Figure 4a and SI Figures S6 and S7). In stark contrast, the benzoylated derivatives PTL-9-4 and PTL-14-4, were found to exhibit a significantly improved activity (compared to PTL) against the complex-karyotype AML cells (AML123009), as indicated by the 2-fold lower  $LD_{50}$  values (Table 2). These results clearly showed the beneficial effect of larger, aromatic substituents at either the C9 or C14 sites toward potentiating PTL antileukemic activity. Accordingly, a set of compounds carrying variously substituted benzoyl groups at each of these positions were synthesized. Notably, most of the resulting semisynthetic derivatives were found to be 2- to 3-fold more potent than parthenolide as illustrated by the dose–response curves in Figure 4a and SI Figures S6 and S7, and as summarized in Table 2. Within the C9-functionalized series, the largest increases in potency were achieved through substitution of the aryl moiety at the *para* position with fluorine (PTL-9-9), a

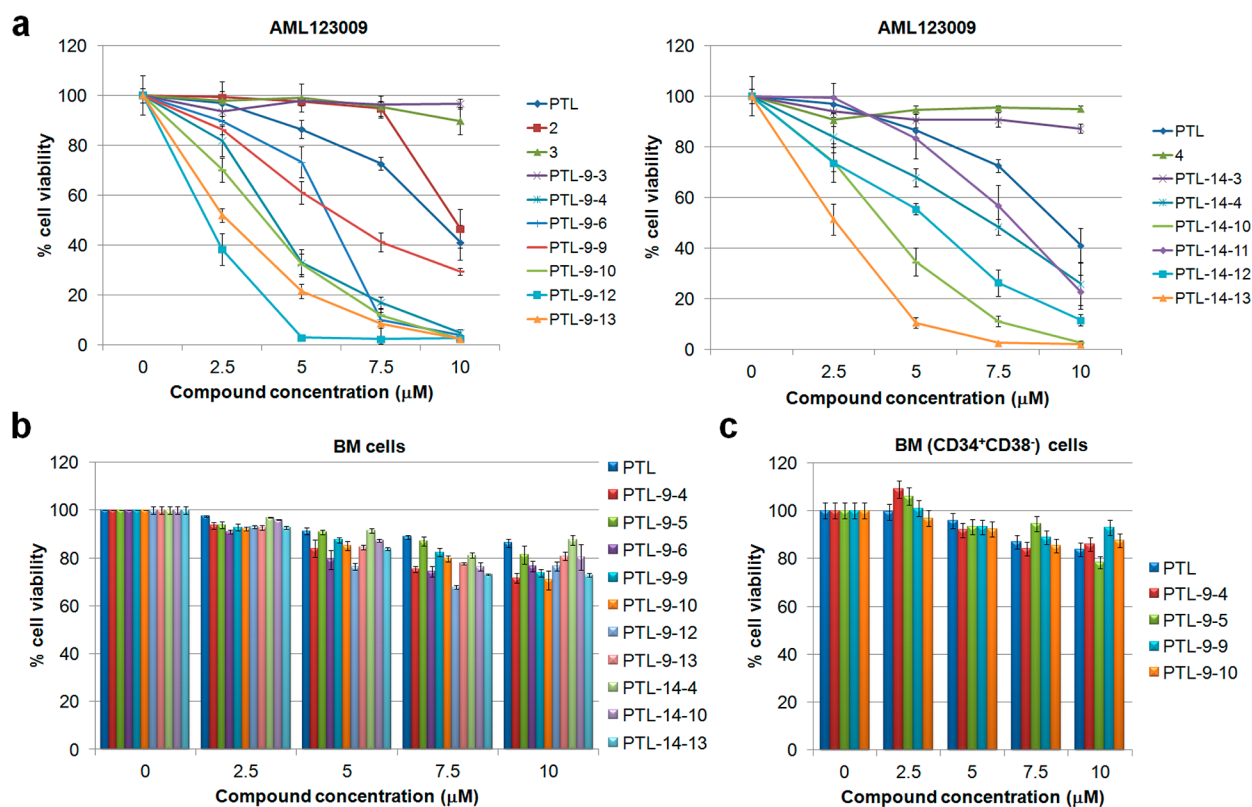


**Figure 4.** Biological activity for representative parthenolide (PTL) analogs. (a) Dose response curves for C9- (left panel) and C14-modified (right panel) PTL derivatives tested against a complex-karyotype primary AML specimen (AML123009). Data for the remaining analogs with a second primary AML specimen (AML100510) cells are provided in SI Figures S6 and S7. (b, c) Cytotoxicity of the most potent PTL analogs against (b) total and (c) primitive (CD34<sup>+</sup>CD38<sup>-</sup>) normal bone marrow cells.

dimethylamino (PTL-9-6), or trifluoromethyl group (PTL-9-10). A similar structure–activity trend was observed for the C14-functionalized series of compounds, although in this case the *para*-trifluoromethyl-benzoyl substituted derivative, PTL-14-10, emerged as the most potent derivative in the context of both AML specimens.

The beneficial effect of increasing the lipophilicity of the aryl moiety further suggested the design of compounds PTL-9/14-12 and PTL-9/14-13. Notably, the addition of a second trifluoromethyl group to the benzoyl moiety brought about a further increase in antileukemic potency for both the C9- and C14-modified analogs and in particular against AML123009 cells. Overall, the most promising compounds within each series, namely PTL-9-12 (LD<sub>50</sub>: 2.3 μM) and PTL-14-13 (LD<sub>50</sub>: 2.5 μM), were found to exhibit a 4.2- and 3.9-fold enhanced cytotoxicity, respectively, against primary AML cells compared to PTL (LD<sub>50</sub>: 9.7 μM, Table 2).

The most potent parthenolide derivatives identified in these studies were selected for further characterization to evaluate their selectivity against malignant over normal cells. For these studies, normal bone marrow cells (BM cells) obtained from healthy donors were utilized. Importantly, all these compounds, with the exception of PTL-9-6, did not significantly impart the viability of normal cells (Figure 4b), thus presenting the desired high selectivity against leukemic cells. Remarkably, at a concentration sufficient to kill 98% of primary AML cells (10 μM), compounds PTL-9-12 and PTL-9-13 were found to cause only less than 15% reduction in the viability of normal BM cells. For some of the most promising PTL analogs, it was also possible to test their cytotoxic effect on the progenitor

(CD34<sup>+</sup>CD38<sup>-</sup>) cell subpopulation of the bone marrow samples (Figure 4c). Notably, the compounds exhibited comparably low or even lower cytotoxicity than in the context of mature BM cells.

Taken together, these results showed that functionalizations at the C9/C14 sites are not only beneficial in enhancing PTL cytotoxicity but also that such effect is exerted with high selectivity in the context of leukemic cells. As a result, the LD<sub>50</sub>(BM)/LD<sub>50</sub>(AML) ratio of the original compound could be improved by several folds by means of these chemoenzymatic manipulations (e.g., 19 (PTL-9-12) and 39 (PTL-9-13) as compared to 8 for PTL with BM and AML123009 cells, Table 1). Given the relatively broad spectrum of cellular proteins/processes affected by PTL in cancer cells,<sup>5</sup> it is possible that the functional modification at the C9/C14 sites may cause a shift in the protein-targeting profile of the molecule, in a way that affect preferentially the proliferation of malignant cells.

**Conclusion.** In conclusion, we have developed efficient, P450-based chemoenzymatic routes to access novel derivatives of the sesquiterpene lactone parthenolide with potent activity and high selectivity against AML cells. From a methodological point of view, this study demonstrates the efficiency of our P450 fingerprint-based tools as a way to accelerate the development of P450 oxidation catalysts with refined regio- and stereoselectivity, a current bottleneck toward the exploitation of these enzymes for synthetic applications. Since the aliphatic positions targeted by the engineered P450s developed here have so far remained inaccessible to chemical manipulation, this work also highlights the potential of P450-

mediated C–H functionalization as a new, enabling strategy for the late-stage diversification and optimization of complex, bioactive molecules. A particularly relevant result from the present studies is the discovery that the C9 and C14 sites represent two ‘hot spots’ for potentiating the antileukemic activity of parthenolide. Notably, the improvements in anticancer activity against AML cells could be achieved without increasing their cytotoxicity against normal hematopoietic cells, thereby effectively enhancing the therapeutic index of the molecule. These findings have important implications. On one hand, two parallel routes (i.e., via C9 or C14 functionalization) have now become available toward further optimization of parthenolide as a therapeutic agent. In this regard, the tolerance of each of these sites to variously substituted aryl substituents is very promising, as it suggests that a variety of functional groups may be explored at these positions toward this goal. Furthermore, our results raise intriguing questions regarding the biochemical mechanisms at the basis of the improved cytotoxicity of the compounds in the context of malignant cells. Since parthenolide is known to target a variety of cellular components, it is plausible that the newly introduced functionalizations at the C9/C14 sites may shift the protein-targeting profile of the molecule in a way that affects preferentially the proliferation of malignant cells. We envision that future investigation of these aspects could provide valuable insights toward the development of effective pharmacological strategies for selective targeting of leukemia stem cells.

## METHODS

For complete description of the materials and methods including reagents, cloning procedures, protein expression and purification, fingerprint-based analyses, and enzyme characterization, see Supporting Information.

**Preparative-Scale Synthesis of 9(S)-, and 14-Hydroxy-parthenolide.** To prepare 3, purified P450 variant XII-F12 (final concn.: 2.5  $\mu\text{M}$ ; 0.26 mol %) was dissolved in 400 mL 50 mM phosphate buffer (pH 8.0) in the presence of parthenolide (100 mg, final concn.: 0.95 mM), PTDH (2  $\mu\text{M}$ ), NADP<sup>+</sup> (150  $\mu\text{M}$ ), and sodium phosphite (50 mM). The reaction mixture was stirred for 12 h at 4 °C. The crude product was extracted with dichloromethane (3  $\times$  80 mL). The collected organic layers were dried with sodium sulfate, concentrated under vacuum, and purified by flash chromatography (hexanes/ethyl acetate: 1/2) to afford 3 (75 mg, 70% (88% of theoretical maximum)) and 2 (16 mg, 15% (75% of theoretical maximum)). 9(S)-hydroxy-parthenolide (3): <sup>1</sup>H NMR (500 MHz, CDCl<sub>3</sub>):  $\delta$  1.34 (s, 3 H), 1.76 (s, 3 H), 1.97–2.06 (m, 1 H), 2.15–2.27 (m, 4 H), 2.50 (dq, 1 H,  $J$  = 5.2, 12.4 Hz), 2.70 (d, 1 H,  $J$  = 8.7 Hz), 2.83–2.90 (m, 1 H), 3.86 (t, 1 H,  $J$  = 8.5 Hz), 4.27 (dd, 1 H,  $J$  = 2.2, 10.5 Hz), 5.42 (d, 1 H,  $J$  = 11.3 Hz), 5.69 (d, 1 H,  $J$  = 3.2 Hz), 6.36 (d, 1 H,  $J$  = 3.6 Hz); <sup>13</sup>C NMR (125 MHz, CDCl<sub>3</sub>):  $\delta$  10.9, 17.4, 23.9, 36.1, 38.0, 44.5, 61.4, 66.2, 79.7, 81.5, 121.6, 126.5, 136.6, 138.3, 168.8; HRMS (ESI) calcd for C<sub>15</sub>H<sub>20</sub>O<sub>4</sub> [M+H]<sup>+</sup>  $m/z$ : 265.1440; found: 265.1433; [ $\alpha$ ]<sub>D</sub><sup>23</sup> = –83.9° (c: 0.43 g 100 mL<sup>-1</sup>, CH<sub>2</sub>Cl<sub>2</sub>). The 9(S) configuration of 3 was assigned based on the observed strong NOE signal (2.5%) between the 9(H) proton and 1(H) proton. 1(R),10(R)-epoxy-parthenolide (2): <sup>1</sup>H NMR (500 MHz, CDCl<sub>3</sub>):  $\delta$  1.34 (s, 3 H), 1.36–1.42 (m, 4 H), 1.45–1.56 (m, 1 H), 1.56–1.65 (m, 1 H), 2.01–2.29 (m, 4 H), 2.47 (dd, 1 H,  $J$  = 8.1, 14.0 Hz), 2.70–2.76 (m, 1 H), 2.85 (d, 1 H,  $J$  = 12.2 Hz), 2.90 (d, 1 H,  $J$  = 8.9 Hz), 3.93 (t, 1 H,  $J$  = 8.9 Hz), 5.62 (d, 1 H,  $J$  = 3.0 Hz), 6.33 (d, 1 H,  $J$  = 3.0 Hz); <sup>13</sup>C NMR (125 MHz, CDCl<sub>3</sub>):  $\delta$  17.0, 17.5, 24.0, 26.0, 35.1, 40.1, 47.6, 60.7, 63.7, 64.6, 81.8, 101.2, 121.4, 138.8, 168.9. HRMS (ESI) calcd for C<sub>15</sub>H<sub>20</sub>O<sub>4</sub> [M+H]<sup>+</sup>  $m/z$ : 265.1440; found: 265.1441; [ $\alpha$ ]<sub>D</sub><sup>23</sup> = –71.0° (c: 0.24 g 100 mL<sup>-1</sup>, CH<sub>2</sub>Cl<sub>2</sub>).

To prepare 4, purified P450 variant VII-H11 (final concn.: 3  $\mu\text{M}$ ; 0.32 mol %) was dissolved in 400 mL 50 mM phosphate buffer (pH 8.0) in the presence of parthenolide (100 mg, final concn.: 0.95 mM),

PTDH (2  $\mu\text{M}$ ), NADP<sup>+</sup> (150  $\mu\text{M}$ ), and sodium phosphite (50 mM). The reaction mixture was stirred for 12 h at 4 °C. The crude product was extracted with dichloromethane (3  $\times$  80 mL). The collected organic layers were dried with sodium sulfate, concentrated under vacuum, and purified by flash chromatography (hexanes/ethyl acetate: 1/2) to afford 4 (77 mg, 72% (90% of theoretical maximum)) and 2 (17 mg, 16% (79% of theoretical maximum)). 14-hydroxy-parthenolide (4): <sup>1</sup>H NMR (500 MHz, CDCl<sub>3</sub>):  $\delta$  1.31 (s, 3 H), 1.32–1.38 (m, 1 H), 1.82–1.92 (m, 1 H), 2.09–2.16 (m, 1 H), 2.20–2.32 (m, 3 H), 2.50 (dq, 1 H,  $J$  = 5.0, 13.4 Hz), 2.82–2.90 (m, 3 H), 3.92 (t, 1 H,  $J$  = 8.7 Hz), 4.16 (d, 1 H,  $J$  = 11.3 Hz), 4.46 (d, 1 H,  $J$  = 11.8 Hz), 5.43 (dd, 1 H,  $J$  = 4.1, 12.4 Hz), 5.68 (d, 1 H,  $J$  = 3.2 Hz), 6.39 (d, 1 H,  $J$  = 3.8 Hz). <sup>13</sup>C NMR (125 MHz, CDCl<sub>3</sub>):  $\delta$  = 16.9, 23.7, 31.4, 36.3, 47.3, 59.8, 61.1, 66.2, 82.4, 121.4, 129.0, 137.8, 139.2, 169.3. HRMS (ESI) calcd for C<sub>15</sub>H<sub>20</sub>O<sub>4</sub> [M+H]<sup>+</sup>  $m/z$ : 265.1440; found: 265.1440; [ $\alpha$ ]<sub>D</sub><sup>23</sup> = –61.7° (c: 0.13 g 100 mL<sup>-1</sup>, CH<sub>2</sub>Cl<sub>2</sub>).

**General Procedure for Synthesis of Parthenolide Derivatives.** To a solution of compound 3 (or 4) in 3 mL of anhydrous dichloromethane under argon atmosphere was added 4-dimethylaminopyridine (1 equiv.), triethylamine (5 equiv.), and the corresponding acid chloride (5 equiv.). Reaction was stirred at RT until complete disappearance of the starting material (ca. 2 h). At this point, the reaction mixture was added with saturated sodium bicarbonate solution (5 mL) and extracted with dichloromethane (3  $\times$  5 mL). The combined organic layers were dried over sodium sulfate, concentrated under reduced pressure, and the ester product was isolated by silica gel flash chromatography (5 to 40% ethyl acetate in hexanes). NMR and MS characterization data for these compounds are provided as Supporting Information.

**Cell Isolation and Culture.** Primary human AML and normal bone marrow (BM) cells were obtained from volunteer donors. Informed consent was obtained in accordance with the Declaration of Helsinki. All manipulation and analysis of human specimens was approved by the University of Rochester Institutional Review Board. In some cases, cells were cryopreserved in freezing medium of Iscove modified Dulbecco medium (IMDM), 40% fetal bovine serum (FBS), and 10% dimethylsulfoxide (DMSO) or in CryoStor CS-10 (VWR, West Chester, PA). Cells were cultured in serum-free medium (SFM)19 for 1 h before the addition of parthenolide or its derivatives.

**Cell Viability Assays.** Apoptosis assays were performed as described.<sup>62</sup> Briefly, after 24 h of treatment, normal BM cells and AML specimens were stained for the surface antibodies CD38-allophycocyanin (APC), CD34-PECy7, and CD123-phycoerythrin (Becton Dickinson, San Jose, CA) for 15 min. Cells were washed in cold PBS and resuspended in 200  $\mu\text{L}$  of annexin-V buffer (0.01 M HEPES/NaOH, 0.14 M NaCl, and 2.5 mM CaCl<sub>2</sub>). Annexin-V-fluorescein isothiocyanate (FITC) and 7-aminoactinomycin (7-AAD; Molecular Probes, Eugene, OR) were added, and the tubes were incubated at RT for 15 min then analyzed on a BD LSRII flow cytometer (BD Biosciences, San Jose, CA). Analyses for phenotypically described stem cell subpopulations were performed by gating CD34<sup>+</sup>/CD38<sup>-</sup> populations. Viable cells were scored as Annexin-V negative/7-AAD negative. The percent viability data provided are normalized to untreated control specimens.

## ASSOCIATED CONTENT

### Supporting Information

Chemical structures of probes P1–P5, oligonucleotide sequences, additional data corresponding to the fingerprint-based predictions and characterization of P450 variants, results from spin-shift experiments, characterization data for parthenolide derivatives. This material is available free of charge via the Internet at <http://pubs.acs.org>.

## AUTHOR INFORMATION

### Corresponding Author

\*E-mail: [fasan@chem.rochester.edu](mailto:fasan@chem.rochester.edu).

**Present Address**

<sup>§</sup>Division of Hematology, University of Colorado, Aurora, Colorado 80045, United States of America

**Author Contributions**

R.F. and C.T.J. conceived the project. J.N.K. conducted all the experiments concerning the engineering of the P450 catalysts and synthesis of the parthenolide derivatives. K.M.O. performed all the cellular and biochemical experiments concerning the biological activity of the compounds. R.F. wrote the manuscript with input from all the other coauthors.

**Notes**

The authors declare no competing financial interest.

**ACKNOWLEDGMENTS**

This work was supported by the National Institute of Health R01 grant GM098628 awarded to R.F. C.T.J. was supported by a grant from the Leukemia and Lymphoma Society (TRP 6230-11). MS instrumentation was supported by the National Science Foundation grants CHE-0840410 and CHE-0946653. The authors are grateful to Bill Brennessel for assistance with the X-ray crystallographic analyses.

**REFERENCES**

- (1) Ghantous, A., Gali-Muhtasib, H., Vuorela, H., Saliba, N. A., and Darwiche, N. (2010) What made sesquiterpene lactones reach cancer clinical trials? *Drug Discovery Today* 15, 668–678.
- (2) Janecka, A., Wyrebska, A., Gach, K., Fichna, J., and Janecki, T. (2012) Natural and synthetic  $\alpha$ -methylene lactones and  $\alpha$ -methylene lactams with anticancer potential. *Drug Discovery Today* 17, 561–572.
- (3) Guzman, M. L., and Jordan, C. T. (2005) Feverfew: Weeding out the root of leukaemia. *Expert Opin. Biol. Ther.* 5, 1147–1152.
- (4) Kreuger, M. R., Grootjans, S., Biavatti, M. W., Vandenabeele, P., and D'Herde, K. (2012) Sesquiterpene lactones as drugs with multiple targets in cancer treatment: Focus on parthenolide. *Anticancer Drugs* 23, 883–896.
- (5) Guzman, M. L., Rossi, R. M., Karnischky, L., Li, X. J., Peterson, D. R., Howard, D. S., and Jordan, C. T. (2005) The sesquiterpene lactone parthenolide induces apoptosis of human acute myelogenous leukemia stem and progenitor cells. *Blood* 105, 4163–4169.
- (6) Guzman, M. L., Karnischky, L., Li, X. J., Neering, S. J., Rossi, R. M., and Jordan, C. T. (2004) Selective induction of apoptosis in acute myelogenous leukemia stem cells by the novel agent parthenolide. *Blood* 104, 697a–697a.
- (7) Guzman, M. L., Rossi, R. M., Li, X. J., Corbett, C., Hassane, D. C., Bushnell, T., Carroll, M., Sullivan, E., Neelakantan, S., Crooks, P. A., and Jordan, C. T. (2006) A novel orally available parthenolide analog selectively eradicates AML stem and progenitor cells. *Blood* 108, 74a–74a.
- (8) Lapidot, T., Sirard, C., Vormoor, J., Murdoch, B., Hoang, T., Cacerescortes, J., Minden, M., Paterson, B., Caligiuri, M. A., and Dick, J. E. (1994) A cell initiating human acute myeloid-leukemia after transplantation into SCID mice. *Nature* 367, 645–648.
- (9) Bonnet, D., and Dick, J. E. (1997) Human acute myeloid leukemia is organized as a hierarchy that originates from a primitive hematopoietic cell. *Nat. Med.* 3, 730–737.
- (10) van Rhenen, A., Feller, N., Kelder, A., Westra, A. H., Rombouts, E., Zweegman, S., van der Pol, M. A., Waisfisz, Q., Ossenkoppele, G. J., and Schuurhuis, G. J. (2005) High stem cell frequency in acute myeloid leukemia at diagnosis predicts high minimal residual disease and poor survival. *Clin. Cancer Res.* 11, 6520–6527.
- (11) Graham, S. M., Jorgensen, H. G., Allan, E., Pearson, C., Alcorn, M. J., Richmond, L., and Holyoake, T. L. (2002) Primitive, quiescent, Philadelphia-positive stem cells from patients with chronic myeloid leukemia are insensitive to ST1571 *in vitro*. *Blood* 99, 319–325.

- (12) Costello, R. T., Mallet, F., Gaugler, B., Sainty, D., Arnoulet, C., Gastaut, J. A., and Olive, D. (2000) Human acute myeloid leukemia CD34<sup>+</sup>/CD38<sup>-</sup> progenitor cells have decreased sensitivity to chemotherapy and Fas-induced apoptosis, reduced immunogenicity, and impaired dendritic cell transformation capacities. *Cancer Res.* 60, 4403–4411.

- (13) Guzman, M. L., Swiderski, C. F., Howard, D. S., Grimes, B. A., Rossi, R. M., Szilvassy, S. J., and Jordan, C. T. (2002) Preferential induction of apoptosis for primary human leukemic stem cells. *Proc. Natl. Acad. Sci. U.S.A.* 99, 16220–16225.

- (14) Sweeney, C. J., Mehrotra, S., Sadaria, M. R., Kumar, S., Shortle, N. H., Roman, Y., Sheridan, C., Campbell, R. A., Murry, D. J., Badve, S., and Nakshatri, H. (2005) The sesquiterpene lactone parthenolide in combination with docetaxel reduces metastasis and improves survival in a xenograft model of breast cancer. *Mol. Cancer Ther.* 4, 1004–1012.

- (15) Zhou, J., Zhang, H., Gu, P., Bai, J., Margolick, J. B., and Zhang, Y. (2008) NF- $\kappa$ B pathway inhibitors preferentially inhibit breast cancer stem-like cells. *Breast Cancer Res. Treat.* 111, 419–427.

- (16) Zhang, D., Qiu, L., Jin, X., Guo, Z., and Guo, C. (2009) Nuclear factor- $\kappa$ B inhibition by parthenolide potentiates the efficacy of Taxol in non-small cell lung cancer *in vitro* and *in vivo*. *Mol. Cancer Res.* 7, 1139–1149.

- (17) Kawasaki, B. T., Hurt, E. M., Kalathur, M., Duhagon, M. A., Milner, J. A., Kim, Y. S., and Farrar, W. L. (2009) Effects of the sesquiterpene lactone parthenolide on prostate tumor-initiating cells: An integrated molecular profiling approach. *Prostate* 69, 827–837.

- (18) Wen, J., You, K. R., Lee, S. Y., Song, C. H., and Kim, D. G. (2002) Oxidative stress-mediated apoptosis. The anticancer effect of the sesquiterpene lactone parthenolide. *J. Biol. Chem.* 277, 38954–38964.

- (19) Park, J. H., Liu, L., Kim, I. H., Kim, J. H., You, K. R., and Kim, D. G. (2005) Identification of the genes involved in enhanced fenretinide-induced apoptosis by parthenolide in human hepatoma cells. *Cancer Res.* 65, 2804–2814.

- (20) Zanutto-Filho, A., Braganhol, E., Schroder, R., de Souza, L. H., Dalmolin, R. J., Pasquali, M. A., Gelain, D. P., Battastini, A. M., and Moreira, J. C. (2011) NF $\kappa$ B inhibitors induce cell death in glioblastomas. *Biochem. Pharmacol.* 81, 412–424.

- (21) Yip-Schneider, M. T., Nakshatri, H., Sweeney, C. J., Marshall, M. S., Wiebke, E. A., and Schmidt, C. M. (2005) Parthenolide and sulindac cooperate to mediate growth suppression and inhibit the nuclear factor- $\kappa$ B pathway in pancreatic carcinoma cells. *Mol. Cancer Ther.* 4, 587–594.

- (22) Zuch, D., Giang, A. H., Shapovalov, Y., Schwarz, E., Rosier, R., O'Keefe, R., and Eliseev, R. A. (2012) Targeting radioresistant osteosarcoma cells with parthenolide. *J. Cell Biochem.* 113, 1282–1291.

- (23) Garcia-Pineres, A. J., Castro, V., Mora, G., Schmidt, T. J., Strunck, E., Pahl, H. L., and Merfort, I. (2001) Cysteine 38 in p65/NF- $\kappa$ B plays a crucial role in DNA binding inhibition by sesquiterpene lactones. *J. Biol. Chem.* 276, 39713–39720.

- (24) Garcia-Pineres, A. J., Lindenmeyer, M. T., and Merfort, I. (2004) Role of cysteine residues of p65/NF- $\kappa$ B on the inhibition by the sesquiterpene lactone parthenolide and N-ethyl maleimide, and on its transactivating potential. *Life Sci.* 75, 841–856.

- (25) Hehner, S. P., Heinrich, M., Bork, P. M., Vogt, M., Ratter, F., Lehmann, V., Schulze-Osthoff, K., Droge, W., and Schmitz, M. L. (1998) Sesquiterpene lactones specifically inhibit activation of NF- $\kappa$ B by preventing the degradation of I $\kappa$ B- $\alpha$  and I $\kappa$ B- $\beta$ . *J. Biol. Chem.* 273, 1288–1297.

- (26) Gopal, Y. N., Chanchorn, E., and Van Dyke, M. W. (2009) Parthenolide promotes the ubiquitination of MDM2 and activates p53 cellular functions. *Mol. Cancer Ther.* 8, 552–562.

- (27) Zhang, S., Ong, C. N., and Shen, H. M. (2004) Involvement of proapoptotic Bcl-2 family members in parthenolide-induced mitochondrial dysfunction and apoptosis. *Cancer Lett.* 211, 175–188.

- (28) Skalska, J., Brookes, P. S., Nadtochiy, S. M., Hilchey, S. P., Jordan, C. T., Guzman, M. L., Maggior, S. B., Briehl, M. M., and Bernstein, S. H. (2009) Modulation of cell surface protein free thiols:

A potential novel mechanism of action of the sesquiterpene lactone parthenolide. *PLoS One* 4, e8115.

(29) Wang, W., Adachi, M., Kawamura, R., Sakamoto, H., Hayashi, T., Ishida, T., Imai, K., and Shinomura, Y. (2006) Parthenolide-induced apoptosis in multiple myeloma cells involves reactive oxygen species generation and cell sensitivity depends on catalase activity. *Apoptosis* 11, 2225–2235.

(30) Liu, Z., Liu, S., Xie, Z., Pavlovicz, R. E., Wu, J., Chen, P., Aimuwu, J., Pang, J., Bhasin, D., Neviani, P., Fuchs, J. R., Plass, C., Li, P. K., Li, C., Huang, T. H., Wu, L. C., Rush, L., Wang, H., Perrotti, D., Marcucci, G., and Chan, K. K. (2009) Modulation of DNA methylation by a sesquiterpene lactone parthenolide. *J. Pharmacol. Exp. Ther.* 329, 505–514.

(31) Gopal, Y. N., Arora, T. S., and Van Dyke, M. W. (2007) Parthenolide specifically depletes histone deacetylase 1 protein and induces cell death through ataxia telangiectasia mutated. *Chem. Biol.* 14, 813–823.

(32) Neelakantan, S., Nasim, S., Guzman, M. L., Jordan, C. T., and Crooks, P. A. (2009) Aminoparthenolides as novel anti-leukemic agents: Discovery of the NF- $\kappa$ B inhibitor, DMAPT (LC-1). *Bioorg. Med. Chem. Lett.* 19, 4346–4349.

(33) Nasim, S., and Crooks, P. A. (2008) Antileukemic activity of aminoparthenolide analogs. *Bioorg. Med. Chem. Lett.* 18, 3870–3873.

(34) Hwang, D. R., Chang, C. W., Lien, T. W., Chen, W. C., Tan, U. K., Hsu, J. T. A., and Hsieh, H. P. (2006) Synthesis and anti-viral activity of a series of sesquiterpene lactones and analogues in the subgenomic HCV replicon system. *Bioorgan. Med. Chem.* 14, 83–91.

(35) Han, C., Barrios, F. J., Rioski, M. V., and Colby, D. A. (2009) Semisynthetic derivatives of sesquiterpene lactones by palladium-catalyzed arylation of the  $\alpha$ -methylene- $\gamma$ -lactone substructure. *J. Org. Chem.* 74, 7176–7179.

(36) Woods, J. R., Mo, H., Bieberich, A. A., Alavanja, T., and Colby, D. A. (2011) Fluorinated amino-derivatives of the sesquiterpene lactone, parthenolide, as (19)f NMR probes in deuterium-free environments. *J. Med. Chem.* 54, 7934–7941.

(37) Kwok, B. H., Koh, B., Ndubuisi, M. I., Elofsson, M., and Crews, C. M. (2001) The anti-inflammatory natural product parthenolide from the medicinal herb Feverfew directly binds to and inhibits I $\kappa$ B kinase. *Chem. Biol.* 8, 759–766.

(38) Zhang, K., El Damaty, S., and Fasan, R. (2011) P450 fingerprinting method for rapid discovery of terpene hydroxylating P450 catalysts with diversified regioselectivity. *J. Am. Chem. Soc.* 133, 3242–3245.

(39) Zhang, K., Shafer, B. M., Demars, M. D., 2nd, Stern, H. A., and Fasan, R. (2012) Controlled oxidation of remote  $sp^3$  C–H bonds in artemisinin via P450 catalysts with fine-tuned regio- and stereo-selectivity. *J. Am. Chem. Soc.* 134, 18695–18704.

(40) Glieder, A., Farinas, E. T., and Arnold, F. H. (2002) Laboratory evolution of a soluble, self-sufficient, highly active alkane hydroxylase. *Nat. Biotechnol.* 20, 1135–1139.

(41) Fasan, R., Chen, M. M., Crook, N. C., and Arnold, F. H. (2007) Engineered alkane-hydroxylating cytochrome P450(BM3) exhibiting native-like catalytic properties. *Angew. Chem., Int. Ed.* 46, 8414–8418.

(42) Rentmeister, A., Arnold, F. H., and Fasan, R. (2009) Chemoenzymatic fluorination of unactivated organic compounds. *Nat. Chem. Biol.* 5, 26–28.

(43) Whitehouse, C. J., Bell, S. G., Tufton, H. G., Kenny, R. J., Ogilvie, L. C., and Wong, L. L. (2008) Evolved CYP102A1 (P450BM3) variants oxidize a range of non-natural substrates and offer new selectivity options. *Chem. Commun.*, 966–968.

(44) Li, S., Chaulagain, M. R., Knauff, A. R., Podust, L. M., Montgomery, J., and Sherman, D. H. (2009) Selective oxidation of carbonyl C–H bonds by an engineered macrolide P450 monooxygenase. *Proc. Natl. Acad. Sci. U.S.A.* 106, 18463–18468.

(45) Weber, E., Seifert, A., Antonovici, M., Geinitz, C., Pleiss, J., and Urlacher, V. B. (2011) Screening of a minimal enriched P450 BM3 mutant library for hydroxylation of cyclic and acyclic alkanes. *Chem. Commun.* 47, 944–946.

(46) Robin, A., Roberts, G. A., Kisch, J., Sabbadin, F., Grogan, G., Bruce, N., Turner, N. J., and Flitsch, S. L. (2009) Engineering and improvement of the efficiency of a chimeric [P450cam-RhFRed reductase domain] enzyme. *Chem. Commun.*, 2478–2480.

(47) Bordeaux, M., Galarneau, A., Fajula, F., and Drone, J. (2011) A regioselective biocatalyst for alkane activation under mild conditions. *Angew. Chem., Int. Ed.* 50, 2075–2079.

(48) Rea, V., Kolkman, A. J., Vottero, E., Stronks, E. J., Ampt, K. A., Honing, M., Vermeulen, N. P., Wijmenga, S. S., and Commandeur, J. N. (2012) Active site substitution A82W improves the regioselectivity of steroid hydroxylation by cytochrome P450 BM3 mutants as rationalized by spin relaxation nuclear magnetic resonance studies. *Biochemistry* 51, 750–760.

(49) Fasan, R. (2012) Tuning P450 enzymes as oxidation catalysts. *ACS Catal.* 2, 647–666.

(50) Narhi, L. O., and Fulco, A. J. (1987) Identification and characterization of two functional domains in cytochrome P-450BM-3, a catalytically self-sufficient monooxygenase induced by barbiturates in *Bacillus megaterium*. *J. Biol. Chem.* 262, 6683–6690.

(51) Bloszyk, E., Budesinsky, M., Daniewski, W. M., Peskova, E., Drozd, B., and Holub, M. (1990) Sesquiterpene lactones of *Inula aschersoniana*. *Collect. Czech. Chem. Commun.* 55, 1562–1567.

(52) Abdel Sattar, E., Galal, A. M., and Mossa, G. S. (1996) Antitumor germacranolides from *Anvillea garcinii*. *J. Nat. Prod.* 59, 403–405.

(53) Galal, A. M., Ibrahim, A. R. S., Mossa, J. S., and El-Feraly, F. S. (1999) Microbial transformation of parthenolide. *Phytochemistry* 51, 761–765.

(54) Nasim, S., Pei, S., Hagen, F. K., Jordan, C. T., and Crooks, P. A. (2011) Melampomagnolide B: A new antileukemic sesquiterpene. *Bioorg. Med. Chem.* 19, 1515–1519.

(55) Gonzalez, A. G., Galindo, A., Afonso, M. M., Mansilla, H., and Lopez, M. (1988) The biomimetic cyclization of melampomagnolide-B. *Tetrahedron* 44, 4585–4589.

(56) Cuisart, B., Touffet, F., Cremilleux, B., Bureau, R., and Rault, S. (2002) The maximum common substructure as a molecular depiction in a supervised classification context: Experiments in quantitative structure/biodegradability relationships. *J. Chem. Inf. Comput. Sci.* 42, 1043–1052.

(57) Cao, Y., Jiang, T., and Girke, T. (2008) A maximum common substructure-based algorithm for searching and predicting drug-like compounds. *Bioinformatics* 24, 366–374.

(58) Rahman, S. A., Bashton, M., Holliday, G. L., Schrader, R., and Thornton, J. M. (2009) Small molecule subgraph detector (SMSD) toolkit. *J. Cheminform.* 1, 1–13.

(59) Sevrioukova, I. F., Li, H., Zhang, H., Peterson, J. A., and Poulos, T. L. (1999) Structure of a cytochrome P450-redox partner electron-transfer complex. *Proc. Natl. Acad. Sci. U.S.A.* 96, 1863–1868.

(60) Oliver, C. F., Modi, S., Sutcliffe, M. J., Primrose, W. U., Lian, L. Y., and Roberts, G. C. (1997) A single mutation in cytochrome P450 BM3 changes substrate orientation in a catalytic intermediate and the regioselectivity of hydroxylation. *Biochemistry* 36, 1567–1572.

(61) McLachlan, M. J., Johannes, T. W., and Zhao, H. (2008) Further improvement of phosphite dehydrogenase thermostability by saturation mutagenesis. *Biotechnol. Bioeng.* 99, 268–274.

(62) Guzman, M. L., Neering, S. J., Upchurch, D., Grimes, B., Howard, D. S., Rizzieri, D. A., Luger, S. M., and Jordan, C. T. (2001) Nuclear factor- $\kappa$ B is constitutively activated in primitive human acute myelogenous leukemia cells. *Blood* 98, 2301–2307.

(63) Quick, A., and Rogers, D. (1976) Crystal and molecular-structure of parthenolide [4,5-epoxygermacra-1(10),11(13)-dien-12,6-olactone]. *J. Chem. Soc., Perkin Trans. 2*, 465–469.

Supplemental Information for

## **Discovery of potent parthenolide-based antileukemic agents enabled by late-stage P450-mediated C—H functionalization**

Joshua N. Kolev<sup>1</sup>, Kristen M. O'Dwyer<sup>2</sup>, Craig T. Jordan<sup>2,3</sup>, and Rudi Fasan<sup>1,\*</sup>

<sup>1</sup>*Department of Chemistry, University of Rochester, Rochester, New York 14627, USA.*

<sup>2</sup>*Department of Hematology/Oncology, School of Medicine and Dentistry, University of Rochester, Rochester, New York 14627, USA.*

<sup>3</sup>*Current address: Division of Hematology, University of Colorado, Aurora, Colorado 80045, USA.*

\*[fasan@chem.rochester.edu](mailto:fasan@chem.rochester.edu)

### **Table of contents:**

Supplementary Figure S1-S7	Pages S2-S8
Supplementary Table S1-S3	Pages S10-S13
Experimental Procedures	Pages S14-S18
Synthesis of parthenolide derivatives	Pages S19-S30
X-Ray Crystallography Data	Pages S31
References	Page S32
Spectra	Pages S33-S84

**Figure S1.** Chemical structures of the five probes used for high-throughput fingerprinting of the P450 libraries. The synthesis of these compounds was described earlier<sup>1</sup>.

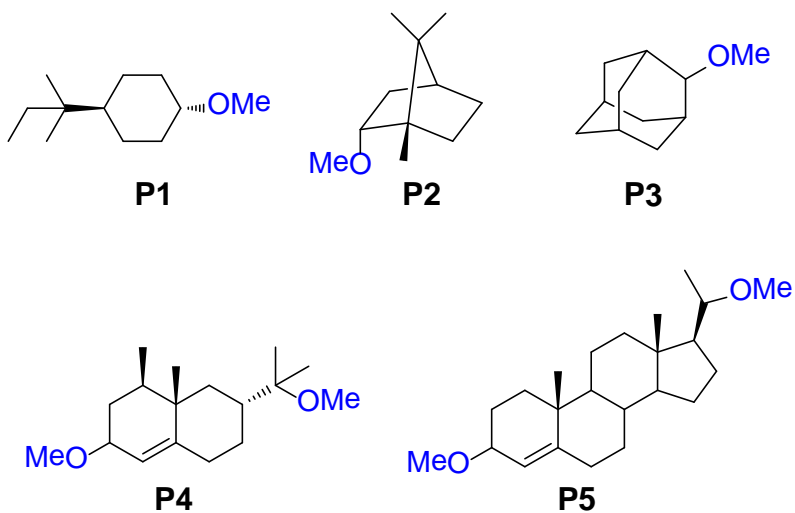


**Figure S2.** Fingerprint-based prediction of parthenolide reactivity via fingerprint multi-component analysis (MCA). (a) Plot of experimental versus calculated PTL activity from multiple linear regression analysis of PTL reactivity/fingerprint correlation across the P450 training set (**Table S3**). (b) Ranking of the 522 P450 variants according to their predicted PTL activity calculated based on the resulting fingerprint-based model. (c) Total turnovers in PTL oxidation for the 75 top-scoring P450 variants arranged from the least to the most active variant.

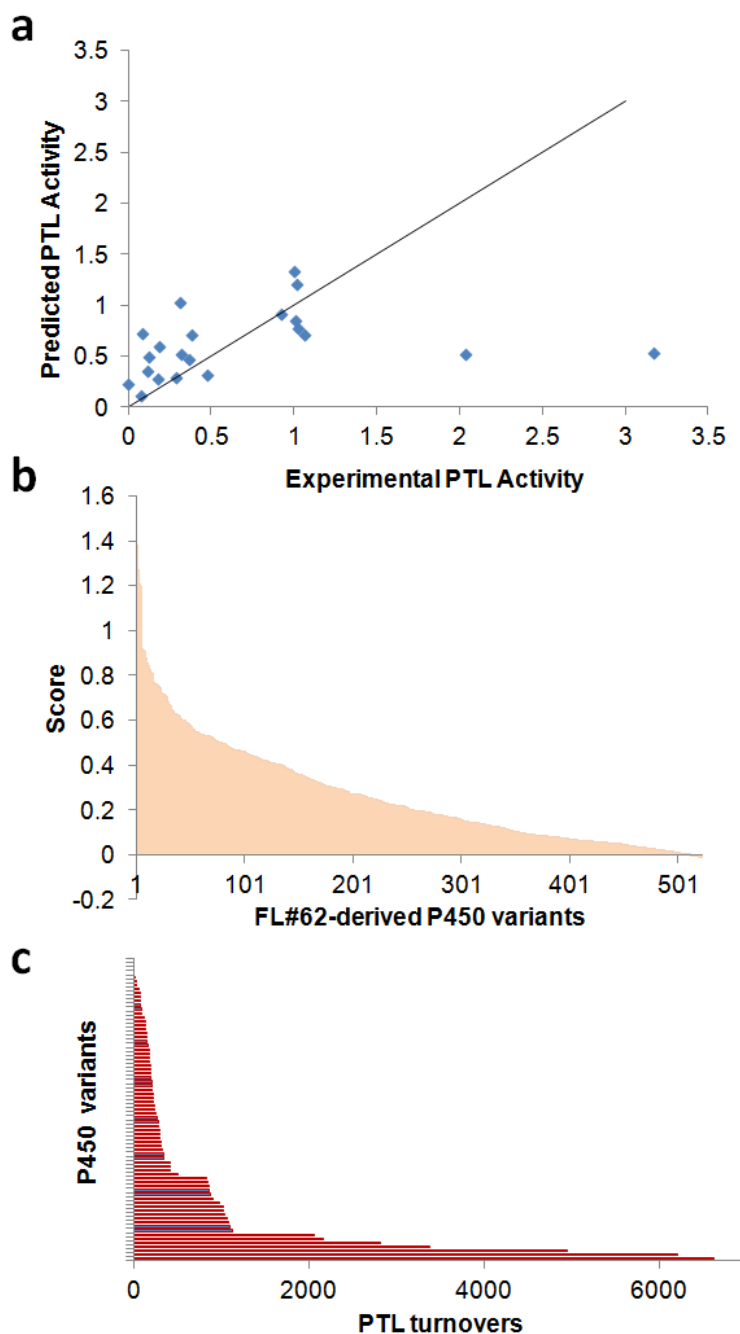


**Figure S3.** Visible spectra of the P450 variants of **Table 1** recorded before (red line) and after (black line) addition of parthenolide (1.5 mM), illustrating the shift in heme spin state upon addition of parthenolide.

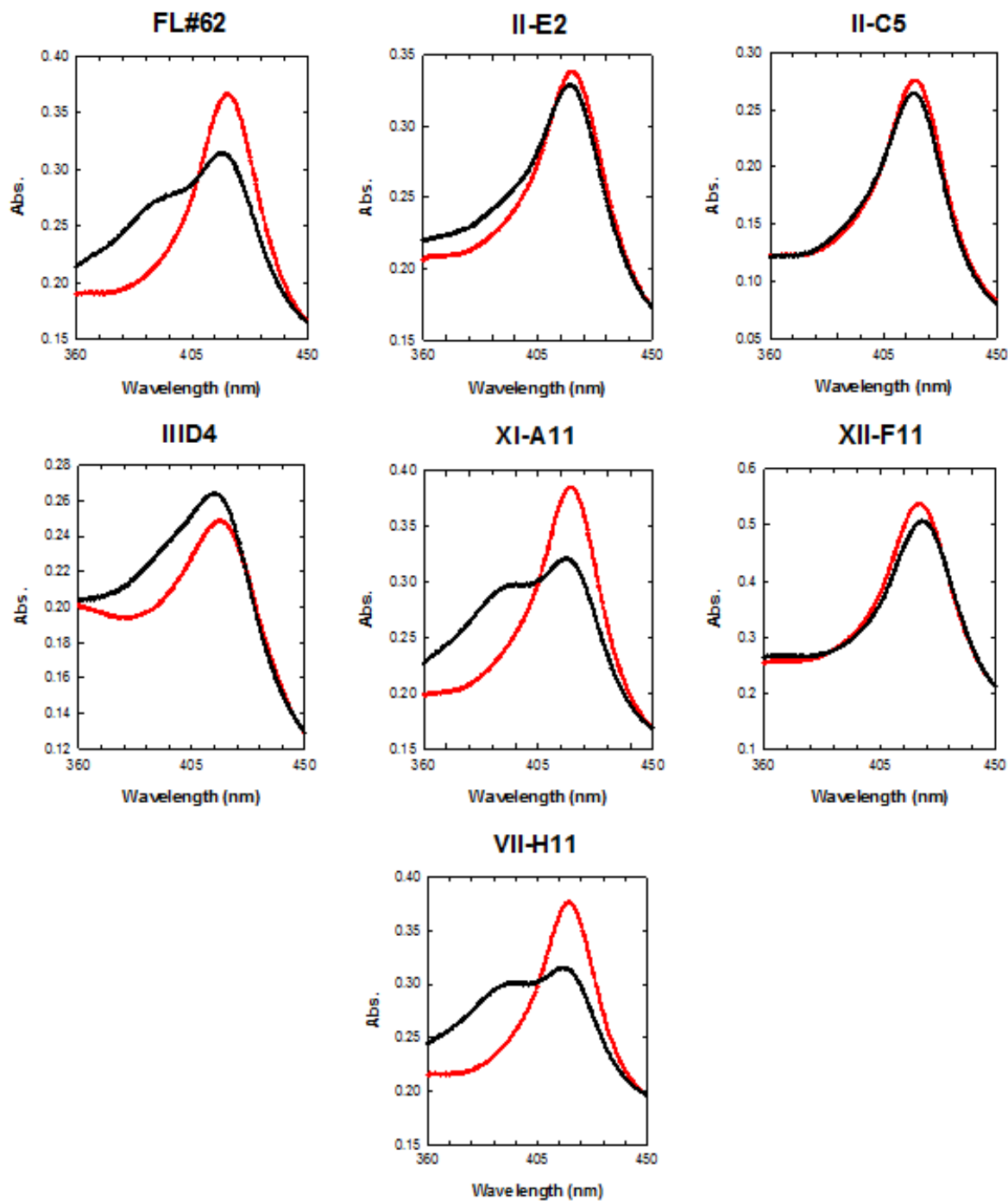


**Figure S4.** Plots of parthenolide-induced heme spin shift *versus* parthenolide concentration for the P450 variants described in **Table 1**. The experimental data (dots) were fitted to a non-cooperative 1:1 binding model equation (solid line).

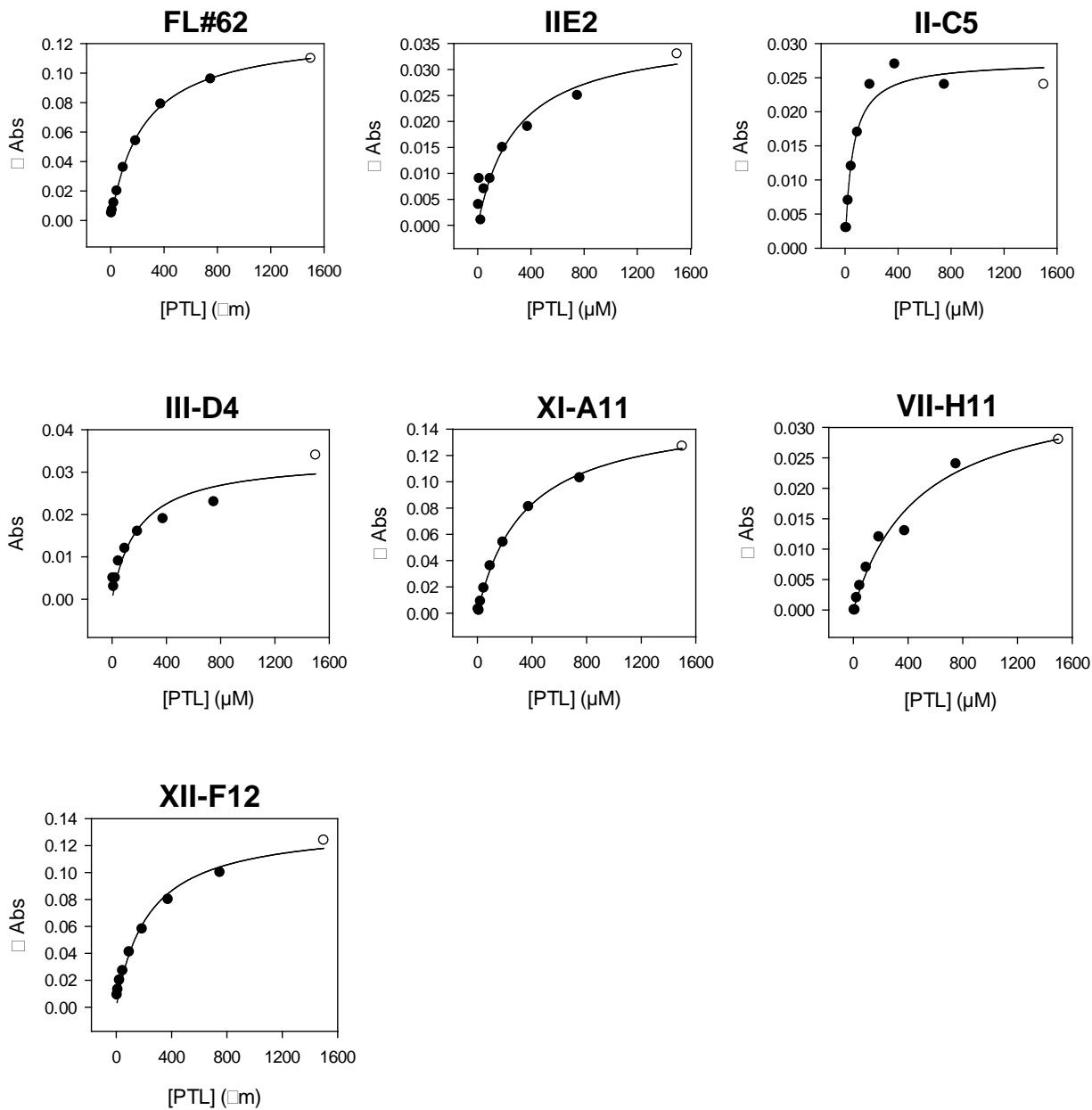


**Figure S5.** Fingerprint profiles for the P450 variants described in **Table 1**, after normalization with reference P450<sub>BM3</sub>(F87A). Standard deviation for activity values are <15%.

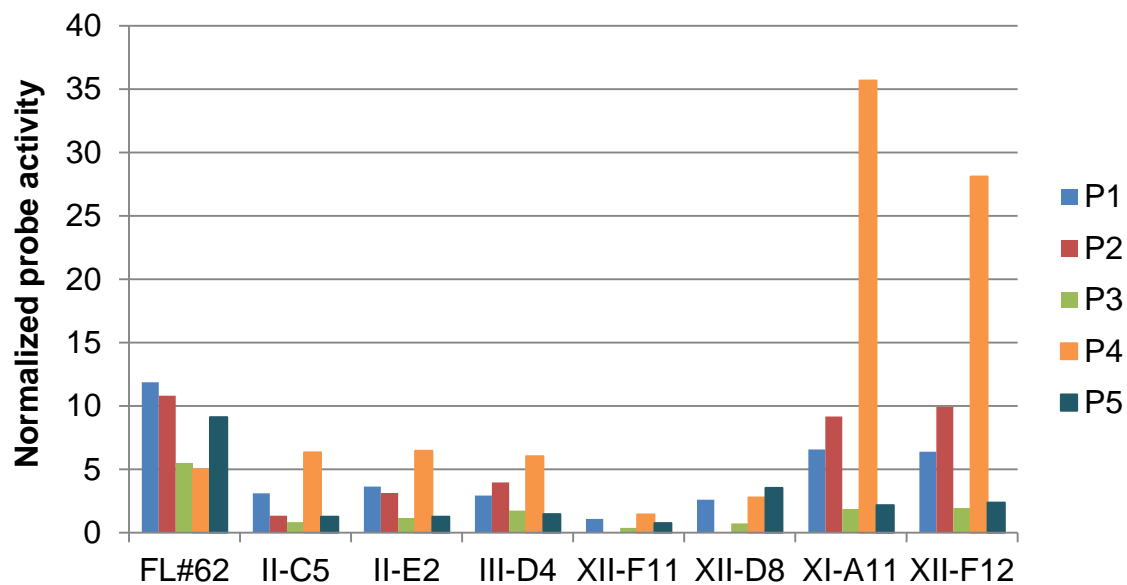


**Figure S6.** Cytotoxicity of PTL and the C9-functionalized PTL analogs against AML123009 and AML100510 cells.

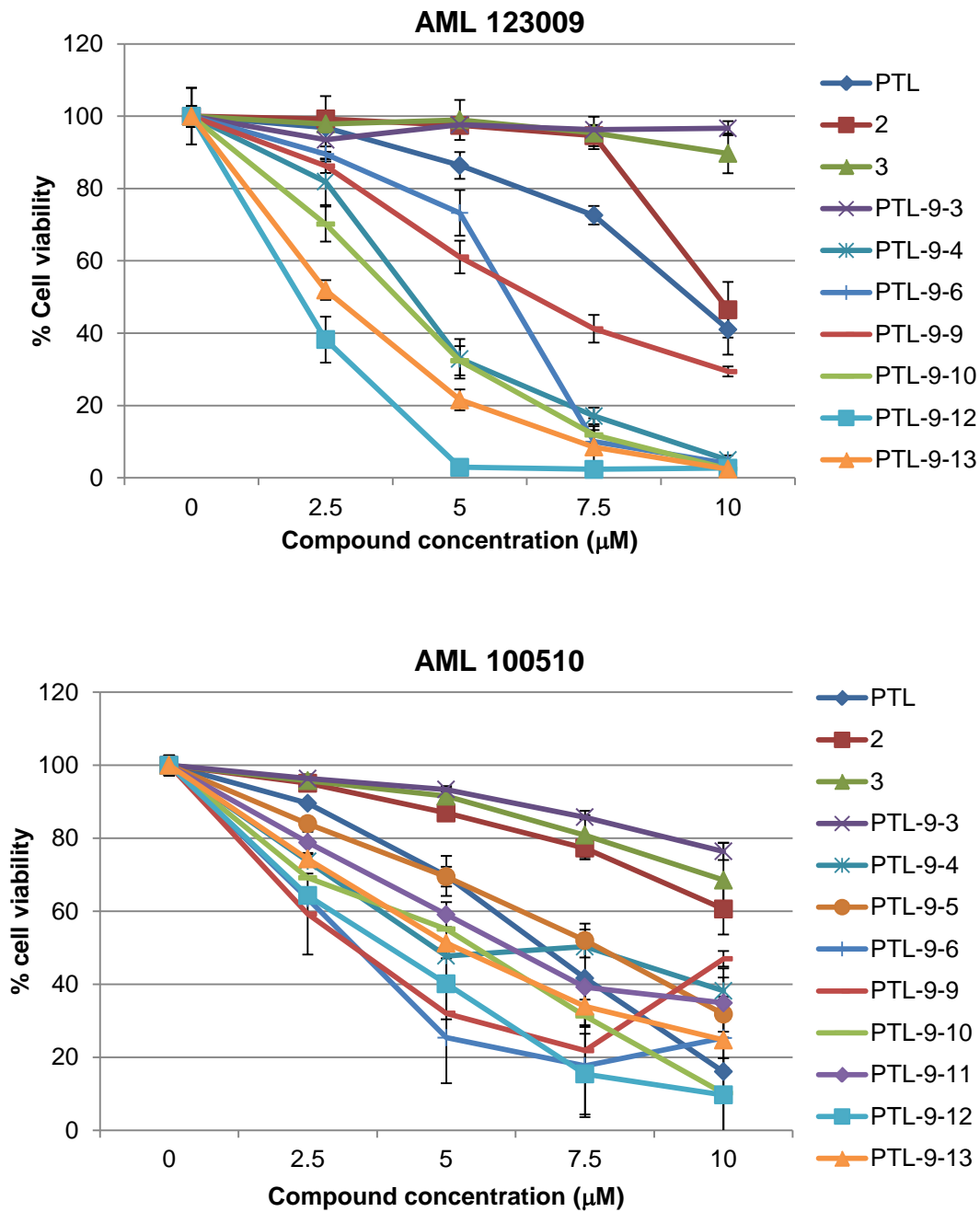


**Figure S7.** Cytotoxicity of PTL and the C14-functionalized PTL analogs against AML123009 and AML100510 cells.

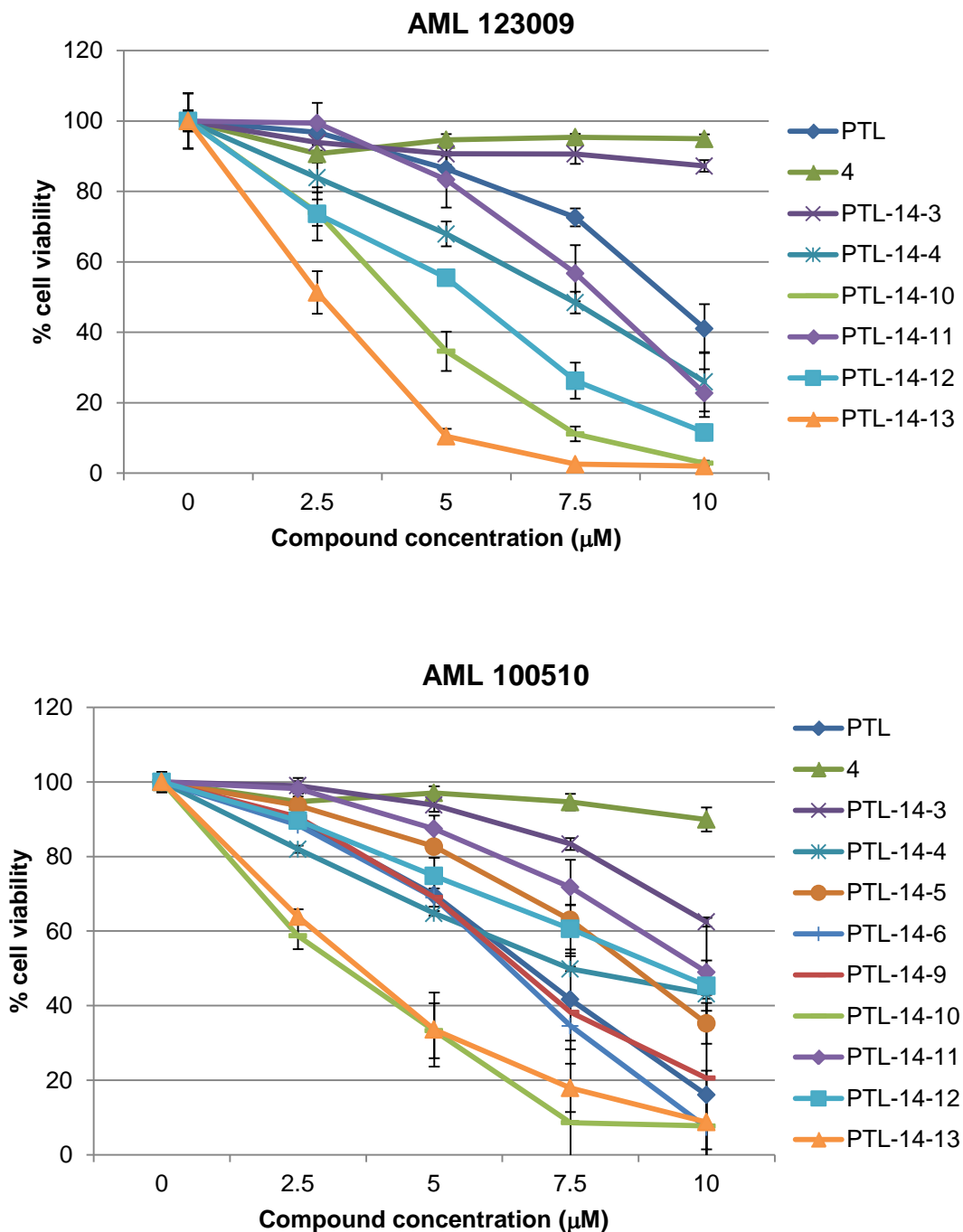


**Table S1.** Sequence of the oligonucleotides used for the preparation of the P450 libraries.

<b>Primer</b>	<b>Sequence</b>
74NNK_for	5'-CTTAAGTCAANNKCTTAAATTTAATCGTG-3'
74NNK_rev	5'-CACGATTAAATTTAAGMNNTTGACTIONAAG-3'
75NNK_for	5'-CTTAAGTCAAGCGNNKAAATTTAATCG-3'
75NNK_rev	5'-CGATTAAATTTMNNCGCTTGACTIONAAG-3'
IIC5-82NNK_for	5'-CGTGATATTNNKGGAGACGGG-3'
IIC5-82NNK_rev	5'-CCCGTCTCCMNAATATCACG-3'
87NNK_for	5'-AGACGGGTTANNKACAAGCTGG-3'
87NNK_rev	5'-CCAGCTTGTMNNTAACCCGTCT-3'
180NNK_for	5'-GGTCCGTNNKCTGGATGAAG-3'
180NNK_rev	5'-CTTCATCCAGMNNACGGACC-3'
181NNK_for	5'-GGTCCGTACANNKGATGAAGTAATG-3'
181NNK_rev	5'-CATTACTTCATCMNNTGTACGGACC-3'
184NNK_for	5'-CTGGATGAANNKATGAACAAGCTG-3'
184NNK_rev	5'-CAGCTTGTTTCATMNNTTCATCCAG-3'
263NNK_for	5'-CATTCTTANNKGC GGACACG-3'
263NNK_rev	5'-CGTGTC CCGCMNNTAAGAATG-3'
328NNK_for	5'-GGCCA ACTNNKCCTGCGTTTTCC-3'
328NNK_rev	5'-GGAAAACGCAGGMN NAGTTGGCC-3'
IIC5-A87S_for	5'-GAGACGGGTTAAGCAC AAGCTGGAC-3'
IIC5-A87S_rev	5'-GTCCAGCTTGTGCTTAACCCGTCTC-3'
IIC5-T180A_for	5'-TAAGTATGGTCCGTGCGCTGGATGAA-3'
IIC5-T180A_rev	5'-TTCATCCAGCGCACGGACCATACTTA-3'

**Table S2.** Catalytic turnovers and regioselectivity of the top 75 FL#62-derived P450 variants ranked based on probe **P4** activity (single component analysis). Variants are grouped according to their site-selectivity toward formation of 1,10-epoxy-PTL **2** (red), 9-hydroxy-PTL **3** (green), and 14-hydroxy-PTL **4** (blue). Variants highlighted in darker colors correspond to those selected for further characterization.

Variant	Product distribution			TTN
	<b>2</b>	<b>3</b>	<b>4</b>	
III-D4	89%	9%	2%	6636
III-D9	90%	8%	2%	6220
III-A5	89%	11%	1%	199
VI-F2	89%	5%	6%	155
V-D8	88%	8%	4%	346
II-H2	88%	8%	4%	3380
IV-F7	88%	8%	5%	141
III-B4	87%	9%	4%	2820
III-B7	87%	11%	2%	2065
III-A3	87%	10%	3%	2173
I-B1	86%	6%	8%	908
I-D2	86%	6%	9%	865
I-C11	86%	6%	9%	865
IV-C3	86%	12%	3%	173
IV-H10	84%	11%	5%	184
II-C12	84%	9%	7%	1133
V-E8	83%	11%	5%	239
V-B8	83%	11%	6%	177
II-B12	83%	10%	7%	1075
III-A12	82%	8%	10%	234
IV-A11	82%	16%	2%	146
I-G12	81%	10%	9%	1020
I-E2	81%	8%	12%	414
VI-C2	81%	9%	10%	157
VI-G9	80%	18%	2%	224
IV-C11	79%	8%	13%	202
I-D12	79%	13%	8%	842
I-B12	79%	12%	9%	1040

I-C12	78%	13%	9%	1022
II-A11	78%	13%	9%	1093
I-F5	78%	13%	10%	985
II-H11	77%	14%	9%	412
I-A1	77%	11%	12%	421
I-B4	76%	14%	10%	825
II-F11	76%	14%	10%	298
I-H4	76%	14%	10%	249
II-G12	74%	15%	11%	267
II-F12	74%	15%	11%	282
II-E11	74%	16%	10%	209
I-D1	74%	19%	7%	1080
II-D12	74%	16%	11%	190
I-E1	72%	7%	21%	202
V-H2	70%	16%	14%	167
II-D1	69%	24%	7%	279
IV-H3	69%	17%	14%	303
III-H2	67%	33%	0%	4961
III-B10	65%	14%	21%	72
IV-F8	64%	12%	24%	77
II-B4	63%	10%	27%	90
IV-H4	63%	25%	12%	130
II-A2	60%	10%	30%	127
III-H10	57%	40%	3%	225
II-B9	57%	12%	31%	90
III-D10	53%	12%	34%	129
II-C5	29%	68%	3%	305
II-C3	34%	61%	5%	173
VI-E10	39%	58%	3%	224
III-C10	44%	53%	3%	307
III-B2	42%	53%	5%	13
III-H4	45%	52%	3%	338
VI-F8	48%	49%	4%	326
I-C10	53%	47%	0%	195
VI-G2	41%	45%	14%	35
III-A11	54%	43%	2%	880
IV-C1	55%	40%	5%	196
II-E2	40%	16%	44%	503
III-F1	37%	19%	43%	295

III-D3	48%	12%	40%	82
VI-A11	43%	18%	39%	50
II-H8	30%	33%	37%	85
III-B3	50%	13%	37%	19
III-A1				0
II-D11				0
IV-B5				0
II-E1				0

**Table S3.** Data corresponding to the P450training set used for calculating the fingerprint-based model for predicting PTL reactivity: fingerprint components (= normalized activity on probe **P1** to **P5**), PTL turnovers (TTN), and relative PTL activity (normalized to parent FL#62).

Variant	Probe Activity					TTN	Normalized Activity
	1	2	3	4	5		
#62	11.88	10.80	5.50	5.00	9.11	1,065	1.00
IIA11	6.76	3.37	1.30	6.43	1.51	1,090	1.02
IIA2	5.21	0.39	0.71	7.57	1.31	127	0.12
IIB12	7.45	3.70	1.36	6.83	1.56	1,075	1.01
IIB4	1.85	6.45	3.23	9.68	1.49	90	0.08
IIC12	6.24	3.13	1.21	6.09	1.36	1,135	1.07
IIC5	3.11	1.35	0.84	6.34	1.27	305	0.29
IID11	3.31	0.71	0.80	6.95	1.44	0	0.00
IIE2	3.63	3.14	1.17	6.47	1.27	341	0.32
IIH11	6.22	3.16	1.14	6.69	1.45	412	0.39
IA1	9.42	3.82	1.72	11.97	1.57	336	0.32
IC10	1.43	2.34	1.13	7.44	1.01	195	0.18
ID1	6.27	7.88	2.49	10.05	1.53	1,080	1.01
IE1	2.48	4.73	1.35	10.07	1.17	202	0.19
IF5	7.45	4.12	1.14	12.22	1.42	985	0.92
IID4	2.20	2.02	1.73	5.06	1.02	510	0.48
IIH2	4.38	3.06	1.68	6.85	1.73	3,380	3.17
IIH8	1.42	1.97	11.83	6.23	3.61	85	0.08
IIIA11	2.65	3.42	1.67	9.34	1.26	392	0.37
IIID7	6.76	0.48	0.75	4.67	1.15	131	0.12
IIIA3	3.09	3.74	1.61	5.91	1.46	2,170	2.04

## **MATERIALS, METHODS, AND EXPERIMENTAL PROCEDURES**

**Reagents and Analytical Methods.** Chemical reagents, substrates, and solvents were purchased from Sigma-Aldrich, TCI, Fluka, and Tocris Bioscience. Silica gel chromatography purifications were carried out using AMD Silica Gel 60 230-400 mesh. Gas chromatography analyses were carried out on a Shimadzu GC2010, an FID detector, a Restek RTX-5 column (15 m x 0.25 mm x 0.25  $\mu$ m film), and the following separation program: 200°C inlet, 300°C detector, 130°C oven, 12°C/min ramp to 290°C, and 290°C for 2 min. 1D and 2D NMR experiments were carried out on a Bruker 500 MHz spectrometer. Data for  $^1\text{H}$  NMR spectra are reported in the conventional form: chemical shift ( $\delta$  ppm), multiplicity (s=singlet, d=doublet, t=triplet, q=quartet, m=multiplet, br=broad), coupling constant (Hz), integration. Data for  $^{13}\text{C}$  NMR spectra are reported in terms of chemical shift ( $\delta$  ppm).  $^{19}\text{F}$  NMR spectra were carried out on a Bruker 400MHz spectrometer calibrated to trifluorotoluene and reported in terms of chemical shift ( $\delta$  ppm). Mass spectra were collected by direct infusion on a Thermo Scientific LTQ Velos ESI/ion-trap mass spectrometer. The oligonucleotides for the mutagenesis experiments were obtained from IDT DNA Technology. Restriction enzymes were purchased from New England Biolabs.

**Cloning and fingerprinting of P450 libraries.** Site-saturation (NNK) mutagenesis libraries were prepared using pCWori\_FL#62 (or corresponding parent enzyme) as template, primers BamHI\_2\_fwd (5'-GGAAACAGGATCCATCGATGC-3') and SacI\_2\_rev (5'-AATATCGAGCTCGTAGTTTGTATGATC-3') as megaprimers, and the oligonucleotides of **Table S1** as mutagenizing primers. The target gene product (1.5 Kbp) were prepared by PCR overlap extension mutagenesis, digested with *BamH* I and *Sac* I restriction enzymes, and ligated to *BamH* I/*Sac* I double-digested pCWori\_FL#62 vector. The ligation mixtures were transformed

in chemically competent DH5 $\alpha$  cells and plated on LB agar plates containing ampicillin (100 mg L<sup>-1</sup>) followed by overnight incubation at 37 °C. High-throughput fingerprinting of the P450 libraries was carried out as described earlier.<sup>1, 2</sup> Briefly, recombinant colonies were arrayed and grown in 96-deep well plates first in LB medium (37°C, overnight) and then in TB medium for protein expression. Each plate included a row (8 wells) with cells expressing the parent enzyme as a reference. Protein expression was induced by IPTG (0.25 mM) and carried out at 27 °C and 150 rpm for 18 hrs. Cell lysates were prepared by enzymatic treatment of the cell pellets (400  $\mu$ L lysis buffer: U deoxyribonuclease I, 0.8 mg mL<sup>-1</sup> lysozyme, 10 mM MgCl<sub>2</sub>, 50 mM phosphate buffer, pH 7.5; incubation at 37°C for 60 min) and clarified by centrifugation. P450 demethylation activity on probe **P1-P5 (Figure S1)** was quantified using a TECAN Infinity plate reader (550 nm) according to the previously reported procedure.<sup>2</sup> The enzyme fingerprints were obtained by normalizing the demethylation activity of the P450 variant on probes **P1-P5** to that of the parent enzyme from the same plate.

**P450 reactivity predictions via SCA and MCA.** The P450 variants displaying a unique fingerprint based on the primary screening (criteria: (a) >10% of parent activity on at least one probe; and (b) larger than 20% variation in activity on at least one probe compared to parent enzyme or any other member of the library) were re-fingerprinted in 96-well plates (triplicate) using P450<sub>BM3</sub> (F87A) as the reference enzyme. For the SCA analyses, the P450 variants were simply ranked according to their fingerprint component corresponding to the decaline-based probe **P4**. For MCA analyses, FL#62 and other 19 randomly chosen, parthenolide-oxidizing variants identified by SCA were used as training set. Their total parthenolide oxidation activity (measured in TTN and normalized to that of FL#62 (TTN(P450 variant)/TTN(FL#62))) were then

correlated with the corresponding fingerprints using multiple linear regression (MLR) analysis using the equation:  $y = b_0 + b_1x_1 + b_2x_2 + b_3x_3 + b_4x_4 + b_5x_5$ , where  $y$  corresponds to relative parthenolide reactivity,  $x_1$  to  $x_5$  correspond to the five fingerprint components (activity on probe **P1** to **P5**, respectively), and  $b_1$  to  $b_5$  correspond to the regression coefficients for the five independent variables  $x_1$  to  $x_5$ . This process yielded the plot of calculated *versus* experimental parthenolide reactivity presented in **Figure S2b**, with the calculated regression coefficients being  $b_1 = 0.07926$ ,  $b_2 = 0.10353$ ,  $b_3 = 0.00912$ ,  $b_4 = 0.00019$ , and  $b_5 = -0.08490$ . The RMSD value (0.8340) indicated an excellent fit between the calculated and experimental values. This model was then used to rank the P450 variants of the collection according to their predicted parthenolide reactivity (**Figure S2c**).

**Protein expression and purification.** The P450 enzymes were expressed from pCWori-based vectors and purified by ion-exchange chromatography as described previously.<sup>1</sup> P450 concentration was determined from CO binding difference spectra ( $\epsilon_{450-500} = 91,000 \text{ M}^{-1} \text{ cm}^{-1}$ ). The vector encoding for the thermostable phosphite dehydrogenase (PTDH) was kindly provided by the Zhao group.<sup>3</sup> PTDH was expressed and purified via Ni-affinity chromatography according to the published procedure.<sup>3</sup>

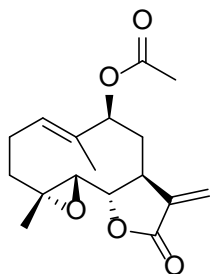
**Determination of total turnovers and regioselectivity of the P450 variants.** Analytical-scale reactions (1 mL) were carried out using 0.2–1  $\mu\text{M}$  P450, 1.5 mM parthenolide, 2  $\mu\text{M}$  PTDH, 100  $\mu\text{M}$  NADP<sup>+</sup>, and 50 mM sodium phosphite in potassium phosphate buffer (50 mM, pH 8.0). The P450 variants described in **Table 1** were characterized in purified form, while those described in **Table S3** were characterized directly from cell lysates. After 12 hours at 4°C, the reaction

mixtures were added with 500  $\mu\text{M}$  guaiacol (as internal standard), extracted with dichloromethane and analyzed by gas chromatography (see Supporting Information for details). TTN values were calculated based on the total amount of oxidation products as quantified based on the calibration curves generated using purified **2-4**. Mean and standard deviation values reported for P450 variants in **Table 1** were calculated from experiments performed at least in triplicate.

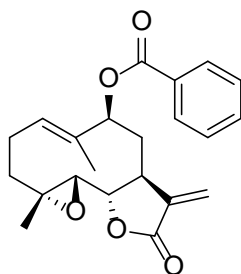
**Measurement of kinetic parameters, substrate binding affinity ( $K_D$ ) and coupling efficiency.** Initial product formation rates were measured from 1 mL scale reactions containing 1 mM parthenolide, 0.1-1.0  $\mu\text{M}$  purified P450, and 1 mM NADPH in potassium phosphate buffer (50 mM, pH 8.0) at room temperature. After 60 seconds, the samples were added with 500  $\mu\text{M}$  Guaiacol and extracted with dichloromethane. Cofactor oxidation rate in the presence of parthenolide was measured by monitoring NADPH depletion at 340 nm ( $\epsilon = 6.22 \text{ mM}^{-1} \text{ cm}^{-1}$ ) using 0.1-0.5  $\mu\text{M}$  purified P450, 1.0 mM parthenolide, and 200  $\mu\text{M}$  NADPH. Coupling efficiency was calculated from the ratio between the initial product formation rate and the initial NADPH oxidation rate. Reported mean and standard deviation values were calculated from experiments performed at least in triplicate. Binding experiments were performed using 3  $\mu\text{M}$  purified P450 in potassium phosphate buffer (50 mM, pH 8.0) by titrating increasing amounts of parthenolide (5.9  $\mu\text{M}$  to 1.5 mM) from an ethanol stock solution (20 mM). At each concentration, a difference spectrum from 360 to 500 nm was recorded and binding curves were generated by plotting the change in absorbance at 390 nm and 420 nm corresponding to the high-spin and low-spin state of the enzyme, respectively, against the parthenolide concentration. Variant III-D4 displayed an unusual spin difference spectrum with minimum at 403 nm and

maximum at 430 nm and the difference in absorbance at these two wavelengths was utilized for  $K_D$  determination.  $K_D$  values were calculated using Sigma Plot via non-linear fitting of the experimental binding curves to an equation describing a standard 1:1 binding interaction.

## SYNTHESIS AND CHARACTERIZATION OF PARTHENOLIDE DERIVATIVES

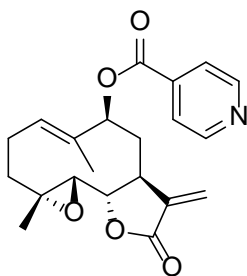


**PTL-9-003:** Standard procedure was applied using (*S*)-9-hydroxy-parthenolide (6.5 mg, 0.025 mmol), 4-dimethylaminopyridine (1.5 mg, 0.0125 mmol), triethylamine (35  $\mu$ L, 0.25 mmol), and acetyl chloride (9  $\mu$ L, 0.125 mmol). Isolated PTL-9-003: 1.7 mg, 22% yield.  $^1\text{H}$  NMR (500 MHz,  $\text{CDCl}_3$ ):  $\delta$  = 1.22-1.29 (m, 1 H), 1.33 (s, 3 H), 1.74 (s, 3 H), 2.00-2.06 (m, 1 H), 2.09 (s, 3 H), 2.15-2.21 (m, 2 H), 2.23-2.29 (m, 1 H), 2.48 (dq, 1 H,  $J$  = 5.31, 12.52 Hz), 2.71 (d, 1 H,  $J$  = 8.73 Hz), 2.91 (m, 1 H), 3.86 (t, 1 H,  $J$  = 8.25 Hz), 5.20 (dd, 1 H,  $J$  = 2.23, 10.90 Hz), 5.51 (d, 1 H,  $J$  = 11.78 Hz), 5.69 (d, 1 H,  $J$  = 3.24 Hz), 6.37 (d, 1 H,  $J$  = 3.75);  $^{13}\text{C}$  NMR (125 MHz,  $\text{CDCl}_3$ ):  $\delta$  = 11.7, 17.3, 21.2, 23.8, 36.0, 36.1, 44.1, 61.3, 66.0, 80.7, 81.6, 122.0, 127.8, 133.0, 138.0, 168.6, 170.0; MS (ESI) calcd for  $\text{C}_{17}\text{H}_{22}\text{O}_5$   $[\text{M}+\text{H}]^+$   $m/z$ : 307.15; found: 307.3.

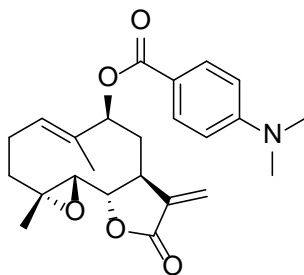


**PTL-9-004:** Standard procedure was applied using (*S*)-9-hydroxy-parthenolide (8mg, 0.03mmol), 4-dimethylaminopyridine (2 mg, 0.015 mmol), triethylamine(42  $\mu$ L, 0.3mmol), and benzoyl chloride (17  $\mu$ L, 0.15 mmol). Isolated PTL-9-004: 5.5 mg, 50% yield.  $^1\text{H}$  NMR (500 MHz,  $\text{CDCl}_3$ ):  $\delta$  = 1.33-1.39 (m, 1 H), 1.41 (s, 3 H), 1.91 (s, 3 H), 2.17-2.29 (m, 2 H), 2.32-2.44

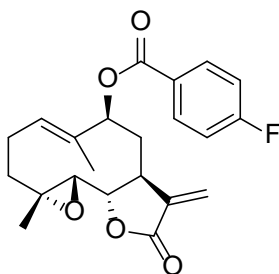
(m, 2 H), 2.57 (dq, 1 H,  $J= 4.8, 12.9$  Hz), 2.81 (d, 1 H,  $J=8.9$  Hz), 3.03-3.10 (m, 1 H), 3.96 (t, 1 H,  $J= 8.9$  Hz), 5.52 (d, 1 H,  $J= 10.1$  Hz), 5.66 (d, 1 H,  $J= 12.1$  Hz), 5.79 (d, 1 H,  $J= 2.4$  Hz), 6.44 (d, 1 H,  $J= 2.8$  Hz), 7.52 (t, 2 H,  $J= 7.7$  Hz), 7.65 (t, 1 H,  $J= 7.3$  Hz), 8.10 (d, 2 H,  $J= 7.2$  Hz);  $^{13}\text{C}$  NMR (125 MHz,  $\text{CDCl}_3$ ):  $\delta = 11.9, 17.4, 23.8, 36.0, 36.2, 44.1, 61.3, 66.1, 81.2, 81.7, 122.2, 127.9, 128.5, 129.6, 130.0, 133.1, 133.3, 138.0, 165.5, 168.6$ ; MS (ESI) calcd for  $\text{C}_{22}\text{H}_{24}\text{O}_5$   $[\text{M}+\text{H}]^+$   $m/z$ : 369.15; found: 369.8.



**PTL-9-005:** Standard procedure was applied using (*S*)-9-hydroxy-parthenolide (8 mg, 0.03 mmol), 4-dimethylaminopyridine (2 mg, 0.015 mmol), triethylamine (63  $\mu\text{L}$ , 0.45 mmol), and isonicotinoyl chloride (27 mg, 0.15 mmol). Isolated PTL-9-005: 3 mg, 27% yield  $^1\text{H}$  NMR (500 MHz,  $\text{CDCl}_3$ ):  $\delta = 1.34-1.40$  (m, 1 H), 1.42 (s, 3 H), 1.90 (s, 3 H), 2.20-2.30 (m, 2 H), 2.33-2.44 (m, 2 H), 2.56 (dq, 1 H,  $J= 5.1, 13.3$  Hz), 2.80 (d, 1 H,  $J= 9.2$  Hz), 3.04-3.10 (m, 1 H), 3.96 (t, 1 H,  $J= 8.2$  Hz), 5.54 (d, 1 H,  $J= 10.2$  Hz), 5.68 (d, 1 H,  $J= 11.2$  Hz), 5.77 (d, 1 H,  $J= 2.5$  Hz), 6.45 (d, 1 H,  $J= 3.6$  Hz), 7.90 (d, 2 H,  $J= 4.8$  Hz), 8.87 (d, 2 H,  $J= 4.8$  Hz);  $^{13}\text{C}$  NMR (125 MHz,  $\text{CDCl}_3$ ):  $\delta = 12.0, 17.4, 24.0, 36.0, 44.1, 61.3, 66.0, 81.4, 82.4, 122.2, 123.4, 129.0, 132.2, 137.7, 138.3, 149.9, 163.7, 168.6$ ; MS (ESI) calcd for  $\text{C}_{21}\text{H}_{23}\text{NO}_5$   $[\text{M}+\text{H}]^+$   $m/z$ : 370.16; found: 370.4.

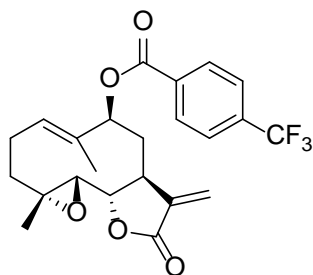


**PTL-9-006:** Standard procedure was applied using (*S*)-9-hydroxy-parthenolide (10 mg, 0.037 mmol) 4-dimethylaminopyridine (2.3 mg, 0.019 mmol), triethylamine(52  $\mu$ L, 0.37 mmol), and 4-(dimethylamino)benzoyl chloride (28 mg, 0.15 mmol). Isolated PTL-9-006: 9 mg, 59% yield.  $^1\text{H}$  NMR (500 MHz,  $\text{CDCl}_3$ ):  $\delta$  =1.25-1.32 (m, 1 H), 1.35 (s, 3 H), 1.84 (s, 3 H), 2.07-2.15 (m, 1 H), 2.17-2.22 (m, 1 H), 2.25-2.37 (m, 2 H), 2.51 (dq, 1 H,  $J$ = 4.7, 13.0 Hz), 2.76 (d, 1 H,  $J$ = 8.9 Hz), 2.97-3.03 (m, 1 H), 3.06 (s, 6 H), 3.90 (t, 1 H,  $J$ = 8.1 Hz), 5.41 (d, 1 H,  $J$ = 11.0 Hz), 5.57 (d, 1 H,  $J$ = 12.0 Hz), 5.74 (d, 1 H,  $J$ = 3.1 Hz), 6.38 (d, 1 H,  $J$ = 3.9 Hz), 6.66 (d, 2 H,  $J$ = 8.9 Hz), 7.91 (d, 2 H,  $J$ = 9.1 Hz);  $^{13}\text{C}$  NMR (125 MHz,  $\text{CDCl}_3$ ):  $\delta$  =12.0, 17.4, 23.8, 36.1, 36.5, 40.6, 44.2, 61.7, 65.9, 80.2, 81.6, 110.7, 116.6, 122.3, 127.4, 131.2, 133.9, 138.2, 153.6, 165.8, 168.9; MS (ESI) calcd for  $\text{C}_{24}\text{H}_{29}\text{NO}_5$   $[\text{M}+\text{H}]^+$   $m/z$ : 412.20; found: 412.3.

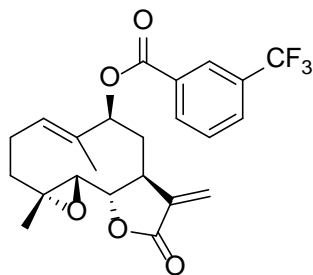


**PTL-9-009:** Standard procedure was applied using (*S*)-9-hydroxy-parthenolide (7 mg, 0.026 mmol), 4-dimethylaminopyridine (1.6 mg, 0.013 mmol), triethylamine(36  $\mu$ L, 0.26 mmol), and 4-fluorobenzoyl chloride (15  $\mu$ L, 0.13 mmol). Isolated PTL-9-009: 3 mg, 30% yield.  $^1\text{H}$  NMR (500 MHz,  $\text{CDCl}_3$ ):  $\delta$  =1.33-1.38 (m, 1 H), 1.41 (s, 3 H), 1.90 (s, 3 H), 2.17-2.29 (m, 2 H), 2.32-

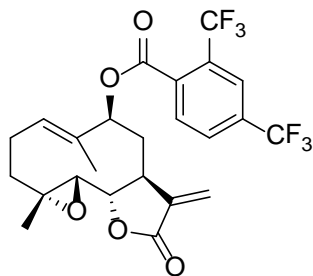
2.42 (m, 2 H), 2.57 (dq, 1 H,  $J= 5.2, 13.0$  Hz), 2.81 (d, 1 H,  $J= 8.5$  Hz), 3.03-3.09 (m, 1 H), 3.96 (t, 1 H,  $J= 8.3$  Hz), 5.50 (d, 1 H,  $J= 11.1$  Hz), 5.66 (d, 1 H,  $J= 11.8$  Hz), 5.78 (d, 1 H,  $J= 3.1$  Hz), 6.49 (d, 1 H,  $J= 3.3$  Hz), 7.19 (t, 2 H,  $J= 8.4$  Hz), 8.11 (t, 2 H,  $J= 6.4$  Hz);  $^{13}\text{C}$  NMR (125 MHz,  $\text{CDCl}_3$ ):  $\delta = 11.9, 17.4, 23.8, 36.0, 36.2, 44.1, 61.3, 66.0, 81.4, 81.6, 115.6, 115.8, 122.15, 126.3, 128.1, 132.2$  (d,  $J= 9.41$  Hz), 132.9, 137.9, 164.5, 168.4.  $^{19}\text{F}$  NMR (376 MHz,  $\text{CDCl}_3$ ):  $\delta = -42.49$ ; MS (ESI) calcd for  $\text{C}_{22}\text{H}_{23}\text{FO}_5$   $[\text{M}+\text{H}]^+$   $m/z$ : 387.15; found: 387.4.



**PTL-9-010:** Standard procedure was applied using (*S*)-9-hydroxy-parthenolide (5 mg, 0.019 mmol), 4-dimethylaminopyridine (1.2 mg, 0.0095 mmol), triethylamine (27  $\mu\text{L}$ , 0.19 mmol), and the 4-(trifluoromethyl)benzoyl chloride (14  $\mu\text{L}$ , 0.095 mmol). Isolated PTL-9-010: 4.4 mg, 53% yield  $^1\text{H}$  NMR (500 MHz,  $\text{CDCl}_3$ ):  $\delta = 1.34-1.39$  (m, 1 H), 1.42 (s, 3 H), 1.90 (s, 3 H), 2.21-2.30 (m, 2 H), 2.33-2.44 (m, 2 H), 2.58 (dq, 1 H,  $J= 4.9, 13.0$  Hz), 2.81 (d, 1 H,  $J= 8.5$  Hz), 3.04-3.10 (m, 1 H), 3.97 (t, 1 H,  $J= 8.5$  Hz), 5.54 (d, 1 H,  $J= 10.1$  Hz), 5.68 (d, 1 H,  $J= 11.8$  Hz), 5.78 (d, 1 H,  $J= 2.8$  Hz), 6.45 (d, 1 H,  $J= 2.8$  Hz), 7.79 (d, 2 H,  $J= 7.7$  Hz), 8.21 (d, 2 H,  $J= 8.1$  Hz);  $^{13}\text{C}$  NMR (125 MHz,  $\text{CDCl}_3$ ):  $\delta = 12.0, 14.1, 17.4, 22.7, 23.9, 35.9, 36.2, 44.1, 61.3, 66.1, 81.6, 81.9, 122.2, 125.6, 128.5, 130.0, 132.6, 133.2, 137.9, 164.5, 168.6$ ;  $^{19}\text{F}$  NMR (376 MHz,  $\text{CDCl}_3$ ):  $\delta = -0.76$ ; HPMS (ESI) calcd for  $\text{C}_{23}\text{H}_{23}\text{F}_3\text{O}_5$   $[\text{M}+\text{H}]^+$   $m/z$ : 437.1576; found: 437.1569

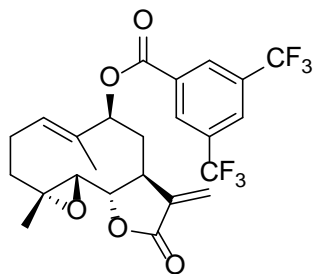


**PTL-9-011:** Standard procedure was applied using (*S*)-9-hydroxy-parthenolide (10 mg, 0.038 mmol), 4-dimethylaminopyridine (2.3 mg, 0.019 mmol), triethylamine (53  $\mu$ L, 0.38 mmol), and 3-(trifluoromethyl)benzoyl chloride (29  $\mu$ L, 0.19 mmol). Isolated PTL-9-011: 7 mg, 42 % yield.  $^1\text{H}$  NMR (400 MHz,  $\text{CDCl}_3$ ):  $\delta$  = 1.26-1.34 (m, 1 H), 1.36 (s, 3 H), 1.85 (s, 3 H), 2.14-2.24 (m, 2 H), 2.26-2.39 (m, 2 H), 2.52 (dq, 1 H,  $J$ = 4.9, 13.1 Hz), 2.75 (d, 1 H,  $J$ = 9.1 Hz), 2.97-3.05 (m, 1 H), 3.91 (t, 1 H,  $J$ = 8.4 Hz), 5.48 (d, 1 H,  $J$ = 11.4 Hz), 5.62 (d, 1 H,  $J$ = 12.1 Hz), 5.73 (d, 1 H,  $J$ = 3.4 Hz), 6.40 (d, 1 H,  $J$ = 3.4 Hz), 7.61 (t, 1 H,  $J$ = 7.7 Hz), 7.85 (d, 1 H,  $J$ = 7.7 Hz), 8.23 (d, 1 H,  $J$ = 7.7 Hz), 8.28 (s, 1 H);  $^{13}\text{C}$  NMR (125 MHz,  $\text{CDCl}_3$ ):  $\delta$  = 11.9, 17.4, 23.8, 36.0, 36.1, 44.1, 61.3, 66.0, 81.5, 81.9, 122.2, 126.5, 128.5, 129.2, 129.8, 130.9, 132.6, 132.8, 137.9, 164.16, 168.6;  $^{19}\text{F}$  NMR (376 MHz,  $\text{CDCl}_3$ ):  $\delta$  = -0.44; MS (ESI) calcd for  $\text{C}_{23}\text{H}_{23}\text{F}_3\text{O}_5$   $[\text{M}+\text{Na}]^+$   $m/z$ : 459.15; found: 459.7.

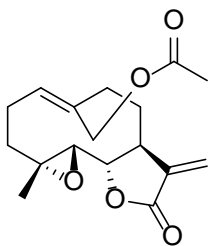


**PTL-9-012:** Standard procedure was applied using (*S*)-9-hydroxy-parthenolide (5 mg, 0.019 mmol), 4-dimethylaminopyridine (12 mg, 0.01 mmol), triethylamine (27  $\mu$ L, 0.19 mmol), and 2,4(bis-trifluoromethyl)benzoyl chloride (18  $\mu$ L, 0.1 mmol). Isolated PTL-9-012: 3 mg, 31 %

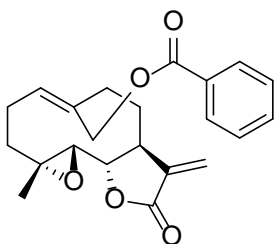
yield  $^1\text{H}$  NMR (500 MHz,  $\text{CDCl}_3$ ):  $\delta$  = 1.33-1.39 (m, 1 H), 1.40 (s, 3 H), 1.84 (s, 3 H), 2.19-2.30 (m, 2 H), 2.34-2.46 (m, 2 H), 2.56 (dq, 1 H,  $J$  = 5.0, 13.0 Hz), 2.80 (d, 1 H,  $J$  = 8.4 Hz), 3.02-3.08 (m, 1 H), 3.95 (t, 1 H,  $J$  = 8.4 Hz), 5.55 (d, 1 H,  $J$  = 10.3 Hz), 5.68 (d, 1 H,  $J$  = 12.6 Hz), 5.77 (d, 1 H,  $J$  = 2.7 Hz), 6.46 (d, 1 H,  $J$  = 3.4 Hz), 7.97 (s, 2 H), 8.08 (s, 1 H);  $^{13}\text{C}$  NMR (125 MHz,  $\text{CDCl}_3$ ):  $\delta$  = 11.7, 17.4, 23.8, 35.5, 36.0, 44.1, 61.2, 66.0, 81.4, 83.3, 122.1, 124.2, 128.8, 130.9, 132.2, 137.7, 164.8, 168.5;  $^{19}\text{F}$  NMR (376 MHz,  $\text{CDCl}_3$ ):  $\delta$  = -0.87, 3.11; HRMS (ESI) calcd for  $\text{C}_{24}\text{H}_{22}\text{F}_6\text{O}_5$   $[\text{M}+\text{H}]^+$   $m/z$ : 505.1453; found: 505.1450.



**PTL-9-013:** Standard procedure was applied using (*S*)-9-hydroxy-parthenolide (9 mg, 0.034 mmol), 4-dimethylaminopyridine (2 mg, 0.017 mmol), triethylamine (47  $\mu\text{L}$ , 0.34 mmol), and 3,5(*bis*-trifluoromethyl)benzoyl chloride (31  $\mu\text{L}$ , 0.17 mmol). Isolated PTL-9-013: 5 mg, 29% yield.  $^1\text{H}$  NMR (400 MHz,  $\text{CDCl}_3$ ):  $\delta$  = 1.27-1.32 (m, 1 H), 1.36 (s, 3 H), 1.85 (s, 3 H), 2.17-2.25 (m, 2 H), 2.27-2.40 (m, 2 H), 2.52 (dq, 1 H,  $J$  = 5.4, 13.0 Hz), 2.75 (d, 1 H,  $J$  = 8.5 Hz), 2.98-3.05 (m, 1 H), 3.91 (t, 1 H,  $J$  = 8.1 Hz), 5.52 (d, 1 H,  $J$  = 10.8 Hz), 5.65 (d, 1 H,  $J$  = 10.8 Hz), 5.72 (s, 1 H), 6.46 (s, 1 H), 8.09 (s, 1 H), 8.46 (s, 2 H);  $^{13}\text{C}$  NMR (125 MHz,  $\text{CDCl}_3$ ):  $\delta$  = 11.9, 17.4, 23.9, 35.9, 36.0, 44.1, 61.3, 66.0, 81.4, 82.6, 122.2, 129.1, 129.7, 132.2, 132.3, 137.8, 162.9, 168.4;  $^{19}\text{F}$  NMR (376 MHz,  $\text{CDCl}_3$ ):  $\delta$  = -0.58; HRMS (ESI) calcd for  $\text{C}_{24}\text{H}_{22}\text{F}_6\text{O}_5$   $[\text{M}+\text{H}]^+$   $m/z$ : 505.1450; found: 505.1443.

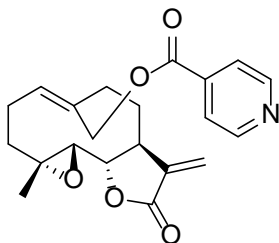


**PTL-14-003:** Standard procedure was applied using 14-hydroxy-parthenolide (3.4 mg, 0.013 mmol), 4-dimethylaminopyridine (0.8 mg, 0.0065 mmol), triethylamine (18  $\mu$ L, 0.13 mmol), and acetyl chloride (5  $\mu$ L, 0.065 mmol). Isolated PTL-14-003: 1.3 mg, 33 % yield.  $^1\text{H}$  NMR (500 MHz,  $\text{CDCl}_3$ ):  $\delta$  = 1.26 (s, 3 H), 1.27-1.35 (m, 1 H), 1.74-1.83 (m, 1 H), 2.08 (s, 3 H), 2.12-2.24 (m, 3 H), 2.26-2.33 (m, 1 H), 2.50 (dq, 1 H,  $J$ =4.9, 13.4 Hz), 2.63 (dd, 1 H,  $J$ =6.1, 14.0 Hz), 2.76-2.85 (m, 2H), 3.86 (t, 1 H,  $J$ =8.8 Hz), 4.68 (d, 1 H,  $J$ =12.1 Hz), 4.80 (d, 1 H,  $J$ =12.3 Hz), 5.50 (dd, 1 H,  $J$ = 3.6, 12.5 Hz), 5.63 (d, 1 H,  $J$ = 3.2 Hz), 6.35 (d, 1 H,  $J$ = 3.6 Hz);  $^{13}\text{C}$  NMR (125 MHz,  $\text{CDCl}_3$ ):  $\delta$  = 17.1, 21.1, 24.1, 31.4, 36.3, 36.8, 47.4, 61.1, 61.3, 66.3, 82.4, 121.6, 132.0, 133.5, 139.1, 169.2, 171.0; MS (ESI) calcd for  $\text{C}_{17}\text{H}_{22}\text{O}_5$   $[\text{M}+\text{H}]^+$   $m/z$ : 307.15; found: 307.1

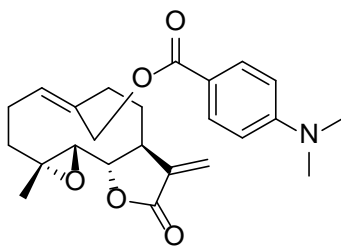


**PTL-14-004:** Standard procedure was applied using 14-hydroxy-parthenolide (12 mg, 0.045 mmol), 4-dimethylaminopyridine (3 mg, 0.023 mmol), triethylamine (63  $\mu$ L, 0.45 mmol), and benzoyl chloride (26  $\mu$ L, 0.23 mmol). Isolated PTL-14-004: 3 mg, 18 % yield.  $^1\text{H}$  NMR (500 MHz,  $\text{CDCl}_3$ ):  $\delta$  = 1.30-1.37 (4 H, m), 1.81-1.90 (1 H, m), 2.15-2.26 (3 H, m), 2.31-2.38 (1 H, m), 2.59 (1 H, dq,  $J$ = 5.2, 13.2 Hz), 2.75 (1 H, dd,  $J$ = 6.0, 14.0 Hz), 2.80 (2 H, m), 3.90 (1 H, t,  $J$ = 8.8 Hz), 4.84 (1 H, d,  $J$ = 11.7 Hz), 5.07 (1 H, d,  $J$ = 12.1 Hz), 5.56 (1 H, dd,  $J$ = 4.0, 12.8 Hz),

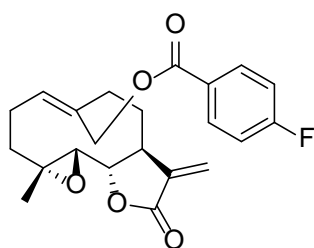
5.63 (1 H, d,  $J= 3.3$  Hz), 6.35 (1 H, d,  $J= 3.6$  Hz), 7.45 (2 H, t,  $J= 7.3$  Hz), 7.58 (1 H, t,  $J= 7.3$  Hz), 8.05 (2 H, d,  $J= 7.7$  Hz).  $^{13}\text{C}$  NMR (125 MHz,  $\text{CDCl}_3$ ):  $\delta = 17.0, 24.0, 31.3, 36.2, 36.6, 47.3, 61.1, 61.6, 66.2, 82.4, 121.6, 128.6, 129.5, 129.8, 131.9, 133.3, 133.5, 139.0, 166.5, 169.1$ . MS (ESI) calcd for  $\text{C}_{22}\text{H}_{24}\text{O}_5$   $[\text{M}+\text{H}]^+$   $m/z$ : 369.16; found: 369.3



**PTL-14-005:** Standard procedure was applied using 14-hydroxy-parthenolide (7 mg, 0.026mmol), 4-dimethylaminopyridine (3 mg, 0.026mmol), triethylamine (40  $\mu\text{L}$ , 0.26mmol), and isonicotinoyl chloride (23 mg, 0.13mmol). Isolated PTL-14-005: 4 mg, 42 % yield.  $^1\text{H}$  NMR (500 MHz,  $\text{CDCl}_3$ ):  $\delta = 1.30$  (s, 3 H), 1.32-1.40 (m, 1 H), 1.75-1.85 (m, 1 H), 2.15-2.28 (m, 3 H), 2.32-2.40 (m, 1 H), 2.58 (dq, 1 H,  $J= 5.8, 13.0$  Hz), 2.73 (dd, 1 H,  $J= 6.1, 13.8$  Hz), 2.78-2.88 (m, 2H), 3.88 (t, 1 H,  $J=8.7$  Hz), 4.82 (d, 1 H,  $J=11.5$  Hz), 4.14 (d, 1 H,  $J=12.4$  Hz), 5.60 (dd, 1 H,  $J= 4.0, 12.4$  Hz), 5.64 (d, 1 H,  $J= 3.2$  Hz), 6.37 (d, 1 H,  $J= 3.7$  Hz), 7.84 (bs, 2 H), 8.82 (bs, 2 H);  $^{13}\text{C}$  NMR (125 MHz,  $\text{CDCl}_3$ ):  $\delta = 17.0, 24.2, 31.2, 36.1, 36.4, 47.2, 60.9, 62.1, 66.1, 82.3, 121.7, 132.6, 132.8, 137.0, 138.8, 150.7, 165.0, 169.0$ ; MS (ESI) calcd for  $\text{C}_{21}\text{H}_{23}\text{NO}_5$   $[\text{M}+\text{H}]^+$   $m/z$ : 370.16; found: 370.2

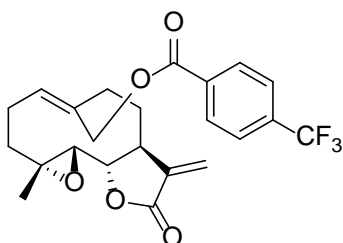


**PTL-14-006:** Standard procedure was applied using 14-hydroxy-parthenolide (7 mg, 0.026 mmol), 4-dimethylaminopyridine (3 mg, 0.026 mmol), triethylamine (40  $\mu$ L, 0.26 mmol), and the 4-(dimethylamino)benzoyl chloride (24 mg, 0.13 mmol). Isolated PTL-14-006: 5 mg, 47% yield.  $^1\text{H}$  NMR (500 MHz,  $\text{CDCl}_3$ ):  $\delta$ =1.32 (s, 3 H), 1.33-1.40 (m, 1 H), 1.84-1.96 (m, 1 H), 2.12-2.26 (m, 3 H), 2.27-2.37 (m, 1 H), 2.51-2.65 (m, 1 H), 2.67-2.77 (m, 1 H), 2.78-2.88 (m, 2H), 3.05 (s, 6H), 3.93 (t, 1 H,  $J$ =8.8Hz), 4.82 (d, 1 H,  $J$ =12.1Hz), 4.97 (d, 1 H,  $J$ =12.4Hz), 5.51 (dd, 1 H,  $J$ = 3.6, 12.7Hz), 5.62 (d, 1 H,  $J$ = 3.4Hz), 6.35 (d, 1 H,  $J$ = 3.6Hz), 6.64 (d, 2H,  $J$ =9.0Hz), 7.86 (d, 2H,  $J$ =8.9Hz);  $^{13}\text{C}$  NMR (125 MHz,  $\text{CDCl}_3$ ):  $\delta$ =16.9, 24.0, 31.6, 36.3, 36.9, 40.0, 47.3, 61.2, 66.2, 82.5, 110.8, 116.2, 121.5, 131.2, 132.6, 134.0, 139.0, 153.4, 166.8, 169.2; MS (ESI) calcd for  $\text{C}_{24}\text{H}_{29}\text{NO}_5$   $[\text{M}+\text{H}]^+$   $m/z$ : 412.20; found: 412.3

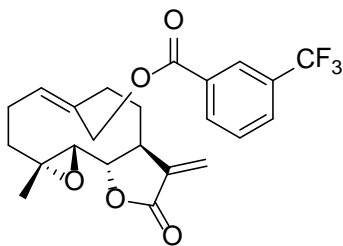


**PTL-14-009:** Standard procedure was applied using 14-hydroxy-parthenolide (14 mg, 0.053 mmol), 4-dimethylaminopyridine (3 mg, 0.027 mmol), triethylamine (74  $\mu$ L, 0.53 mmol), and 4-fluorobenzoyl chloride (31  $\mu$ L, 0.27 mmol). Isolated PTL-14-009: 5.6 mg, 27% yield.  $^1\text{H}$  NMR (500 MHz,  $\text{CDCl}_3$ ):  $\delta$ =1.30 (s, 3 H), 1.31-1.38 (m, 1 H), 1.76-1.87 (m, 1 H), 2.13-2.26 (m, 3 H), 2.30-2.38 (m, 1 H), 2.57 (dq, 1 H,  $J$ =5.3, 13.3Hz), 2.73 (dd, 1 H,  $J$ =6.2, 13.5Hz), 2.78-2.87 (m,

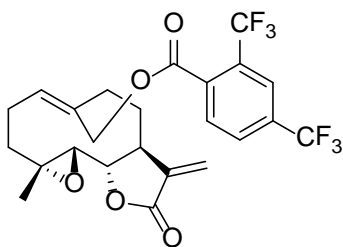
2H), 3.88 (t, 1 H,  $J=8.8\text{Hz}$ ), 4.80 (d, 1 H,  $J=12.4\text{Hz}$ ), 5.07 (d, 1 H,  $J=11.8\text{ Hz}$ ), 5.56 (dd, 1 H,  $J=3.6, 12.4\text{Hz}$ ), 5.62 (d, 1 H,  $J=4.1\text{Hz}$ ), 6.35 (d, 1 H,  $J=3.5\text{Hz}$ ), 7.12 (t, 2H,  $J=8.5\text{Hz}$ ), 8.02 (dt, 2H,  $J=3.3, 5.4\text{Hz}$ );  $^{13}\text{C}$  NMR (125 MHz,  $\text{CDCl}_3$ ):  $\delta=17.0, 24.0, 31.2, 36.2, 36.5, 47.3, 61.0, 61.5, 66.2, 82.3, 115.6, 115.9, 121.6, 132.1, 132.2, 133.4, 138.9, 165.6, 169.0$ ;  $^{19}\text{F}$  NMR (376 MHz,  $\text{CDCl}_3$ ):  $\delta=-42.45$ ; MS (ESI) calcd for  $\text{C}_{22}\text{H}_{23}\text{FO}_5$   $[\text{M}+\text{H}]^+$   $m/z$ : 387.15; found: 387.5.



**PTL-14-010:** Standard procedure was applied using 14-hydroxy-parthenolide (16 mg, 0.061 mmol), 4-dimethylaminopyridine (3.7 mg, 0.03 mmol), triethylamine (85  $\mu\text{L}$ , 0.61 mmol), and 4-(trifluoromethyl)benzoyl chloride (45  $\mu\text{L}$ , 0.3 mmol). Isolated PTL-14-010: 7 mg, 26% yield.  $^1\text{H}$  NMR (500 MHz,  $\text{CDCl}_3$ ):  $\delta=1.31$  (s, 3 H), 1.32-1.39 (m, 1 H), 1.77-1.87 (m, 1 H), 2.19-2.28 (m, 3 H), 2.33-2.39 (m, 1 H), 2.60 (dq, 1 H,  $J=5.5, 13.3\text{Hz}$ ), 2.74 (dd, 1 H,  $J=5.1, 13.7\text{Hz}$ ), 2.79-2.88 (m, 2H), 3.89 (t, 1 H,  $J=8.6\text{Hz}$ ), 4.84 (d, 1 H,  $J=12.1\text{Hz}$ ), 5.13 (d, 1 H,  $J=12.1\text{Hz}$ ), 5.60 (dd, 1 H,  $J=4.3, 12.1\text{Hz}$ ), 5.63 (d, 1 H,  $J=2.7\text{Hz}$ ), 6.36 (d, 1 H,  $J=3.5\text{Hz}$ ), 7.73 (d, 2H,  $J=8.2\text{Hz}$ ), 8.13 (d, 2H,  $J=8.2\text{Hz}$ );  $^{13}\text{C}$  NMR (125 MHz,  $\text{CDCl}_3$ ):  $\delta=17.0, 24.1, 31.2, 36.1, 36.4, 47.3, 61.0, 61.9, 66.1, 82.3, 121.6, 125.6, 130.0, 132.4, 133.0, 138.9, 165.3, 169.0$ ;  $^{19}\text{F}$  NMR (376 MHz,  $\text{CDCl}_3$ ):  $\delta=-0.77$ ; HRMS (ESI) calcd for  $\text{C}_{23}\text{H}_{23}\text{F}_3\text{O}_5$   $[\text{M}+\text{H}]^+$   $m/z$ : 437.1576; found: 437.1572.

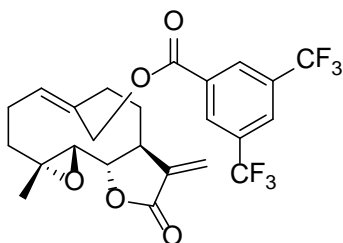


**PTL-14-011:** Standard procedure was applied using 14-hydroxy-parthenolide (13 mg, 0.049 mmol), 4-dimethylaminopyridine (3 mg, 0.025 mmol), triethylamine (68  $\mu$ L, 0.49 mmol), and 3-(trifluoromethyl)benzoyl chloride (37  $\mu$ L, 0.025 mmol). Isolated PTL-14-011: 10 mg, 38% yield.  $^1\text{H}$  NMR (500 MHz,  $(\text{CD}_3)_2\text{CO}$ ):  $\delta$  = 1.36-1.41 (m, 4 H), 2.02-2.07 (m, 1 H), 2.23 (dd, 1 H,  $J$  = 5.0, 12.4 Hz), 2.29-2.39 (m, 3 H), 2.70-2.81 (m, 2 H), 3.03 (d, 1 H,  $J$  = 9.4 Hz), 3.10-3.16 (m, 1 H), 4.13 (t, 1 H,  $J$  = 8.4 Hz), 5.02 (d, 1 H,  $J$  = 11.9 Hz), 5.29 (d, 1 H,  $J$  = 11.9 Hz), 5.78 (d, 1 H,  $J$  = 3.0 Hz), 5.84 (dd, 1 H,  $J$  = 3.5, 12.9 Hz), 6.21 (d, 1 H,  $J$  = 4.0 Hz), 7.85 (t, 1 H,  $J$  = 7.9 Hz), 8.06 (d, 1 H,  $J$  = 7.9 Hz), 8.32 (s, 1 H), 8.36 (d, 1 H,  $J$  = 7.4 Hz);  $^{13}\text{C}$  NMR (125 MHz,  $(\text{CD}_3)_2\text{CO}$ ):  $\delta$  = 17.42, 24.8, 31.9, 37.1, 47.8, 61.6, 63.1, 66.8, 83.4, 120.8, 126.9, 130.7, 131.1, 132.4, 133.1, 134.1, 134.6, 141.5, 165.7, 170.0;  $^{19}\text{F}$  NMR (376 MHz,  $\text{CDCl}_3$ ):  $\delta$  = -0.46; MS (ESI) calcd for  $\text{C}_{23}\text{H}_{23}\text{F}_3\text{O}_5$   $[\text{M}+\text{Na}]^+$   $m/z$ : 459.15; found: 459.7.



**PTL-14-012:** Standard procedure was applied using 14-hydroxy-parthenolide (27 mg, 0.10 mmol), 4-dimethylaminopyridine (6 mg, 0.051 mmol), triethylamine (140  $\mu$ L, 0.1 mmol), and 2,4(bis-trifluoromethyl) benzoyl chloride (90  $\mu$ L, 0.5 mmol). Isolated PTL-14-012: 20 mg, 40% yield.  $^1\text{H}$  NMR (500 MHz,  $(\text{CD}_3)_2\text{CO}$ ):  $\delta$  = 1.30-1.40 (m, 4 H), 1.92-2.00 (m, 1 H), 2.18 (dd, 1 H,

$J= 4.9, 12.5$  Hz), 2.22-2.34 (m, 3 H), 2.65-2.75 (m, 2 H), 2.96 (d, 1 H,  $J= 9.0$  Hz), 3.04-3.10 (m, 1 H), 4.05 (t, 1 H,  $J= 8.7$  Hz), 4.96 (d, 1 H,  $J= 11.9$  Hz), 5.28 (d, 1 H,  $J= 11.9$  Hz), 5.74 (d, 1 H,  $J= 3.2$  Hz), 5.81 (dd, 1 H,  $J= 3.8, 12.5$  Hz), 6.17 (d, 1 H,  $J= 3.5$  Hz), 8.10 (d, 1 H,  $J= 9.1$  Hz), 8.19 (s, 2 H);  $^{13}\text{C}$  NMR (125 MHz,  $(\text{CD}_3)_2\text{CO}$ ):  $\delta = 17.4, 24.7, 31.6, 36.9, 37.0, 47.7, 61.5, 63.9, 66.7, 83.3, 120.7, 124.9, 130.7, 132.2, 133.5, 134.0, 136.1, 141.4, 166.2, 169.9$ ;  $^{19}\text{F}$  NMR (376 MHz,  $\text{CDCl}_3$ ):  $\delta = -0.88, 2.66$ ; MS (ESI) calcd for  $\text{C}_{24}\text{H}_{22}\text{F}_6\text{O}_5$   $[\text{M}+\text{Na}]^+$   $m/z$ : 527.14; found: 527.7.



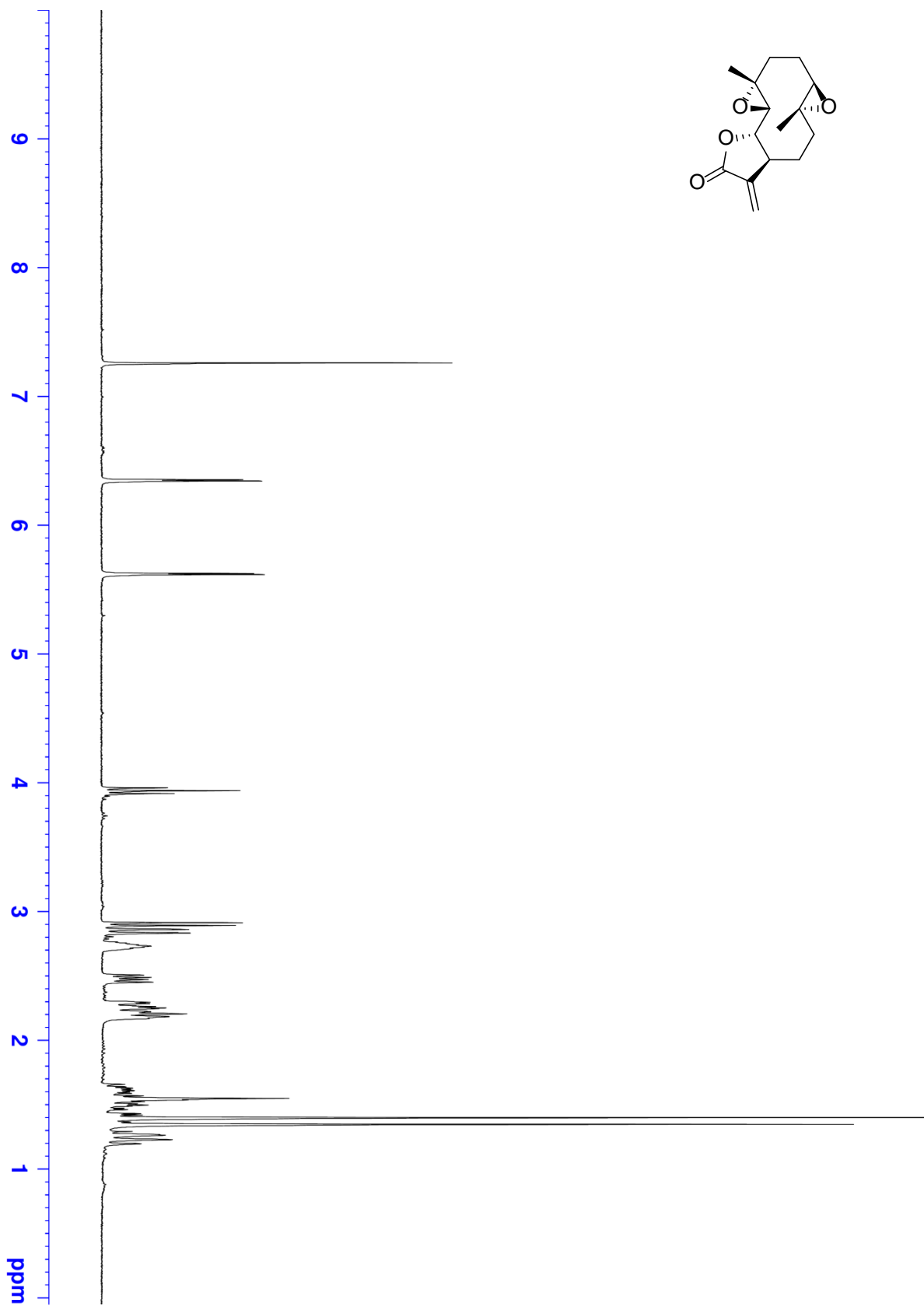
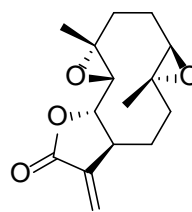
**PTL-14-013:** Standard procedure was applied using 14-hydroxy-parthenolide (15 mg, 0.057 mmol), 4-dimethylaminopyridine (3.5 mg, 0.029 mmol), triethylamine (80  $\mu\text{L}$ , 0.57 mmol), and the 3,5(*bis*-trifluoromethyl)benzoyl chloride (51  $\mu\text{L}$ , 0.29 mmol). Isolated PTL-14-013: 7 mg, 24% yield.  $^1\text{H}$  NMR (500 MHz,  $(\text{CD}_3)_2\text{CO}$ ):  $\delta = 1.30-1.38$  (m, 4 H), 1.94-2.02 (m, 1 H), 2.15-2.22 (m, 1 H), 2.23-2.36 (m, 3 H), 2.67-2.83 (m, 2 H), 2.98 (d, 1 H,  $J= 8.4$  Hz), 3.05-3.12 (m, 1 H), 4.07 (t, 1 H,  $J= 8.4$  Hz), 5.01 (d, 1 H,  $J= 11.2$  Hz), 5.32 (d, 1 H,  $J= 12.1$  Hz), 5.74 (s, 1 H), 5.82 (d, 1 H,  $J= 12.1$  Hz), 6.71 (s, 1 H), 8.36 (s, 1 H), 8.54 (s, 2 H);  $^{13}\text{C}$  NMR (125 MHz,  $(\text{CD}_3)_2\text{CO}$ ):  $\delta = 17.4, 24.8, 31.7, 36.9, 37.0, 47.8, 61.5, 63.4, 66.7, 83.3, 120.7, 123.1, 125.2, 127.6, 130.6, 132.7, 133.0, 133.5, 133.9, 134.3, 141.4, 164.5, 169.8$ ;  $^{19}\text{F}$  NMR (376 MHz,  $\text{CDCl}_3$ ):  $\delta = -0.59$ ; HRMS (ESI) calcd for  $\text{C}_{24}\text{H}_{22}\text{F}_6\text{O}_5$   $[\text{M}+\text{H}]^+$   $m/z$ : 505.1450; found: 505.1454.

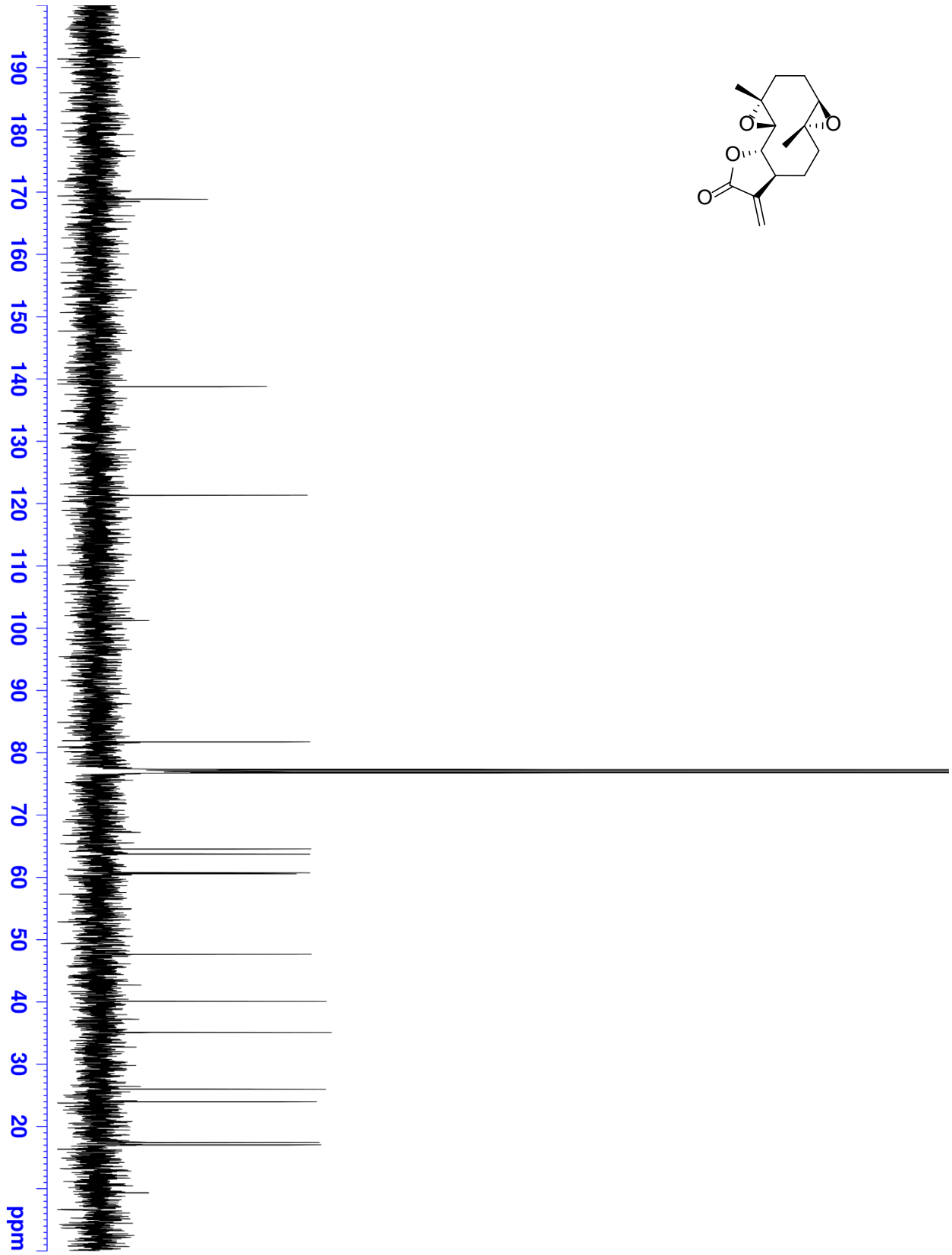
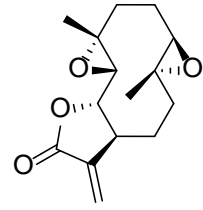
**Crystal Data and Structure Refinement for compound 2.** Crystal structure coordinates have been deposited in the Cambridge Crystallographic Data Centre (CCDC) under the code 966450.

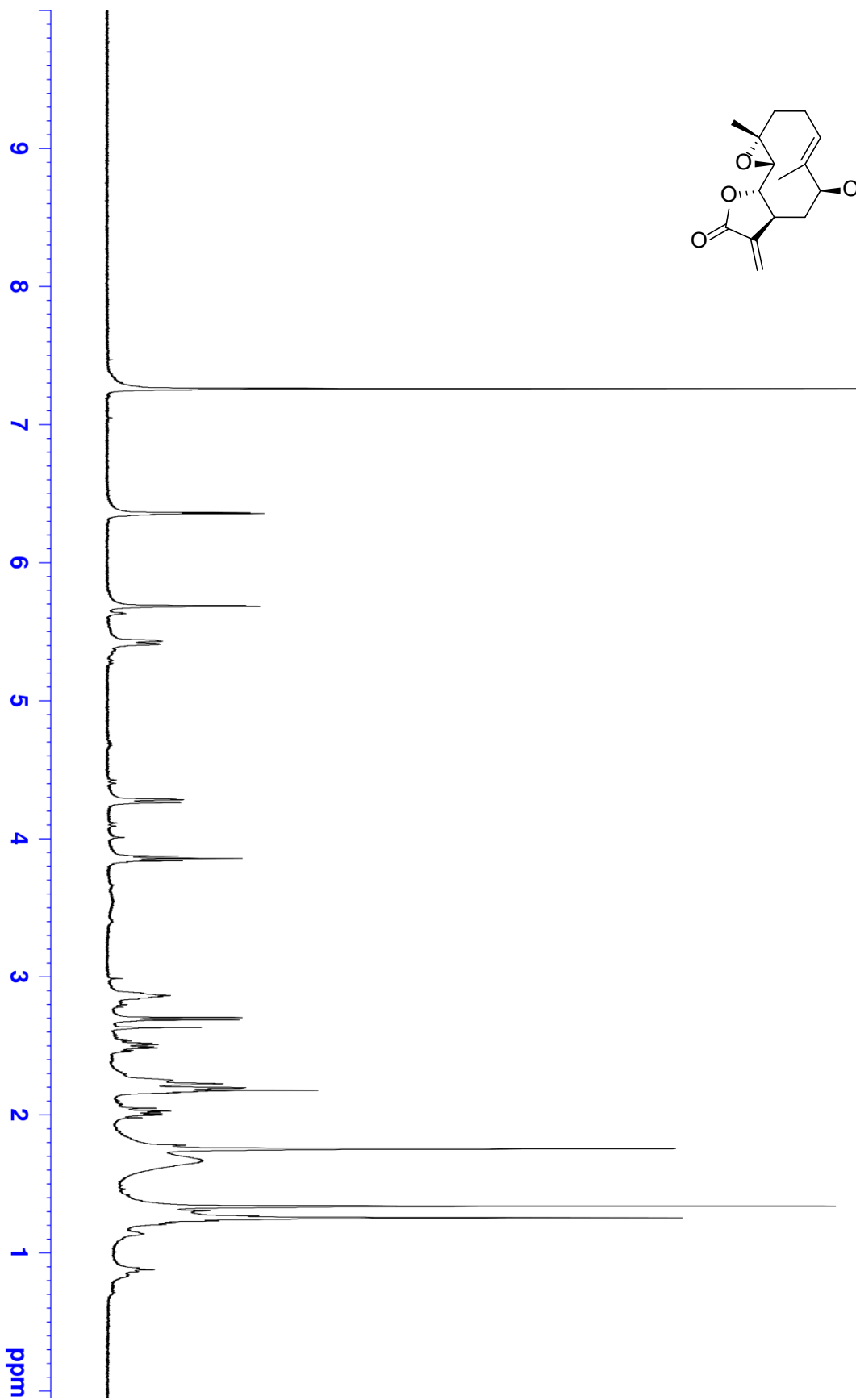
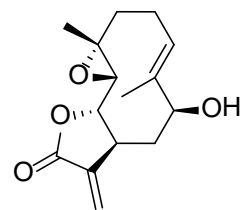
Identification code	fasjk01	
Empirical formula	C <sub>15</sub> H <sub>20</sub> O <sub>4</sub>	
Formula weight	264.31	
Temperature	100.0(1) K	
Wavelength	0.71073 Å	
Crystal system	Monoclinic	
Space group	<i>P</i> 2 <sub>1</sub>	
Unit cell dimensions	<i>a</i> = 10.2867(7) Å	$\alpha = 90^\circ$
	<i>b</i> = 9.2508(6) Å	$\beta = 106.201(1)^\circ$
	<i>c</i> = 15.3155(10) Å	$\gamma = 90^\circ$
Volume	1399.55(16) Å <sup>3</sup>	
<i>Z</i>	4	
Density (calculated)	1.254 Mg/m <sup>3</sup>	
Absorption coefficient	0.090 mm <sup>-1</sup>	
<i>F</i> (000)	568	
Crystal color, morphology	colorless, block	
Crystal size	0.32 x 0.24 x 0.16 mm <sup>3</sup>	
Theta range for data collection	1.38 to 37.78°	
Index ranges	-17 ≤ <i>h</i> ≤ 17, -15 ≤ <i>k</i> ≤ 15, -26 ≤ <i>l</i> ≤ 26	
Reflections collected	51687	
Independent reflections	7850 [ <i>R</i> (int) = 0.0589]	
Observed reflections	5772	
Completeness to theta = 37.78°	99.9%	
Absorption correction	Multi-scan	
Max. and min. transmission	0.9857 and 0.9718	
Refinement method	Full-matrix least-squares on <i>F</i> <sup>2</sup>	
Data / restraints / parameters	7850 / 1 / 503	
Goodness-of-fit on <i>F</i> <sup>2</sup>	0.991	
Final <i>R</i> indices [ <i>I</i> > 2σ( <i>I</i> )]	<i>R</i> 1 = 0.0454, <i>wR</i> 2 = 0.1055	
<i>R</i> indices (all data)	<i>R</i> 1 = 0.0703, <i>wR</i> 2 = 0.1231	
Largest diff. peak and hole	0.351 and -0.201 e.Å <sup>-3</sup>	

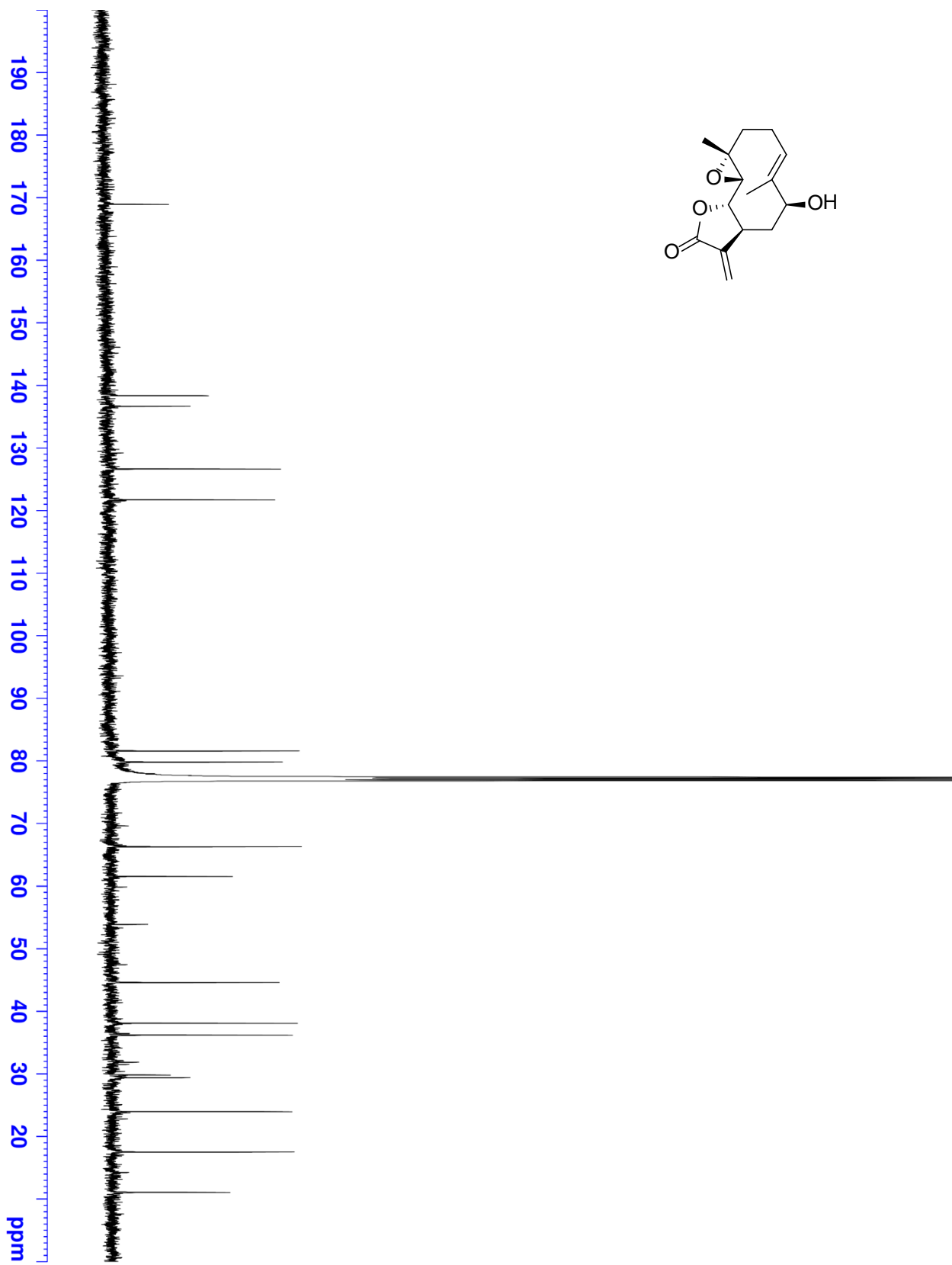
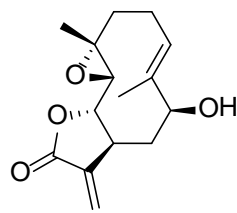
## REFERENCES

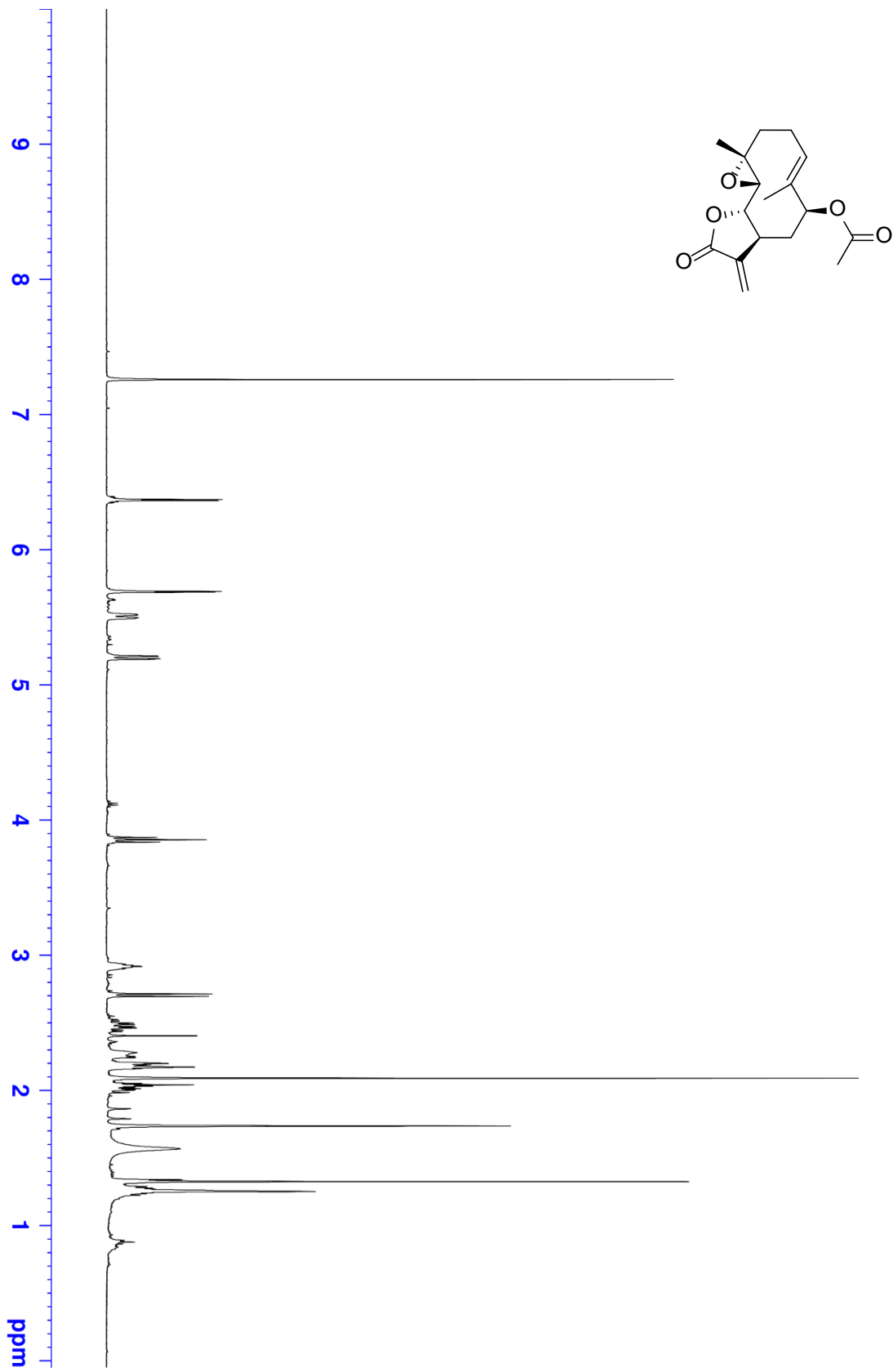
- (1) Zhang, K., El Damaty, S., and Fasan, R. (2011) P450 Fingerprinting Method for Rapid Discovery of Terpene Hydroxylating P450 Catalysts with Diversified Regioselectivity, *J Am Chem Soc* 133, 3242-3245.
- (2) Zhang, K., Shafer, B. M., Demars, M. D., 2nd, Stern, H. A., and Fasan, R. (2012) Controlled oxidation of remote sp<sup>3</sup> C-H bonds in artemisinin via P450 catalysts with fine-tuned regio- and stereoselectivity, *J Am Chem Soc* 134, 18695-18704.
- (3) McLachlan, M. J., Johannes, T. W., and Zhao, H. (2008) Further improvement of phosphite dehydrogenase thermostability by saturation mutagenesis, *Biotechnol. Bioeng.* 99, 268-274.

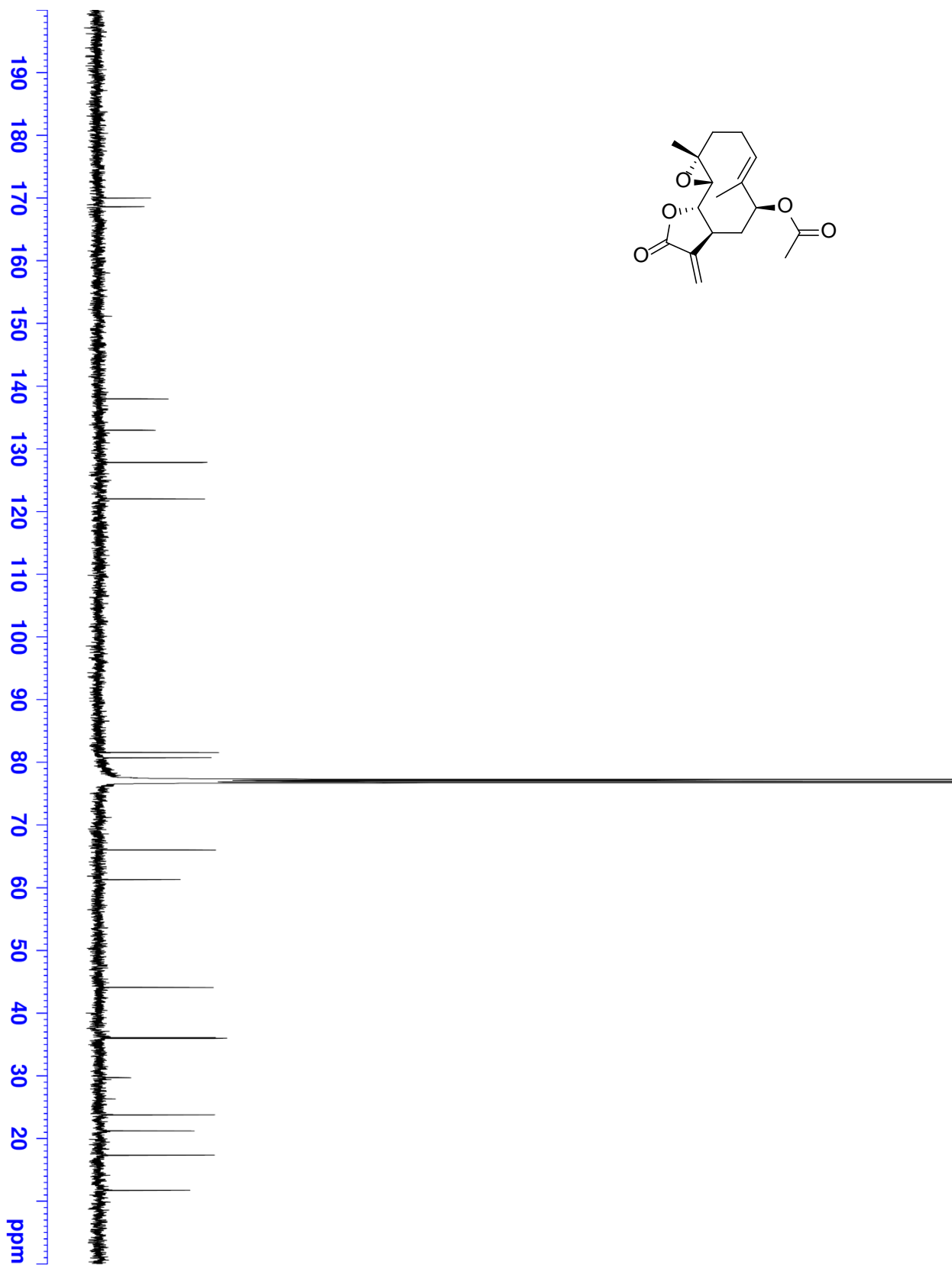
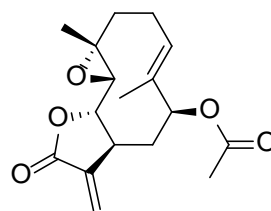


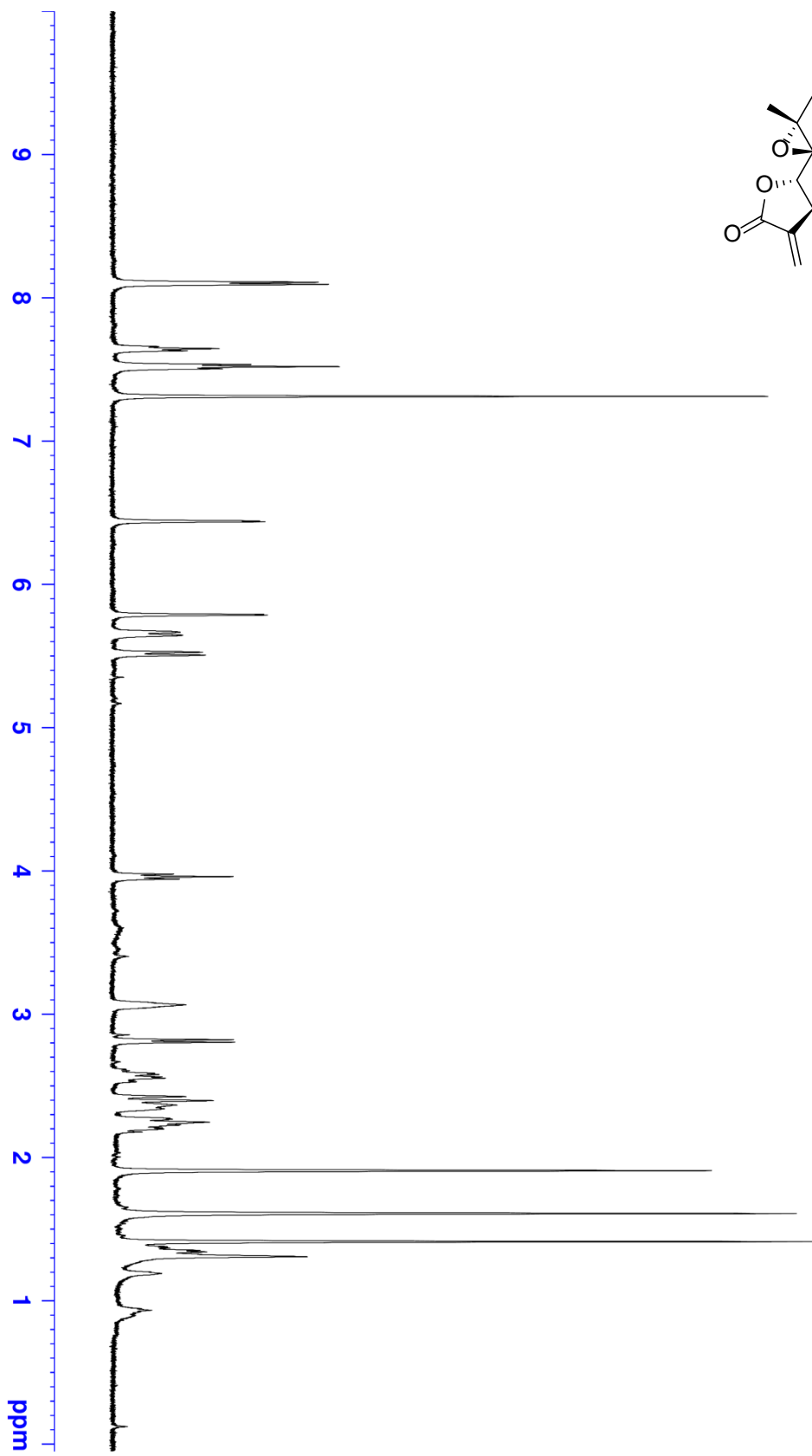
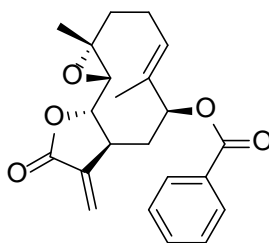


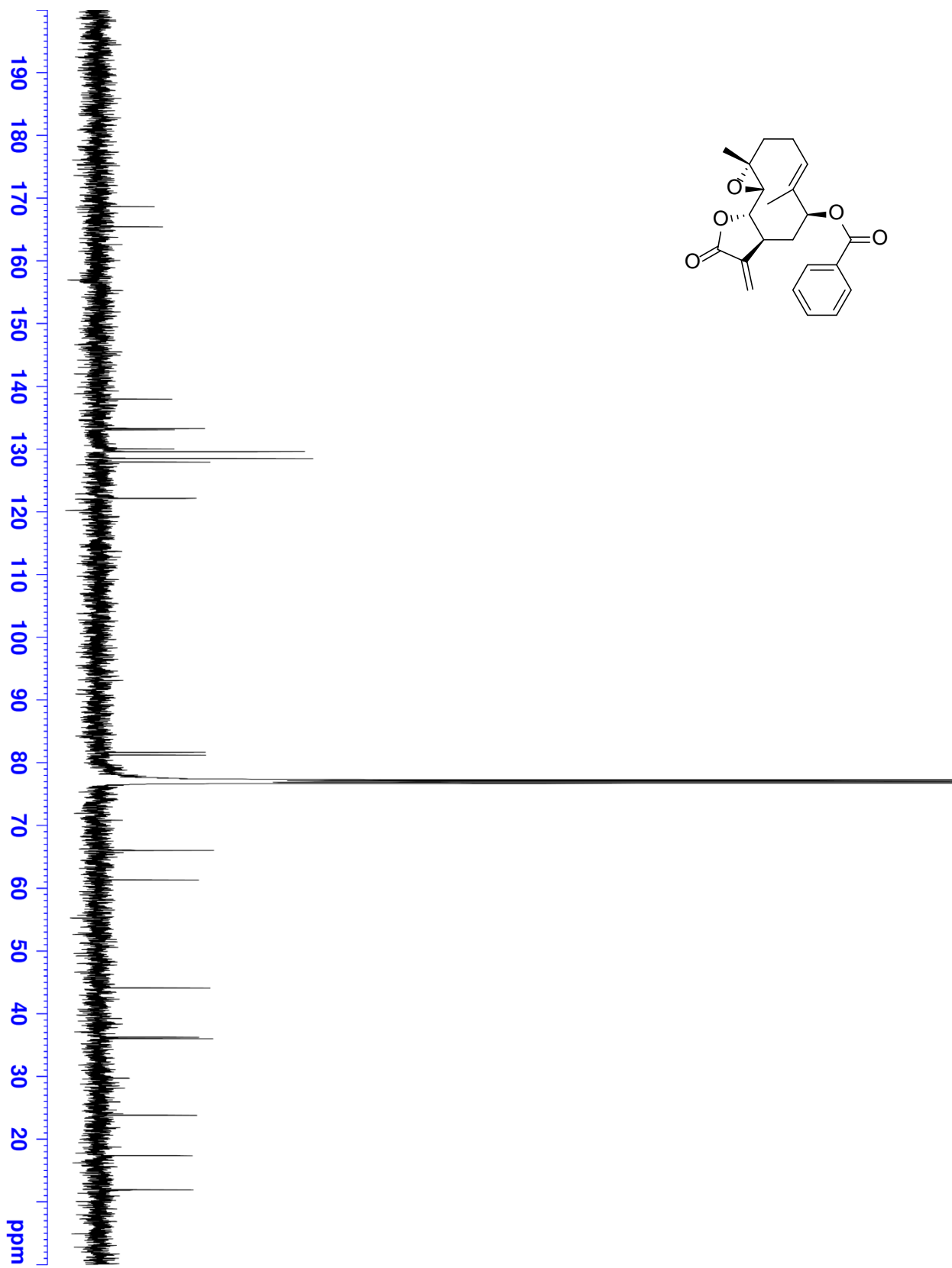
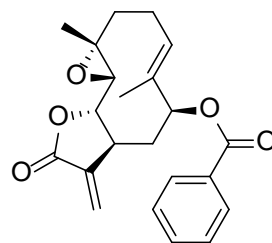


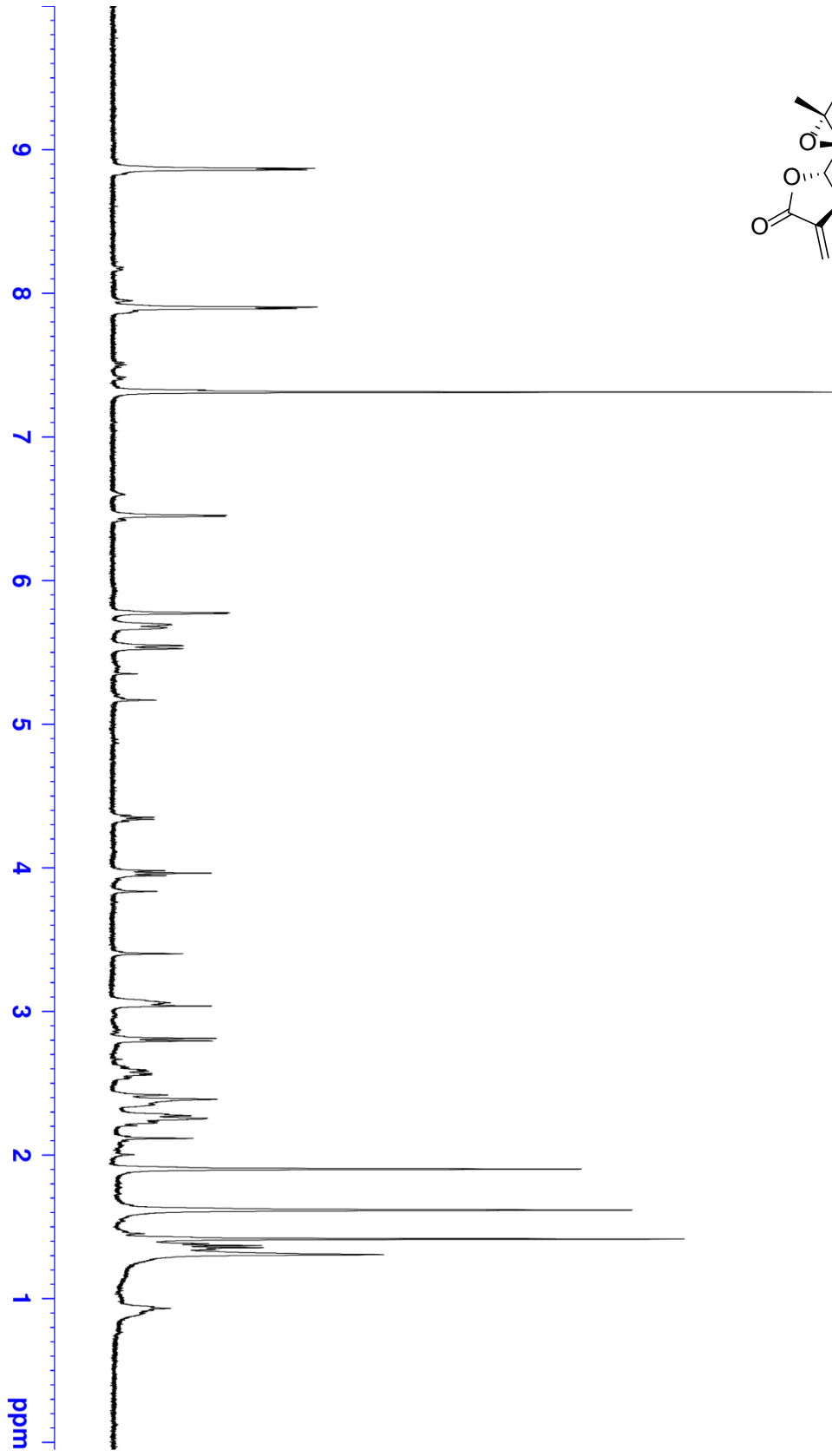
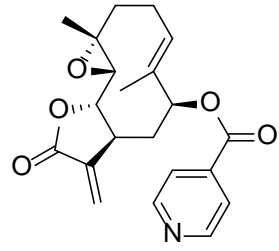


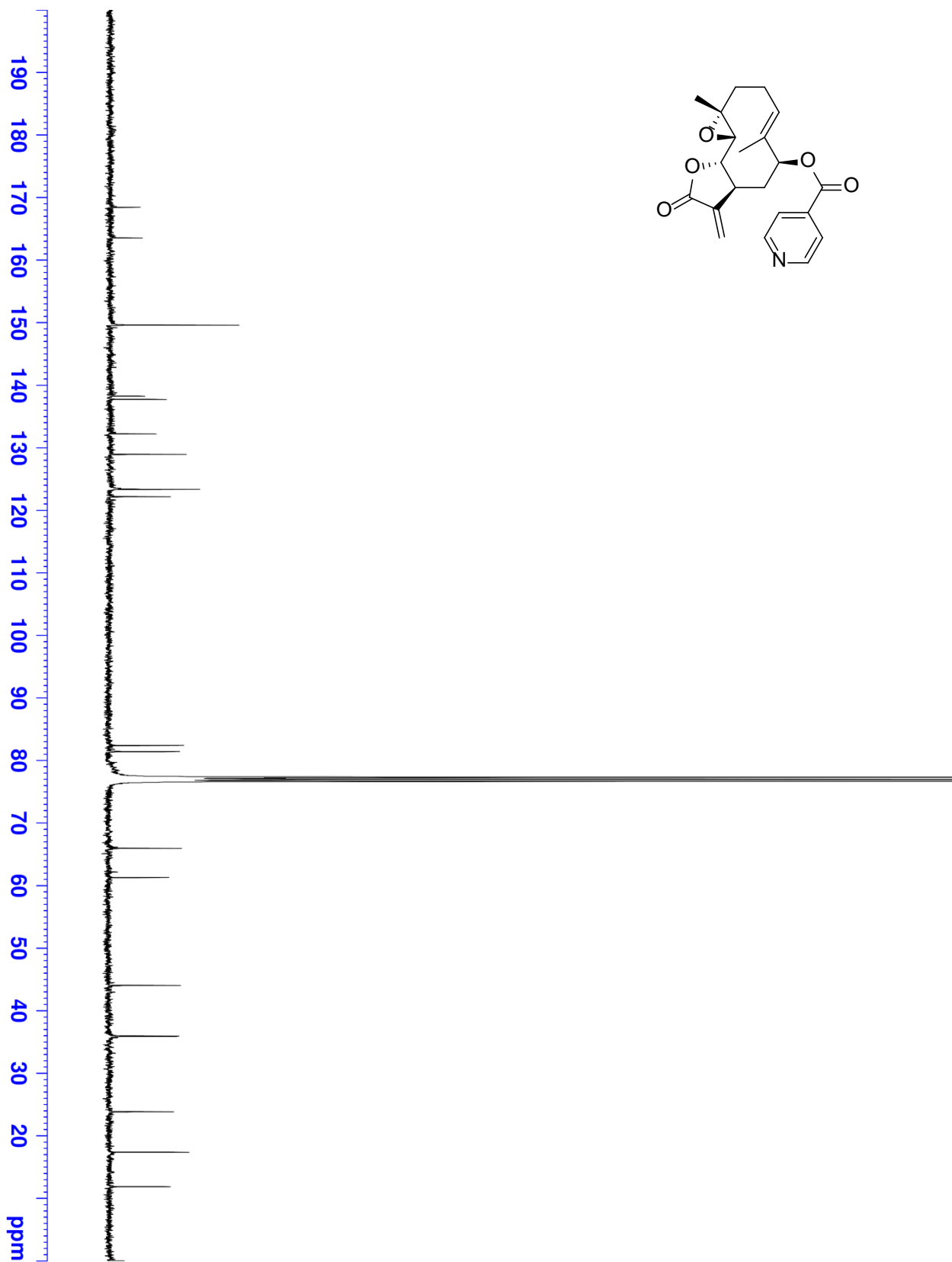
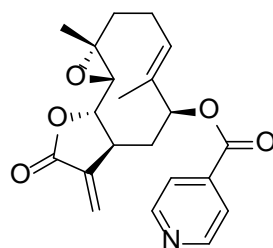


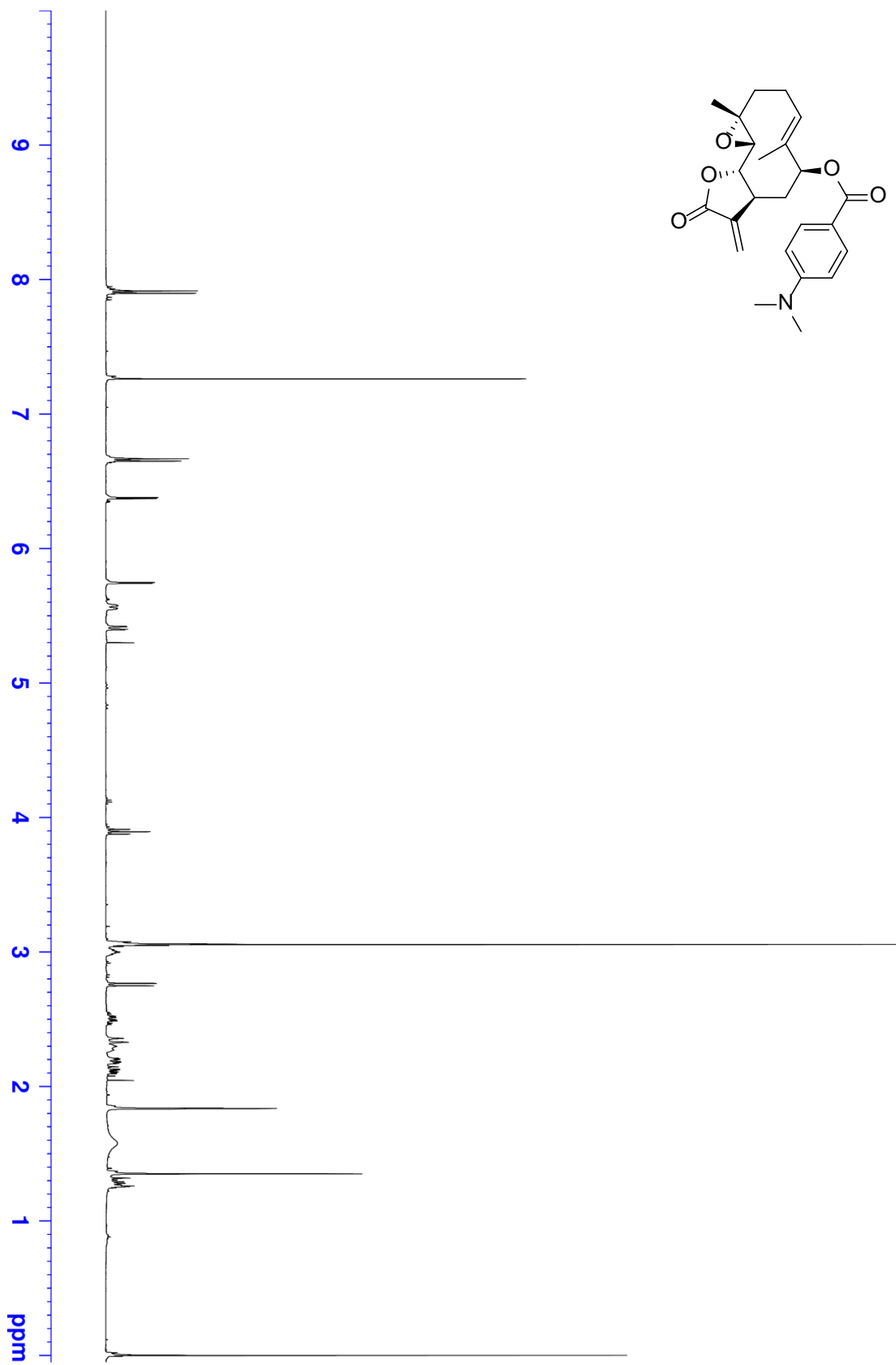
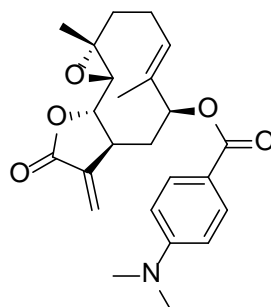


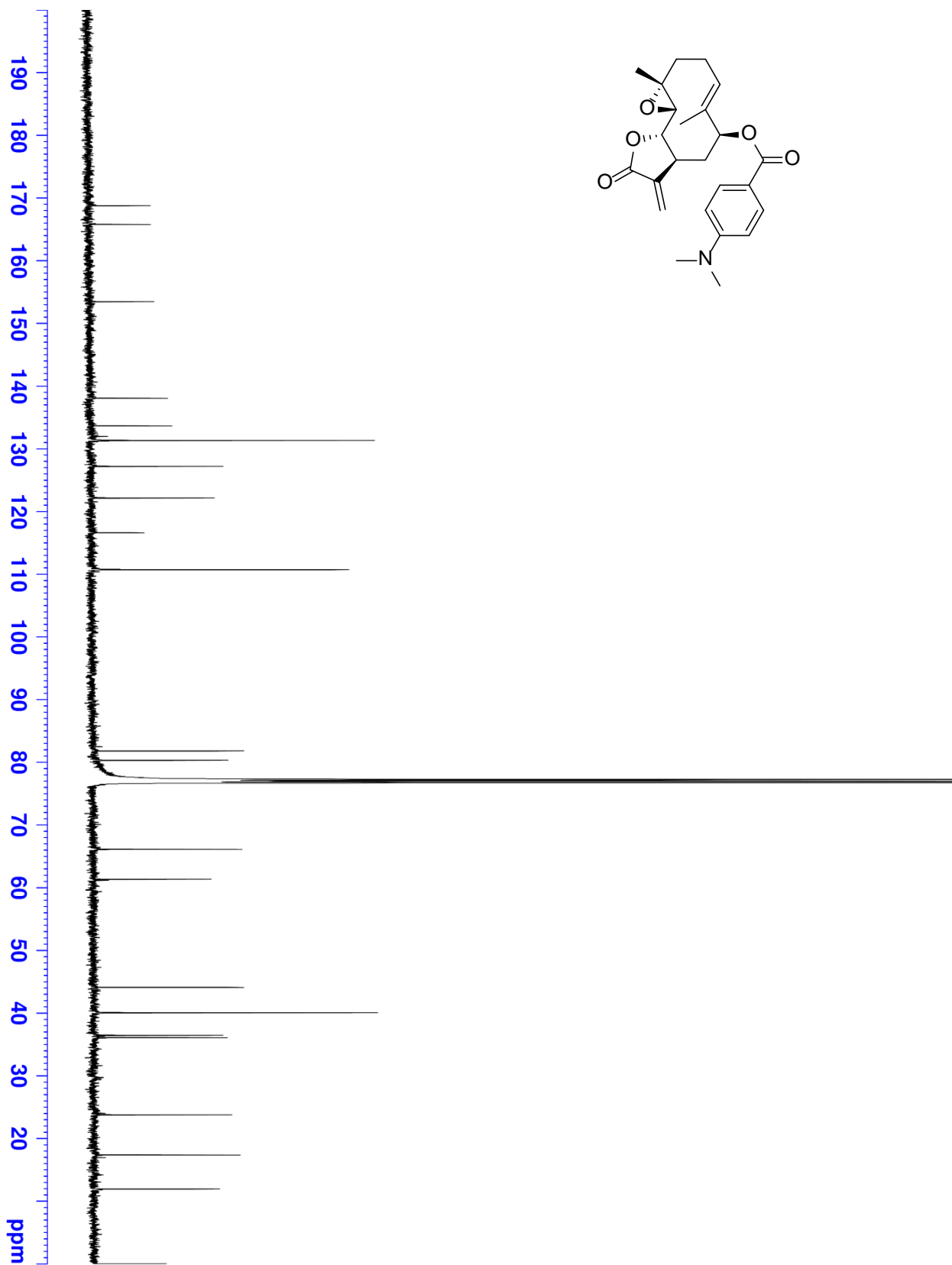
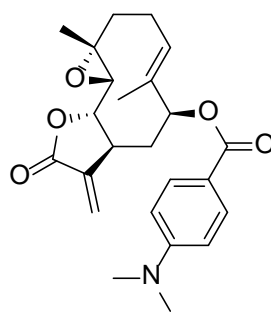


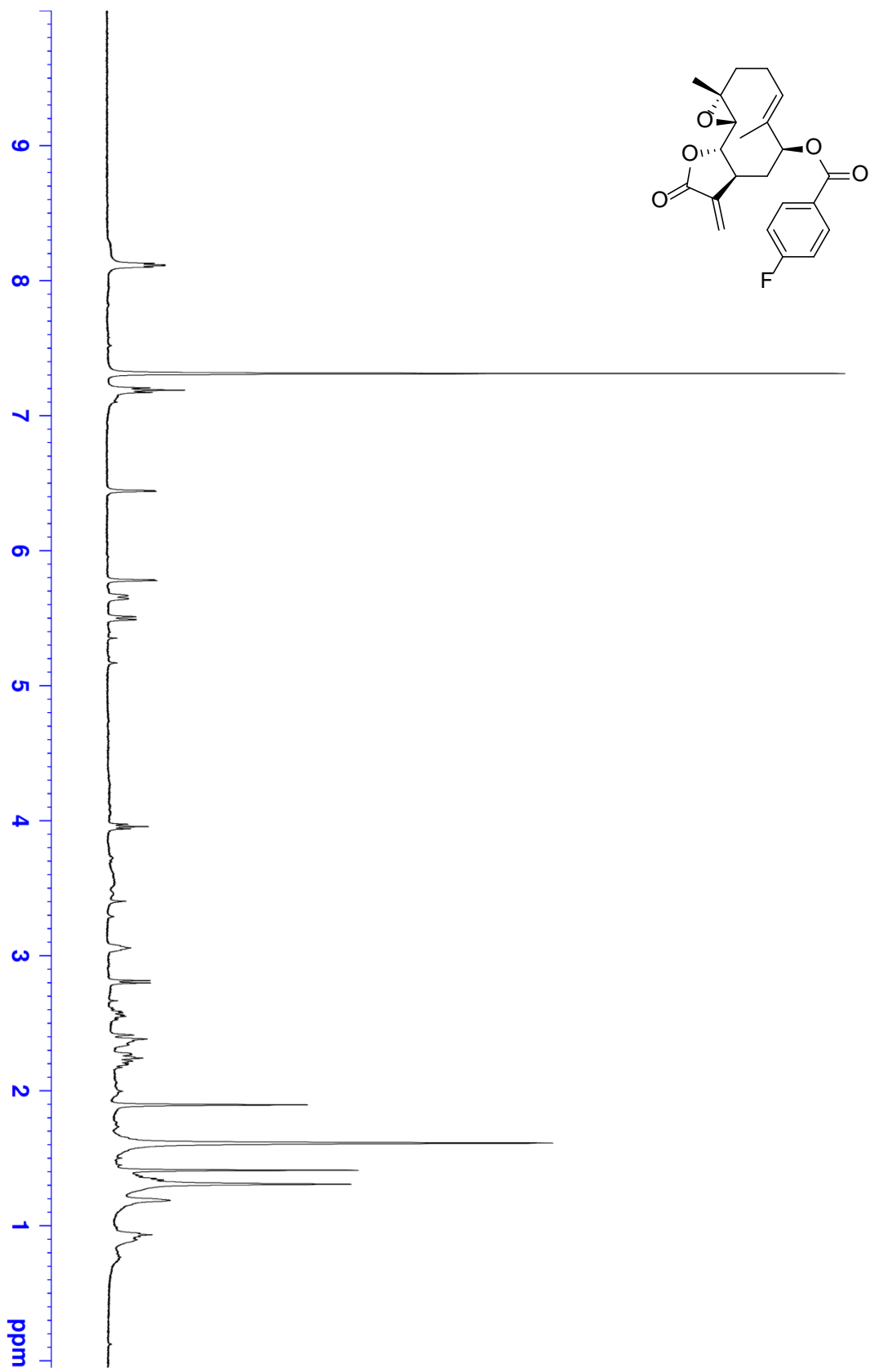


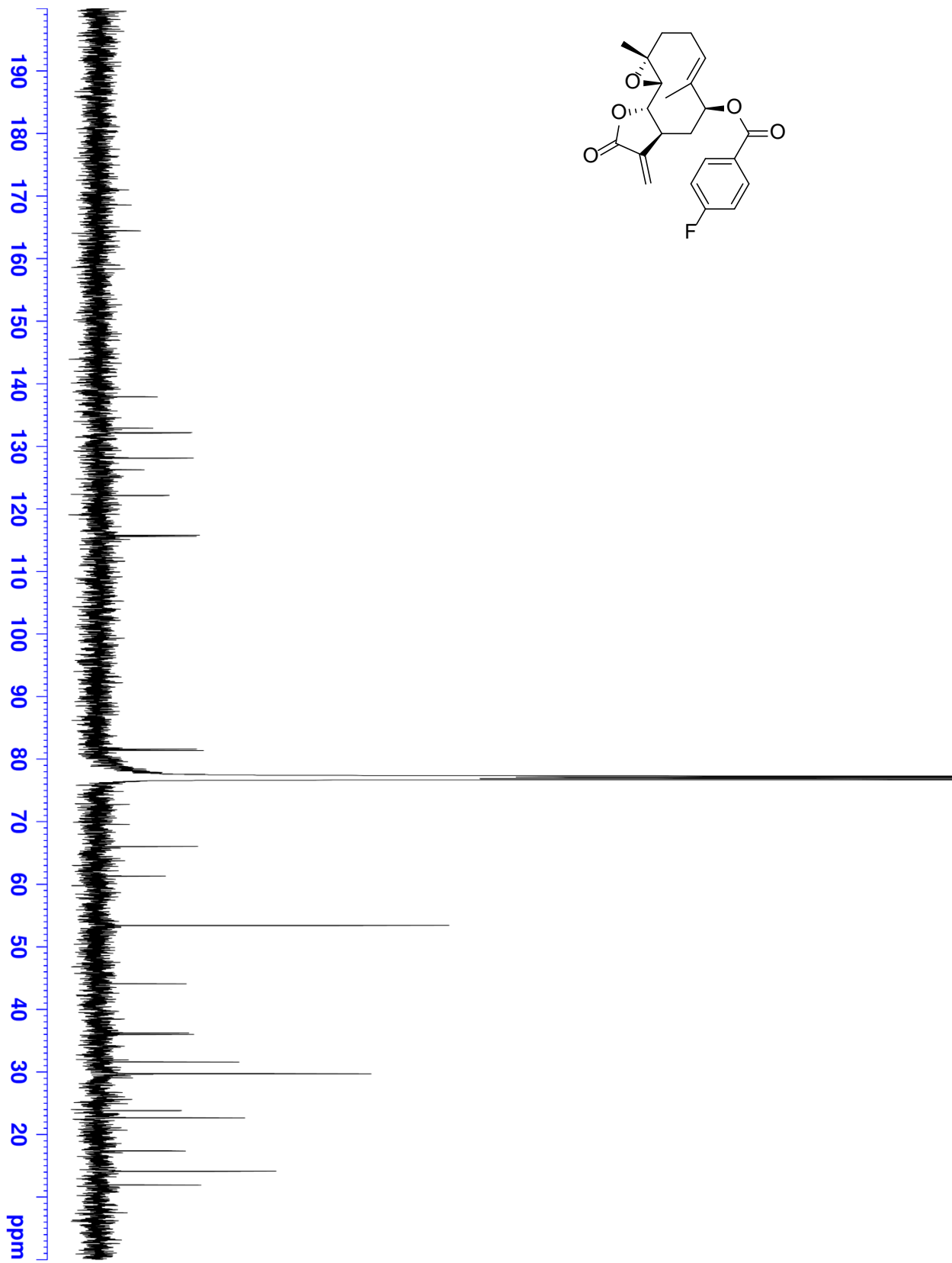
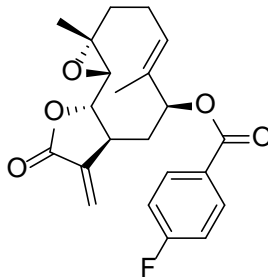


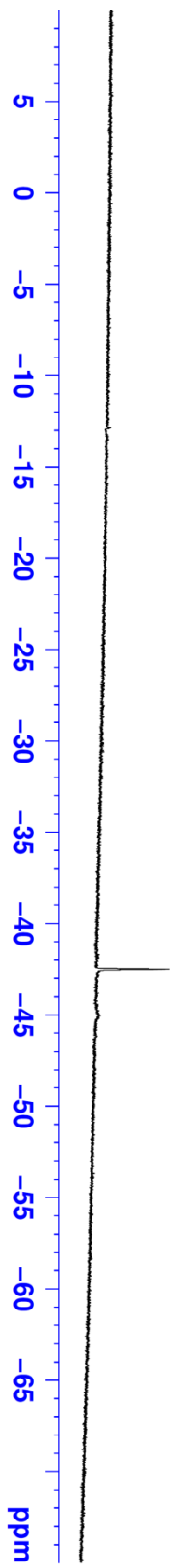
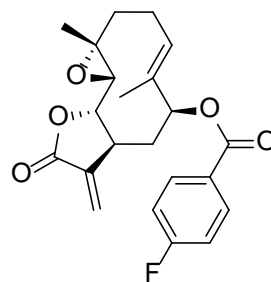


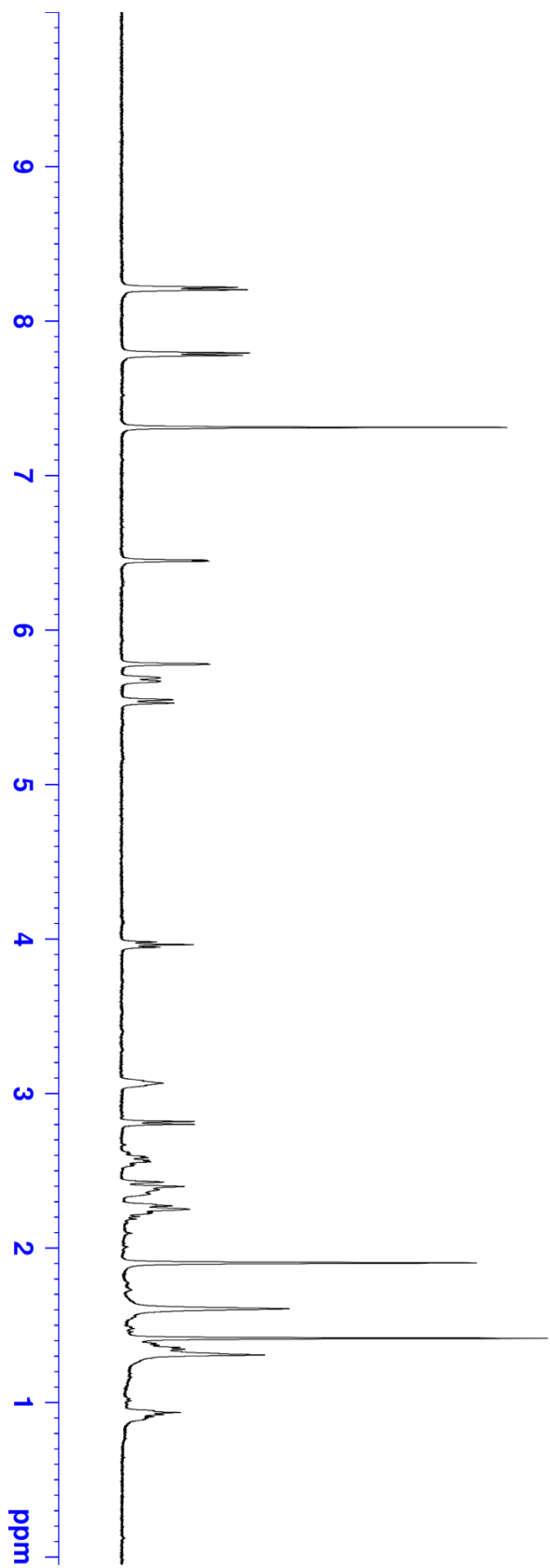
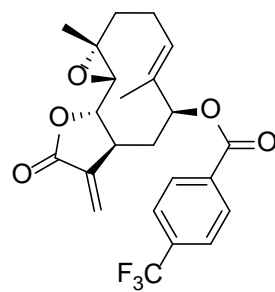


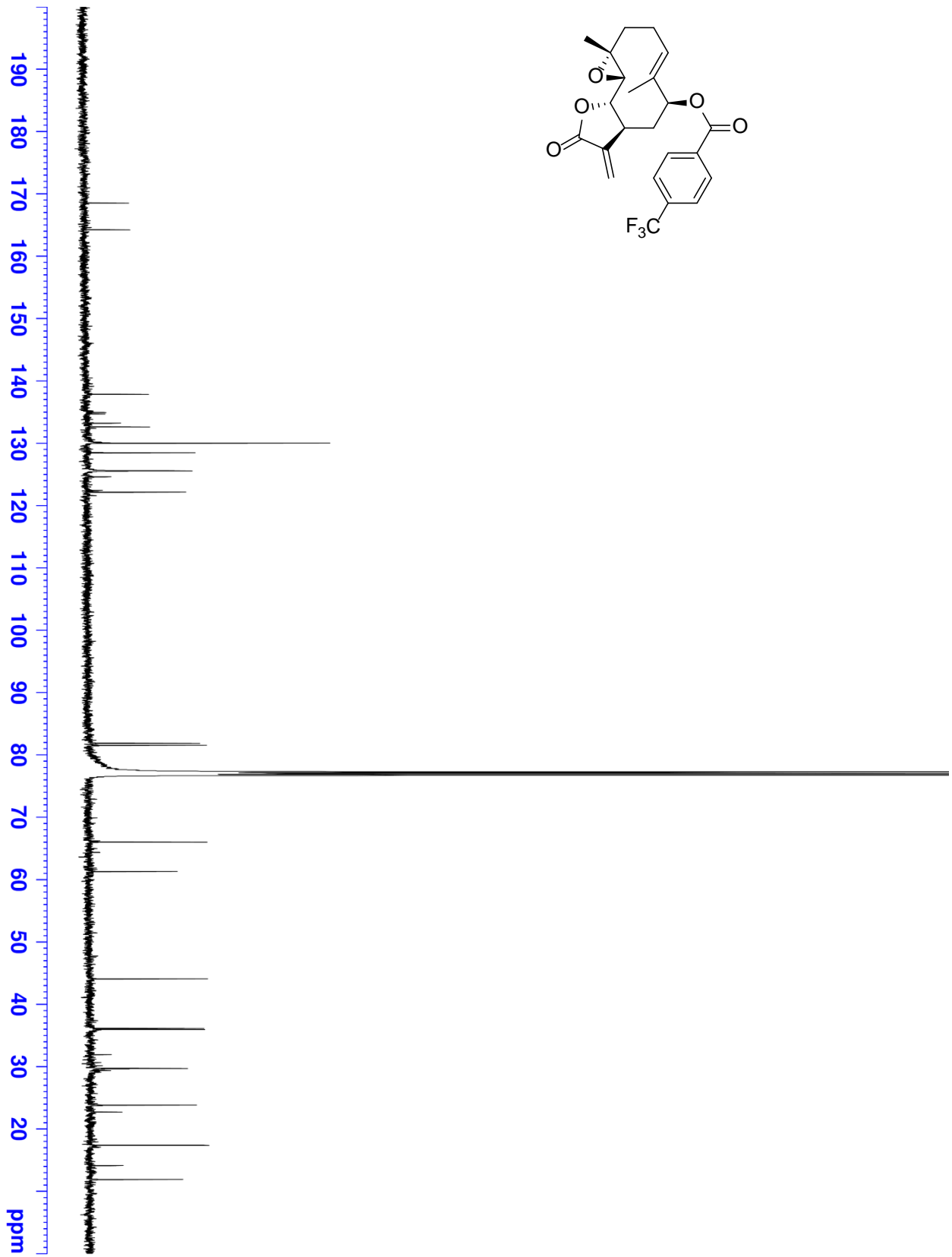
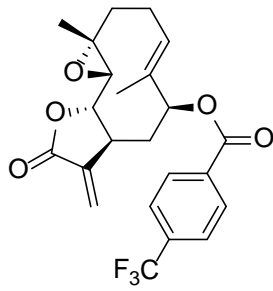


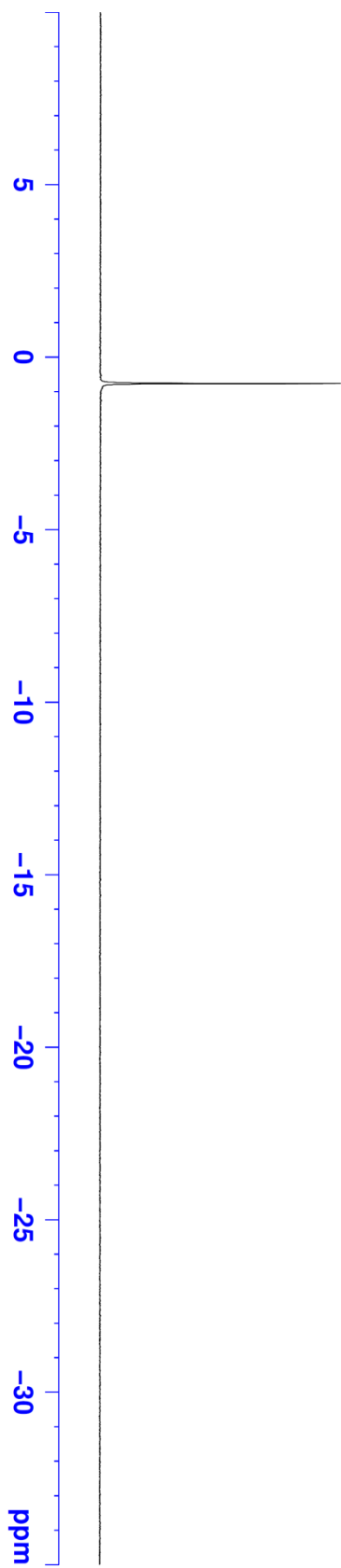
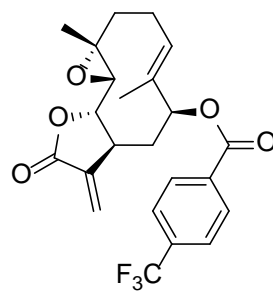


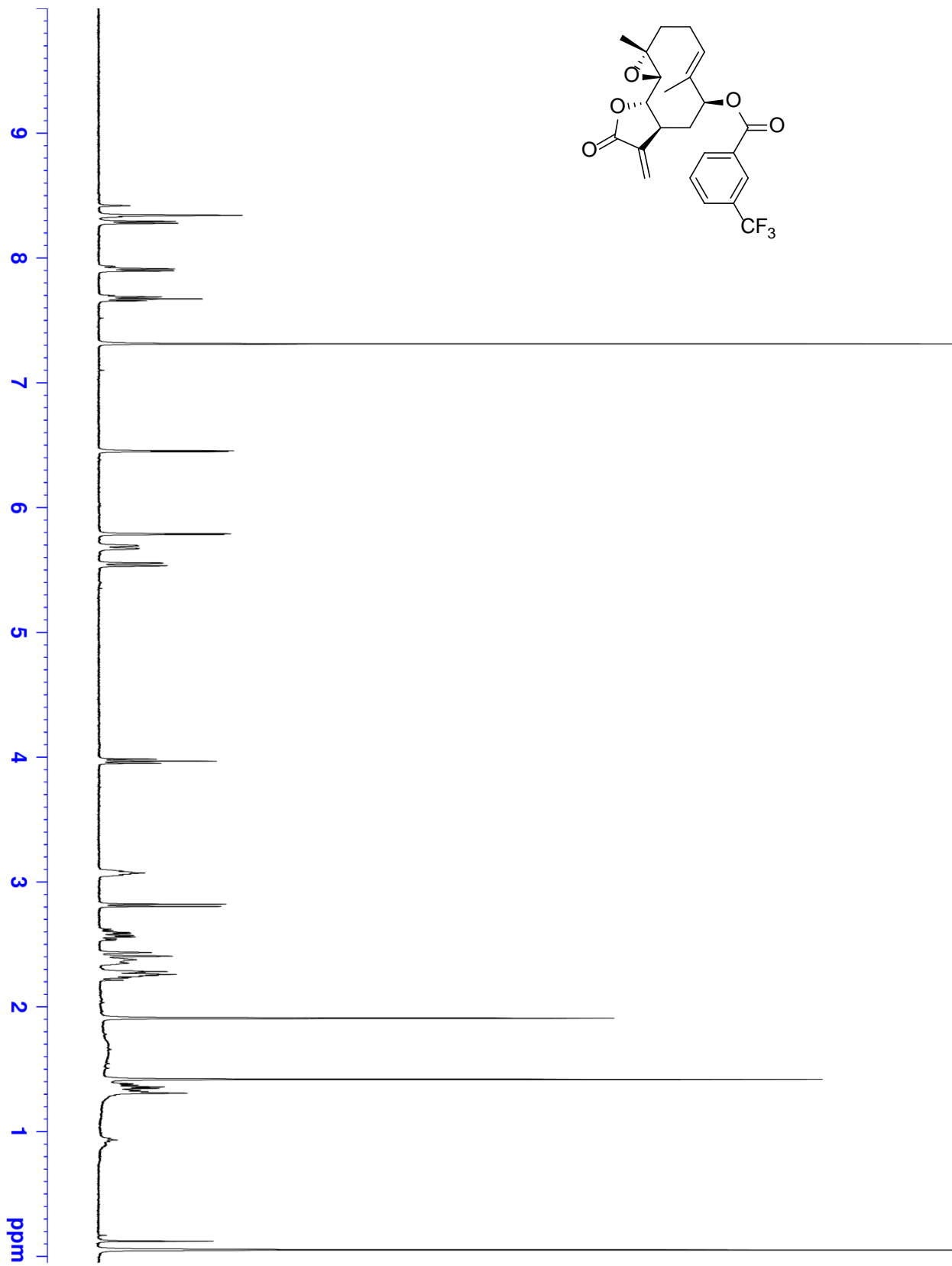


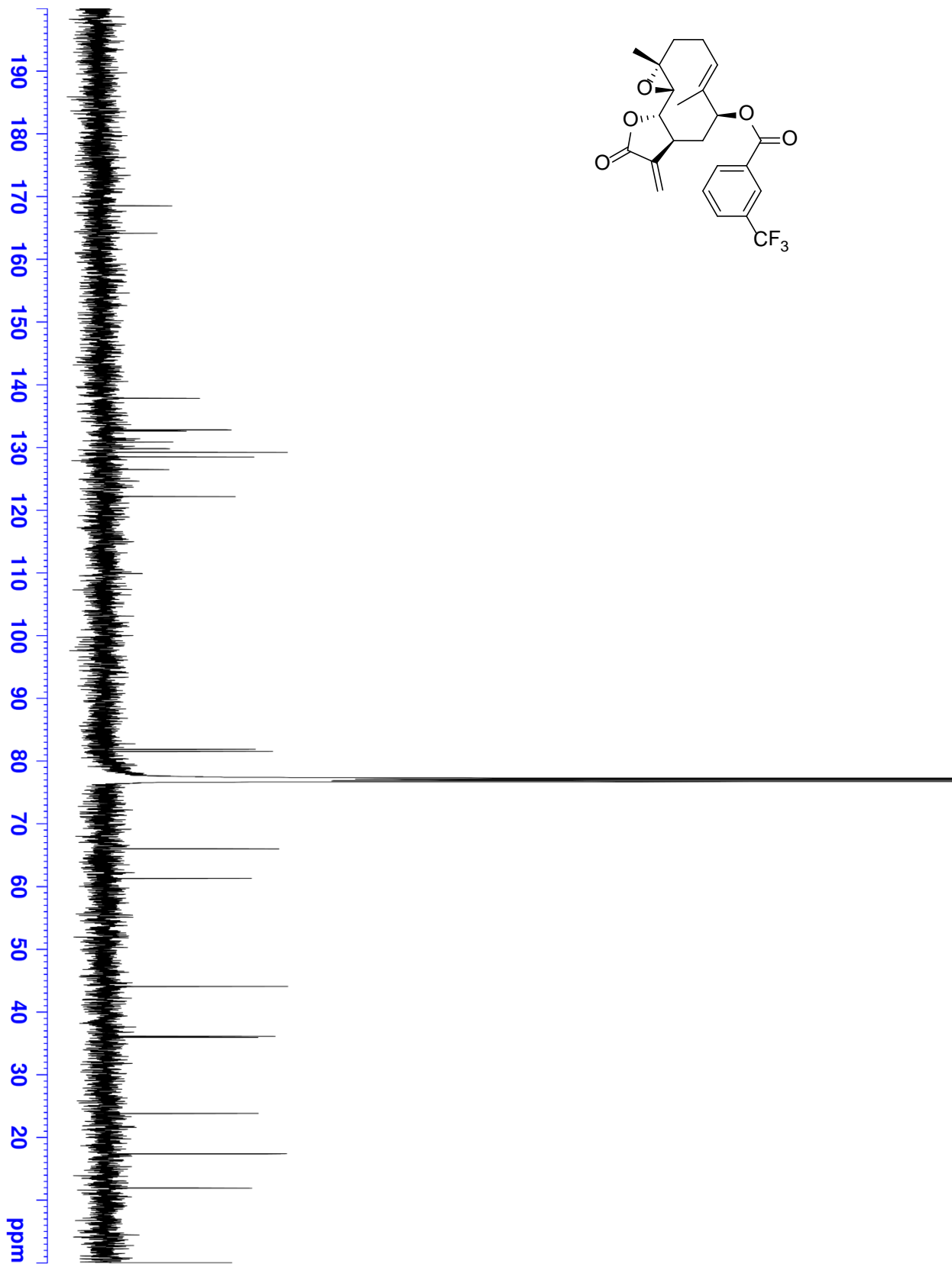
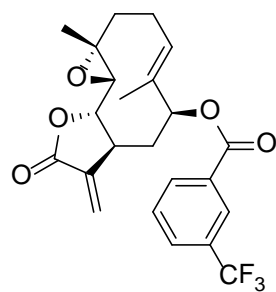


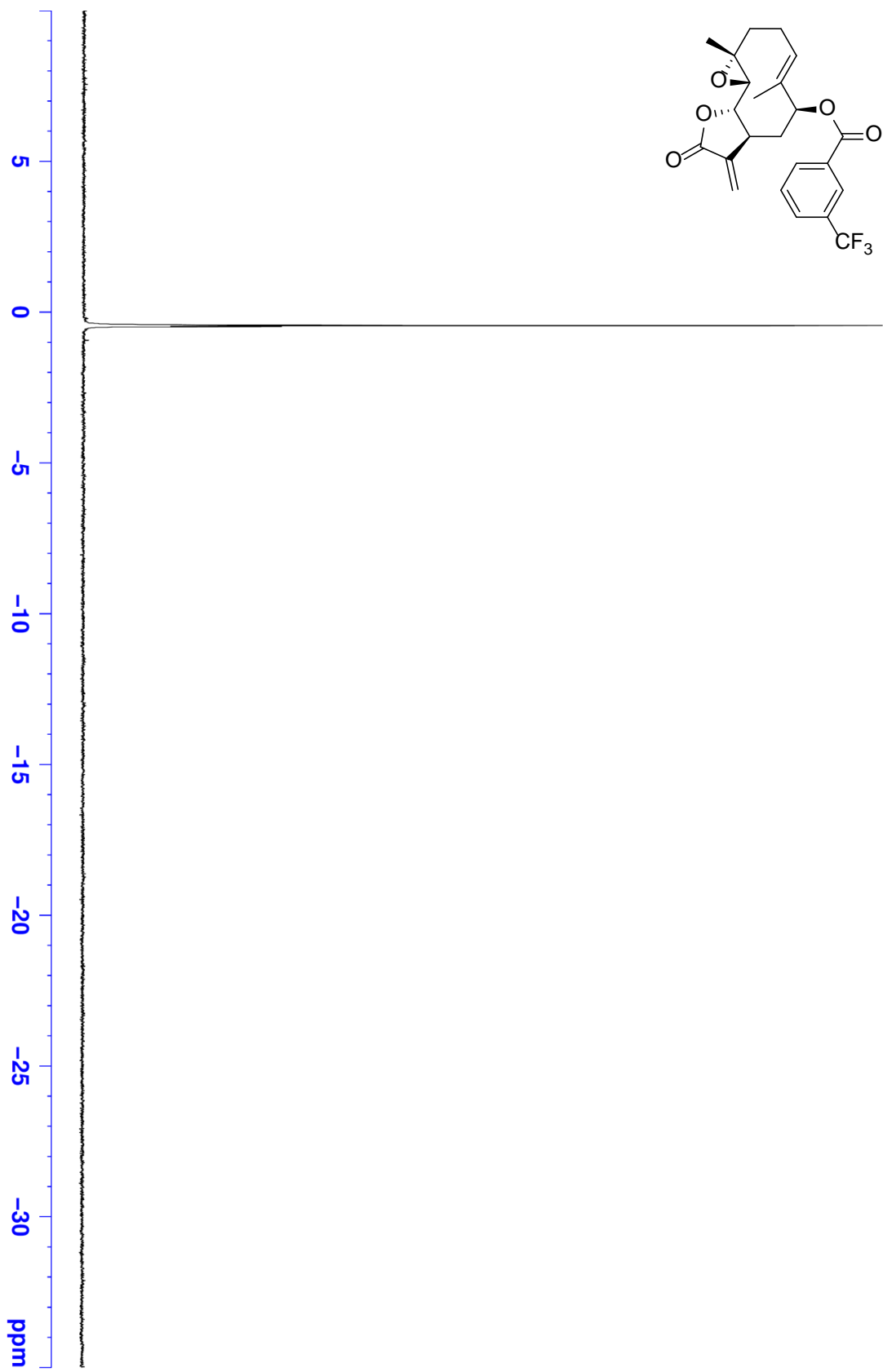


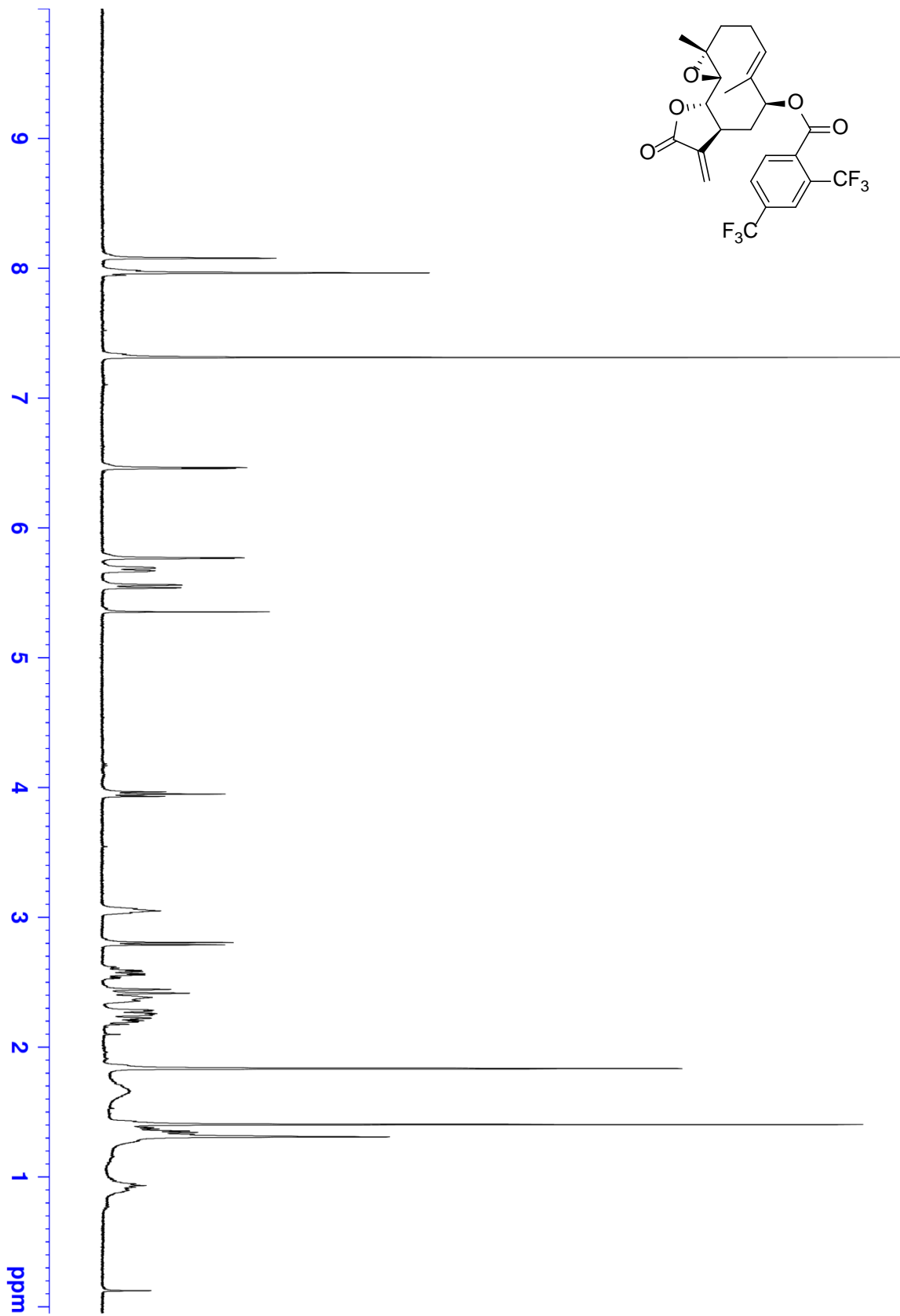


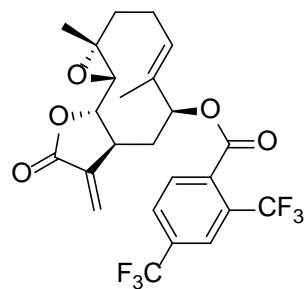
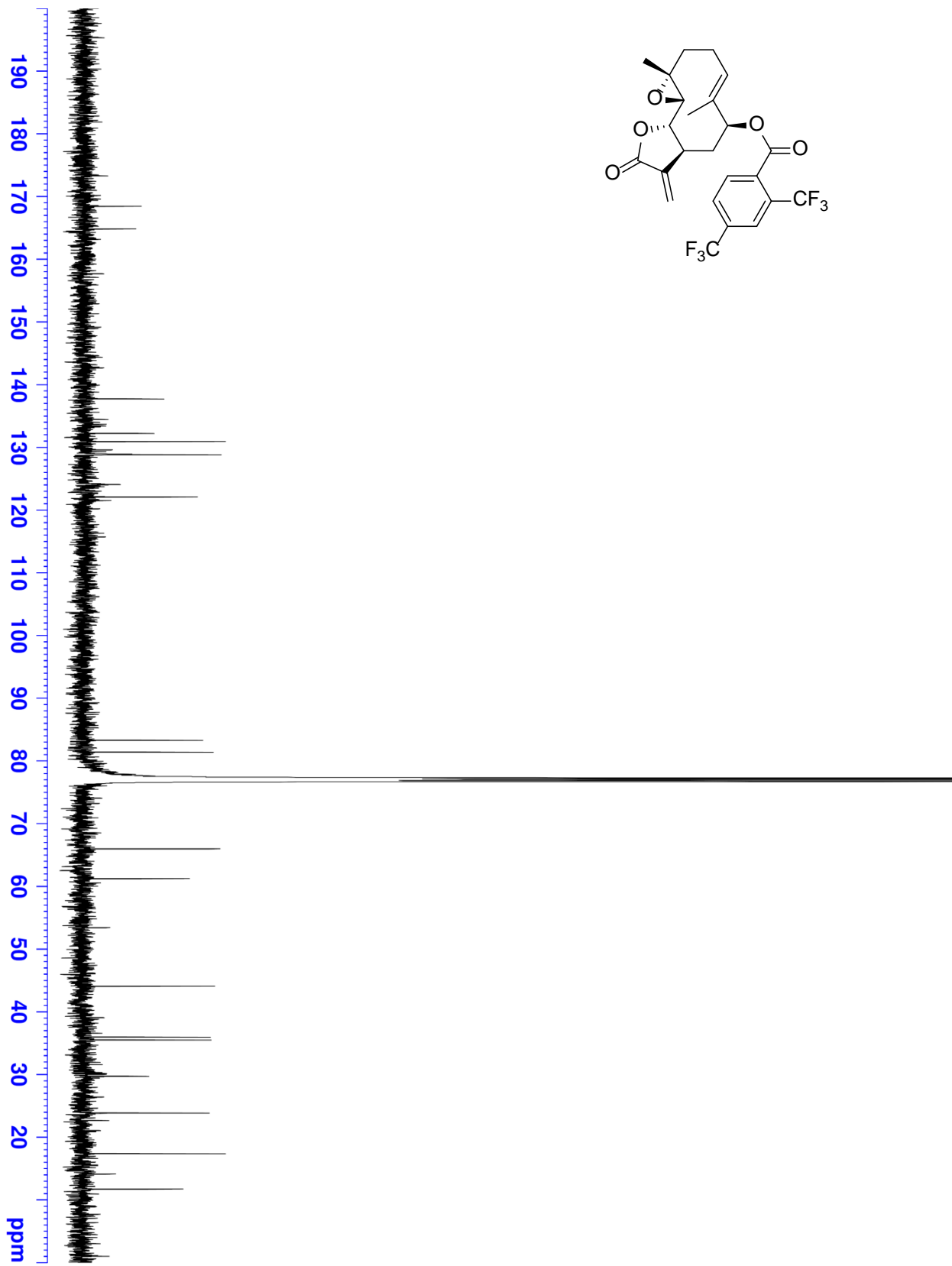


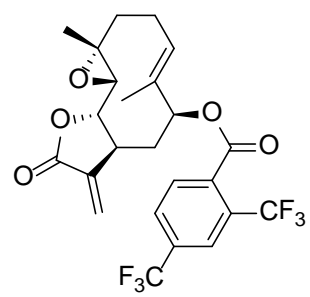
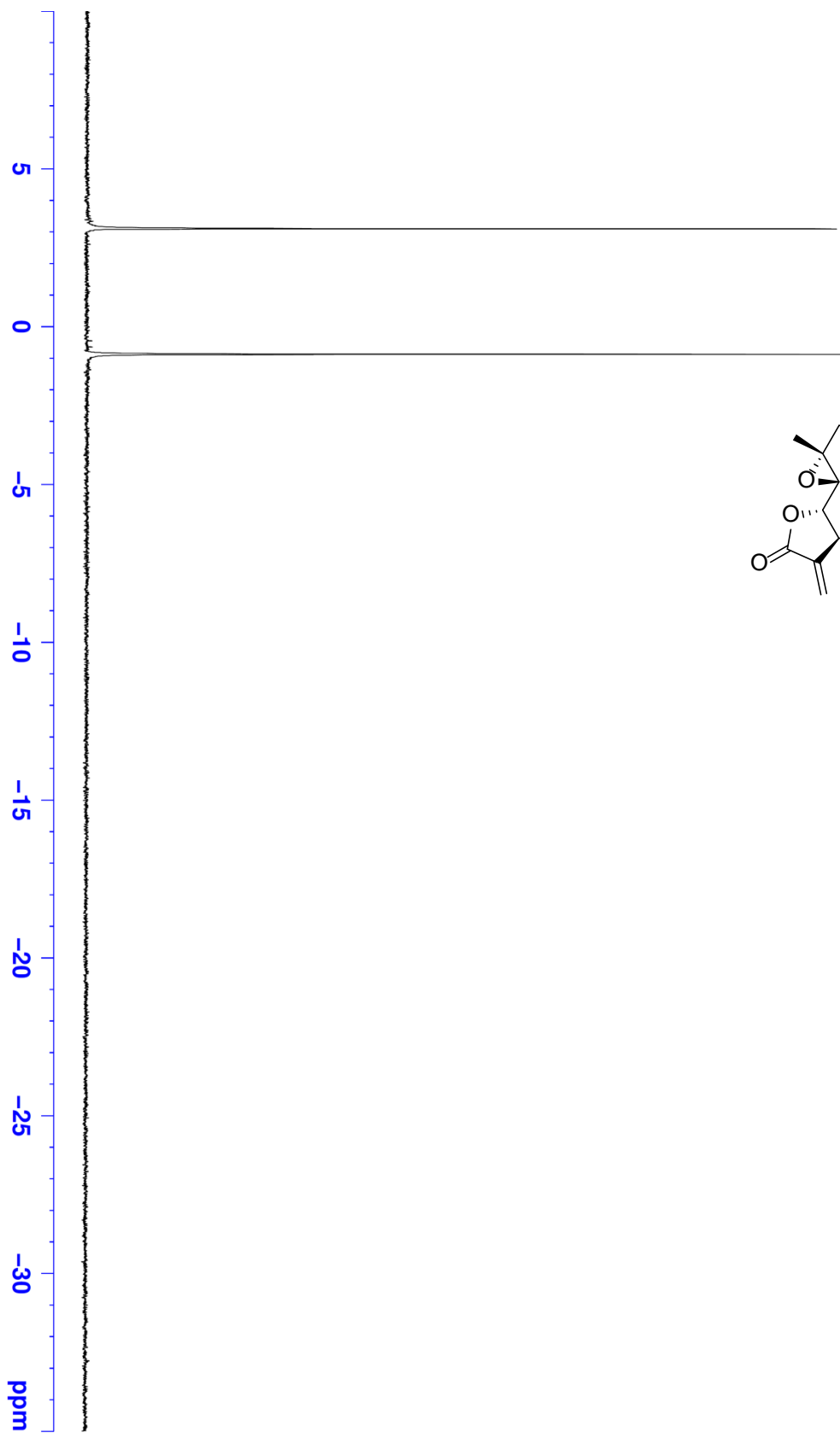












9  
8  
7  
6  
5  
4  
3  
2  
1  
ppm

